CORRELATION OF SOLID-STATE NMR RELAXATION TIMES TO FUNCTIONAL PROPERTIES SUCH AS CHEMICAL STABILITY AND PARTICLE SIZE

By

Kassibla Elodie Dempah

Submitted to the graduate degree program in Pharmaceutical Chemistry and the Graduate Faculty of the University of Kansas in partial fulfillment of the requirements for the degree of Doctor of Philosophy.

_____
Chairperson: Valentino J. Stella

_____
Eric J. Munson

_____
Thomas Tolbert

_____
John F. Stobaugh

_____
Stevin Gehrke

Date Defended: April, 8 2013

The Dissertation Committee for Kassibla Elodie Dempah
certifies that this is the approved version of the following dissertation:

CORRELATION OF SOLID-STATE NMR RELAXATION TIMES TO FUNCTIONAL PROPERTIES SUCH AS CHEMICAL STABILITY AND PARTICLE SIZE

_____
Chairperson Valentino Stella

Date approved: April 8, 2013

Abstract

The purpose of the work presented in this dissertation was to investigate the correlation between the particle size of crystalline active pharmaceutical ingredients (APIs) and their solid-state NMR (SSNMR) proton spin-lattice relaxation times (^{1}H T_1) using model compounds. Dicumarol and salicylic acid were selected as model compounds for this study.

Crystalline samples of the model compounds containing particles with sizes ranging from 1 μm- 800 μm were prepared by sieving, spray-drying, and anti-solvent precipitation. The physical state and the particle size of the materials prepared were characterized. A model that describes the correlation observed between the ^{1}H T_1 time of the dicumarol and the salicylic acid materials and their particle size was proposed. The model was based on the assumption that spin diffusion is the main spin-lattice relaxation mechanism.

The way that SSNMR relaxation time measurements could be used to characterize the polydispersity of crystalline powders using physical mixtures of dicumarol was also investigated. A short investigation of the effect of different compaction forces on the homogeneity of formulated tablets of salicylic acid was also conducted. Different ^{1}H T_1 times were obtained for salicylic acid at all compaction forces, and heavier compaction forces lead to a larger decrease in ^{1}H T_1 time.

Finally, the effect of grinding on the chemical stability of a crystalline API gabapentin was investigated. Changes in ^{1}H T_1 times of ground crystalline gabapentin Form II were correlated with the chemical stability of the material: samples with shorter ^{1}H T_1 times were the least chemical stable. The physical meaning for the reduction in ^{1}H T_1 time observed was

believed to be both the presence of crystal defects and the decrease in particle size of the material.

This research provided evidence that SSNMR can be used to characterize bulk properties as well as molecular level characteristics of pharmaceutical solids. This could improve the characterization of formulated drug products during drug development.

Dedicated to:

My Family

Acknowledgements

I would like to thank my graduate school advisor, Dr. Eric Munson, for his continued guidance and his patience with my questions. I will particularly miss his colorful analogies and his love of his technique that he most certainly passed on to me. I have met many people throughout graduate school and I will not be able to acknowledge every single one of them here. However, I would like to thank the Munson lab members. Thank you, Dr Bob Berendt for correcting my grammar thus making a better speaker and writer. Thank you, Dr Joe Lubach for the summer in San Francisco at Genentech, Donia Arthur for showing me parts of Kentucky that I probably would not have seen without you, and for being a lunch and brownies buddy ☺. Most importantly, thank you, Dr Sarah Pyszczynski for the great company, laughs, helpful advices and many many delicious baked goods. All these things and many many more made for irreplaceable and unforgettable memories.

Thank you to the very helpful staff members of the Pharmaceutical Chemistry department at the University of Kansas, in particular Nancy for answering my many questions and helping so much with the long-distance committee and defense organization. Also, thank you to the graduate students in the department of Pharmaceutical Chemistry who have helped make the department a great collegial environment. Again there are too many to name but I would like to mention Sarah, Rosemary, Ahmed, Diana, Kwame, Josh, Ryan, Barlas, Justin, Randy, Jessica, Josh. The dinners after the physical chemistry exams, and the ice skating trip to Kansas City are some of my favorite graduate school memories. Thank you to Rosemary for providing a listening ear; our sushi dinners are also some of my favorite graduate school memories. Thank you to Katie Sparks also for the fun dance memories.

Moving to another institution in the middle graduate was a little bit of a challenge. Many people were very helpful in easing the transition: thank you, Chris Munson, Catina Rossoll, Todd Sizemore. I have also made some new friends who included me very rapidly in their social lives; thank you, Dayna, Lindsey, Kaci, Eleftheria, Ore, Kyle, Andrei.

My graduate school experience was stressful at times. In addition to Sarah's tasty baked goods that helped ease some of the stress, some friends provided some compassion, or tough love, and helped me put things in perspective. Some often forced me to take breaks and helped me not miss out too much on "real life" while I was busy with grad school. Thank you Marcus, Gladys, Audrey, Lamarre and Quentin.

Finally, thank you to my siblings, Dominique, Linda and Maxime, for supporting me at my best and at my worst.

Thank you to my parents for your undying love, support and confidence in me.

Table of Contents

Table of Contents

Table of Contents

Table of Contents

Table of Contents

Chapter 1

Introduction

1.1 Introduction

The overall objective of the work presented in this dissertation is to characterize the particle size of crystalline solids in pure active pharmaceutical ingredients (API) powders and in formulated drug products using solid-state NMR spectroscopy (SSNMR) relaxation time measurements, and subsequently correlate the measurements to functional pharmaceutical properties such as dissolution rate and drug stability.

The particle size of crystalline pharmaceuticals impacts a number of important pharmaceutical properties such as the dissolution rate, the manufacturability of the powder and the dose uniformity in the final formulated drug product [1-5]. However, it is extremely difficult to measure particle size of drug crystallites after they have been formulated, and in particular in a tablet. Solid-state NMR spectroscopy has emerged as a powerful technique for the characterization of solid pharmaceuticals. One of the main advantages of that technique is that it can be used to characterize APIs within a formulation. SSNMR is generally thought of as a molecular level technique; however, previous work performed in our laboratory suggests that it could be used to characterize bulk properties of solid pharmaceuticals such as particle size.

SSNMR will be discussed in more detail in the following chapter; in this introduction chapter, characteristics of pharmaceutical solids in general, and crystalline solids in particular, are presented. The relevance of the particle size and morphology of solid pharmaceuticals to drug development is also discussed, as well as the impact of processes used during development on these properties. Finally, the motivation for the work presented in this dissertation is presented in more detail and the remainder of the dissertation is outlined.

1.2 Pharmaceutical Solids

Small molecule oral solid-state formulations represent the majority of drug products currently on the market. They offer significant advantages over parenteral formulations like injectable formulations, such as higher stability, cheaper manufacturing cost, and higher patient compliance. Solid drug products are composed of an active pharmaceutical ingredient (API) and excipients, which are the pharmaceutically inactive materials that serve as bulking agents, stabilizers or lubricants. Solid APIs can exist in either the crystalline or amorphous state. The most stable crystalline form of an API is typically preferred when developing a drug candidate because it will not convert into other forms, and is less likely to have chemical stability problems compared to less stable forms such as the amorphous form. Nonetheless, crystalline pharmaceutical solids can also present challenges such as low bioavailability or poor manufacturability, and even physical and chemical instability during the drug development process. A number of these issues arise from the polymorphism of the crystalline solids. Others are due to the size and the morphology of the particles in the solid powder. The research presented in this dissertation focuses extensively on crystalline materials, and in particular on the particle size of crystalline solid pharmaceuticals. For this reason, the properties of crystalline materials will be described in the following sections.

1.3 Crystalline solids

A compound that is crystalline has its molecules ordered in a three-dimensional repeating unit that forms a lattice. The smallest repeating unit, called a unit cell, is composed of one or more molecules that have a fixed conformation and/or arrangement in the unit cell. If the unit cell repeats infinitely without interruption, a single crystal results. Crystals may also be composed of aggregates of smaller single crystals. Crystals may contain some imperfections that

occur as a result of processing or during growth. These imperfections are commonly referred to as crystal defects.

Crystals are often grown from supersaturated solutions, which are solutions where the compound is present at a higher concentration than its equilibrium solubility. Crystal growth begins with nucleation, which occurs when a critical number of molecules come together to create a small crystallite that is thermodynamically stable. Nucleation can be triggered by a number of factors, including the addition of a seed crystal to the supersaturated solution. Crystal formation can result from evaporation of the solvent from a solution, the addition of an anti-solvent, or from a change in pH of the solution. All these actions cause the metastable state of the supersaturated solution to be disturbed, resulting in crystals forming from the solution. The crystallization conditions can be altered in order to obtain crystals of different sizes.

1.3.1 Relevance of particle size and morphology

A polycrystalline material is a collection of crystallites that forms a powdery material, and the properties associated with that powder are highly dependent on the size as well as on the shape, or morphology, of its particles. Some of the pharmaceutically relevant properties of solid powder that are affected by particle size and morphology include the dissolution rate and the manufacturability of the powder [6-8]. In fact, the guidelines issued by the International Conference on Harmonization (ICH) list particle size as one of the physical properties that influence the manufacturability and the performance of solid drug products. The ICH also issued an acceptance criteria flow chart for the particle size distribution of solid pharmaceuticals (Figure 1.1). The way that particle size affects the dissolution rate of solids can often be described by the Noyes-Whitney equation.

$$\frac{dS}{dt} = \frac{DA(C_S - C)}{h} \quad (1.1)$$

Setting acceptance criteria for drug substance particle size distribution

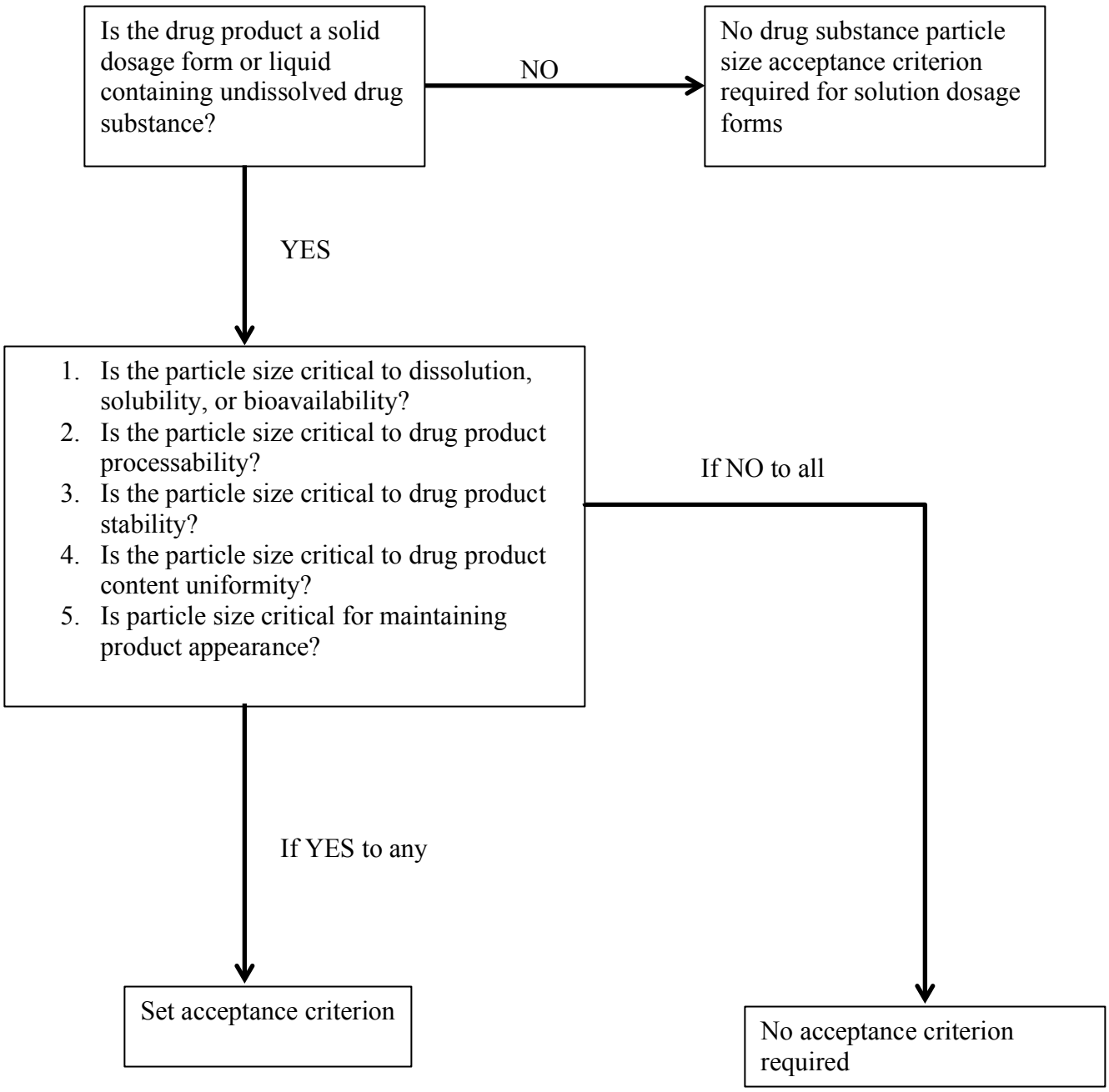

Figure 1.1 ICH guideline Q6A

where dS/dt is the dissolution rate, D is the diffusion coefficient, A is the surface area, Cs is the concentration of the solid in the diffusion layer h immediately surrounding the drug particle, and C is the concentration of the solid in the bulk medium. A decrease in particles size leads to an increase in surface area of the particles, which in turn leads to a faster dissolution rate of the solid material. In theory, an increase in surface area by a factor of 10 leads to an increase in dissolution rate by the same amount, which in turn may improve the bioavailability of the pharmaceutical solid. This ability of smaller size particles to improve the bioavailability of a solid drug has triggered a large volume of investigations on ways to produce nanoparticles of poorly soluble APIs, such as BCS Class II and Class IV compounds [9-12]. Two main approaches for decreasing particle size exist, namely the top-down and the bottom-up approaches. While ways to generate particles as small as hundreds of nanometers have been developed, the physical state characterization of these small size systems poses a challenge. That is because the impact of particle size on the response of commonly used characterization techniques such as differential scanning calorimetry (DSC) is not yet fully understood [13,14].

Apart from impacting the bioavailability of the drug product via modulating the dissolution rate of the material, the particle size of solid pharmaceuticals can also impact the bioavailability of the drug product by dictating the site of drug absorption. This is the case for nasal and pulmonary drug delivery systems where the bioavailability of the drug heavily relies on the size of the particles in the drug product. Particles ranging from 1-5 μm are the ideal size for inhalation and respiratory drug products because their aerodynamic properties dictate that they are deposited in the most vascularized area of the lungs and nose, allowing for the greatest likelihood of drug absorption [15]. On the other hand, the size of the particles of solid drug products for oral delivery is dictated by their manufacturability. Particles for oral dosage

formulations typically range from 100-200 μm because particles in this size range tend to have the best flow properties, which allow for easier manufacturing. Nonetheless, homogeneous mixtures of these larger size particles are not easily obtained, and when a variety of particle sizes are present, segregation can occur [7]. Also, smaller particles (20-50 μm) are preferred for chewable and fast-disintegrating oral tablets because of their faster dissolution rate [15]. The difficulty in obtaining homogeneous mixtures of solid pharmaceuticals can lead to a lack of dose uniformity in the final drug product, especially for low dose (< 5mg) drug products [2]. The impact of particle size on the dose uniformity of the final drug product has been studied, and models that attempt to identify the particle size distribution that will provide the highest dose uniformity for a given drug have been proposed [1,3,4]. However, in certain cases a broad particle size distribution of the API may be desired for drug delivery reasons; for example, a mixture of different particle sizes could be used to tune the release properties of the drug product [15].

The particle morphology of a material can also have a significant effect on the drug product performance and on the powder manufacturability [16,17]. Particles with a spherical morphology are typically easier to manufacture because they have better flow properties. Conversely needle and rod type particles have more resistance to flow. Particle morphology has also been shown to impact the ability to tablet some solid APIs [16]. Also, differences in the shape of the particles within a solid drug product have been shown to cause non-homogenous mixtures [7].

A number of processing steps are used to modify the particle size and the particle morphology of crystalline solids in order to improve their manufacturability and/or improve the drug performance. These include milling, wet and dry granulation, blending with excipients and more. However, some of these processes can cause changes in physical state thus affecting the

physical and/or the chemical stability of the drug product. Common manufacturing processes and their potential effect on the stability of solid pharmaceuticals are discussed below.

1.4 Effect of common processing methods on crystalline solids properties

During manufacturing, solid APIs are often exposed to a variety of temperature and humidity conditions, which combined with the stress of the manufacturing processes, can potentially cause unwanted physical transformations. For example, a material can convert to another solid form such as a different crystalline form, a hydrated or solvated form, or an amorphous form. After a brief discussion of polymorphism, the impact of manufacturing on the physical state of crystalline solid APIs will be discussed.

1.4.1 Polymorphism

Polymorphs of a crystalline material have the same chemical structure but differ in the conformation or arrangement of the molecules in the unit cell. The polymorphs of a material may vary greatly in their physical properties such as density, melting point, solubility, or hygroscopicity. This leads to significant differences in important pharmaceutical properties such as dissolution rate and physical and chemical stability. For this reason, polymorph screening, characterization, and selection are a vital part of the drug development process. Under a particular set of temperature and pressure conditions, one polymorphic form of a compound has the lowest Gibbs free energy and is therefore the most thermodynamically stable. That most stable form is generally preferred for use in the final drug product. It is possible for another polymorphic form to be the most stable form under different conditions; in that case the two forms are said to be enantiotropically related. When one form is more stable than another form at all temperatures and pressures, the relationship between the two forms is described as

monotropic. Figure 1.2 illustrates the difference between monotropic and enantiotropic systems using a graph of energy versus temperature.

1.4.2 Changes in physical state

Milling is often the first step in the manufacturing of solid pharmaceuticals, and is commonly used to improve the powder flowability of solid pharmaceuticals either by reducing the size of the particles in order to obtain a more uniform powder, or by changing the morphology of particles from needles to more spherical [2]. However, milling generates heat and causes mechanical stress that can lead to polymorphic conversions. A number of APIs have been shown to undergo polymorphic conversions when milled [18,19]. Wet-granulation is another commonly-used manufacturing process that is employed to impart better flowability and compressibility to the material. However, wet-granulation is especially prone to causing polymorphic conversions because of the presence of a liquid phase [20,21]. The presence of excipients during wet granulation can also cause changes in physical state [22]. Dry granulation can be used as an alternative to wet granulation in order to avoid the use of a solvent, but the mechanical stress induced by the process can also cause physical state changes. Finally, the compression forces used during tableting of the drug product may be very high and can also lead to physical transformations of the solid API [20,23].

The ability to detect any physical conversions of the API that occurred as a result of processing can be a difficult task due to the complexity of solid formulations, and numerous analytical techniques often have to be used. Moreover, the mechanical stress induced by some of the manufacturing processes discussed above can not only cause polymorphic conversions, they can also lead to changes in the chemical stability of the material [24]. In cases where particle size control of the API is absolutely necessary for effective drug delivery, the particle size must also

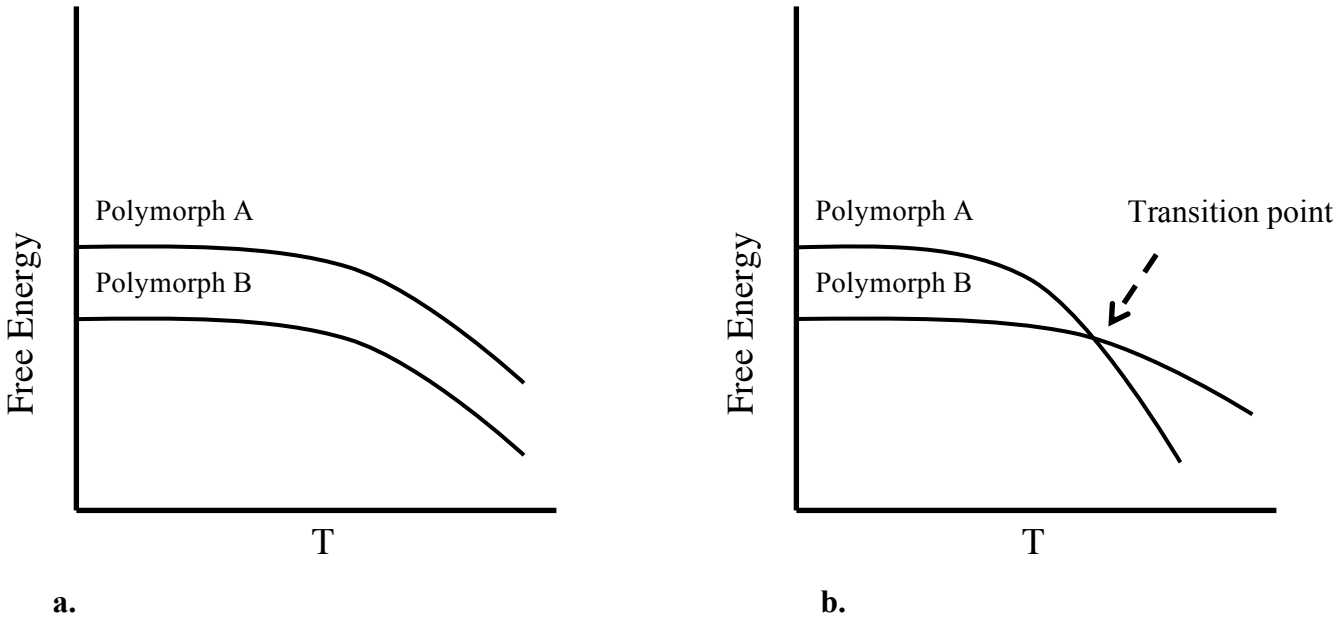

Figure 1.2 Plot of the free energy versus temperature showing how a monotropic and an enantiotropic polymorphic system differ from each other.
a. monotropic polymorphic system; **b.** enantiotropic polymorphic system. In the enantiotropic system the relative stabilities of the polymorphs are reversed past a transition point.

be well characterized. The characterization of the APIs in the presence of the excipients in a formulation is only possible using a handful of analytical techniques, one of which is solid-state NMR.

1.5 Motivation for this work

1.5.1 Advantages of solid-state NMR for the characterization of solid pharmaceuticals

Solid-state NMR (SSNMR) is an superbly powerful tool for the characterization of solid pharmaceuticals, and studies in the Munson laboratory and other laboratories have demonstrated the applicability of SSNMR to the physical state characterization of solid APIs both alone and in the presence of excipients within formulations [25-27]. Solid-State NMR is one of the few analytical techniques available for the characterization of complex solid mixtures containing the API and the excipients. To the best of our knowledge, no study has investigated the ability of SSNMR to characterize other physical properties of crystalline solid pharmaceuticals such as particle size or particle morphology. Part of the reason is that SSNMR is typically thought of as a molecular level technique.

1.5.2 Previous work

Results of previous study performed in the Munson laboratory have suggested that SSNMR proton spin-lattice relaxation (^{1}H T_1) times are sensitive to changes in crystalline solids brought about by common manufacturing processes such as milling. One such study was performed by Lubach and coworkers with lactose monohydrate as a model compound [28]. In their study, Lubach and coworkers cryoground crystalline α-lactose for different lengths of times and obtained ^{1}H T_1 times and ^{13}C SSNMR spectra of all the samples. They found that at longer grinding times, crystalline lactose converted to amorphous lactose. This was obvious by the

significant line broadening observed in the SSNMR spectra. Lactose ground for 2 min remained crystalline, yet its ^{1}H T_1 time was an order of magnitude shorter than that of the unground material. That reduction in ^{1}H T_1 magnitude was believed to be due to the creation of crystal defects. However, particle size reduction also happened during milling, and the influence of particle size on the decrease in ^{1}H T_1 time observed was not investigated. It is this correlation that will be investigated in this dissertation.

1.6 Overview of the dissertation

Chapter 2 contains a description of the techniques, with an emphasis on solid-state NMR relaxation time measurements. Chapter 3 introduces the theory behind the correlation between particle size and ^{1}H T_1 times. Chapter 4 presents the selection of the model compounds used for the remainder of the dissertation and the preparation and physical state characterization of the different samples. Chapter 5 focuses on the correlation between the size of the particles in the samples prepared and the ^{1}H T_1 relaxation times of the materials, and presents a proposed model between particle size and ^{1}H T_1. Chapter 6 shows how the polydispersity of a material can be characterized by its ^{1}H T_1 relaxation, including applications to the study of formulated tablets and a correlation to dissolution rates. In Chapter 7, the correlation between ^{1}H T_1 times and chemical stability of ground samples of a model system, gabapentin, is presented. Finally, Chapter 8 will discuss future possible directions or extensions for this research.

1.6 References

1. Hilden J, Schrad M, Kuehne-Willmore J, Sloan J 2012. A first-principles model for prediction of product dose uniformity based on drug substance particle size distribution. J Pharm Sci 101:2364-2371.

2. Iacocca RG, Burcham CL, Hilden LR 2010. Particle engineering: A strategy for establishing drug substance physical property specifications during small molecule development. J Pharm Sci 99(1):51-75.

3. Rohrs BR, Amidon GE, Meury RH, Secreast PJ, King HM, Skoug CJ 2006. Particle size limits to meet USP content uniformity criteria for tablets and capsules. J Pharm Sci 95:1049-1059.

4. Yalkowsky SH, Bolton S 1990. Particle size and content uniformity. Pharm Res 7:962-966.

5. Sun J, Wang F, Sui Y, She Z, Zhai W, Wang C, Deng Y 2012. Effect of particle size on solubility, dissolution rate, and oral bioavailability: evaluation using coenzyme Q(1)(0) as naked nanocrystals. Int J Nanomedicine 7:5733-5744.

6. Yao T, Yamada M, Yamahara H, Yoshida M 1998. Tableting of Coated Particles. II. Influence of Particle Size of Pharmaceutical Additives on Protection of Coating Membrane from Mechanical Damage during Compression Process. Chemical & Pharmaceutical Bulletin 46(5):826-830.

7. Swaminathan V, Kildsig DO 2002. Polydisperse powder mixtures: effect of particle size and shape on mixture stability. Drug Dev Ind Pharm 28:41-48.

8. Shiraishi T, Sano A, Kondo S, Yuasa H, Kanaya Y 1995. Studies on the granulation process of granules for tableting with a high-speed mixer. II. Influence of particle size of active substance on granulation. Chem Pharm Bull 43:654-659.

9. Kesisoglou F, Panmai S, Wu Y 2007. Nanosizing -- Oral formulation development and biopharmaceutical evaluation. Advanced Drug Delivery Reviews 59(7):631-644.

10. Shekunov B, Chattopadhyay P, Seitzinger J, Huff R 2006. Nanoparticles of Poorly Water-Soluble Drugs Prepared by Supercritical Fluid Extraction of Emulsions. Pharmaceutical Research 23(1):196-204.

11. Van Eerdenbrugh B, Van den Mooter G, Augustijns P 2008. Top-down production of drug nanocrystals: Nanosuspension stabilization, miniaturization and transformation into solid products. International Journal of Pharmaceutics 364(1):64-75.

12. de Waard H, Hinrichs WLJ, Frijlink HW 2008. A novel bottom-up process to produce drug nanocrystals: Controlled crystallization during freeze-drying. Journal of Controlled Release 128(2):179-183.

13. Jillavenkatesa A, Kelly JF 2002. Nanopowder Characterization: Challenges and Future Directions. Journal of Nanoparticle Research 4(5):463-468.

14. Shah RB, Khan MA. 2009. Nanopharmaceuticals: Challenges and Regulatory Perspective. Nanotechnology in Drug Delivery, ed. p 621-646.

15. Shekunov BY, Chattopadhyay P, Tong HHY, Chow AHL 2007. Particle Size Analysis in Pharmaceutics: Principles, Methods and Applications. Pharm Res 24:203-227.

16. Sun C, Grant DJW 2001. Influence of crystal shape on the tableting performance of L-lysine monohydrochloride dihydrate. J Pharm Sci 90(5):569-579.

17. Danjo K, Kinoshita K, Kitagawa K, Iida K, Sunada H, Otsuka A 1989. Effect of particle shape on the compaction and flow properties of powders. Chem Pharm Bull 37:3070-3073.

18. Zhang GGZ, Law D, Schmitt EA, Qiu Y 2004. Phase transformation considerations during process development and manufacture of solid oral dosage forms. Advanced Drug Delivery Reviews 56(3):371-390.

19. Ward GH, Schultz RK 1995. Process-Induced Crystallinity Changes in Albuterol Sulfate and Its Effect on Powder Physical Stability. Pharmaceutical Research 12(5):773-779.

20. Wöstheinrich K, Schmidt PC 2001. Polymorphic Changes of Thiamine Hydrochloride During Granulation and Tableting. Drug Development and Industrial Pharmacy 27(6):481-489.

21. Otsuka M, Hasegawa H, Matsuda Y 1997. Effect of polymorphic transformation during the extrusion-granulation process on the pharmaceutical properties of carbamazepine granules. Chemical and Pharmaceutical Bulletin 45(5):894-898.

22. Airaksinen S, Luukkonen P, Jørgensen A, Karjalainen M, Rantanen J, Yliruusi J 2003. Effects of excipients on hydrate formation in wet masses containing theophylline. J Pharm Sci 92(3):516-528.

23. Chan HK, Doelker E 1985. Polymorphic Transformation of Some Drugs Under Compression. Drug Development and Industrial Pharmacy 11(2-3):315-332.

24. Wardrop J, Law D, Qiu Y, Engh K, Faitsch L, Ling C 2006. Influence of solid phase and formulation processing on stability of Abbott-232 tablet formulations. Journal of Pharmaceutical Sciences 95(11):2380-2392.

25. Sotthivirat S, Lubach JW, Haslam JL, Munson EJ, Stella VJ 2007. Characterization of prednisolone in controlled porosity osmotic pump pellets using solid-state NMR spectroscopy. Journal of Pharmaceutical Sciences 96(5):1008-1017.

26. Harris RK 2007. Applications of solid-state NMR to pharmaceutical polymorphism and related matters*. Journal of Pharmacy and Pharmacology 59(2):225-239.

27. Saindon PJ, Cauchon NS, Sutton PA, Chang Cj, Peck GE, Byrn SR 1993. Solid-State Nuclear Magnetic Resonance (NMR) Spectra of Pharmaceutical Dosage Forms. Pharmaceutical Research 10(2):197-203.

28. Lubach JW, Xu D, Segmuller BE, Munson EJ 2007. Investigation of the effects of pharmaceutical processing upon solid-state NMR relaxation times and implications to solid-state formulation stability. Journal of Pharmaceutical Sciences 96(4):777-787.

Chapter 2

Physical State Characterization and Particle Size Measurements of Pharmaceutical Solids

2.1 Introduction

In this chapter techniques that can be used to characterize the particle size and the physical state of crystalline solid pharmaceuticals, including laser diffraction, microscopy and solid-state NMR (SSNMR) are discussed. In the previous chapter some of the basic properties of crystalline solids and their impact on pharmaceutical properties were presented. In particular, the central role that the particle size of pharmaceutical solids plays on their manufacturability and the way that it can impact the drug product uniformity and the bioavailability of the drug product were discussed. The potential for commonly used manufacturing processes to modify the size and the morphology of solids, to cause changes in the physical state of the API such as polymorphic conversions, or to result in crystalline to amorphous conversions was also mentioned [1-3]. These changes could lead to poorer bioavailability and decreases in chemical stability. As a result, it is important for the particle size and the physical state of the pure solid API and the final formulated drug product to be well characterized.

2.2 Particle size measurement techniques

There are several methods available to measure particle size, and the choice of method used often depends on the expected size of the particles in the sample analyzed. In an excellent review article, Shekunov and coworkers discussed the particle sizing techniques that are applicable to pharmaceuticals as well as the principles of operation and shortcomings of each [4]. Laser diffraction and microscopy are two of the most commonly used techniques. The following is a short description of their principles of operation and the particle size range that they can be used to measure. The limitations of each method will also be discussed.

2.2.1 Laser diffraction techniques

Laser diffraction operates on the principle that particles that are suspended in a liquid produce a diffraction pattern as they pass through a laser beam. This pattern is dependent on the size of the particles. Laser diffraction is used to measure particles ranging from 0.5 to 1000 μm in size [4]. Laser diffraction measurements are volume-based: the angle and the intensity of the scattered light are function of the volume of the particles. Equations relating scattering to volume are then used to calculate the diameter of the particles from the volume measurements and to provide a particle size distribution [4]. The results are often represented in terms of percentile values, where the d10, d50, and d90 values are the numbers below which 10, 50, and 90% of the volume of the sample lies. Laser diffraction measurements require the solid to be suspended in solution often with a surfactant added. For some materials, that step may cause the particles to agglomerate, and therefore sonication is often used to break down these agglomerates and any other agglomerate that may already be present in the sample. Whether a sample is sonicated before measurements and for how long can affect the particle size results obtained, as both aggregates and actual particles can be broken down during sonication. Figure 2.1 illustrates the impact of sonication on laser diffraction results. In Figure 2.1, the laser diffraction data obtained for a sample of dicumarol that was suspended in water with and without prior sonication are shown; the sample that was sonicated contains smaller particles than the unsonicated material. Another parameter that can affect the data obtained by laser diffraction is the morphology of the particles in the solid [4]. The equations used to obtain the diameter of the particles assume that they have a spherical morphology, which is not always the case.

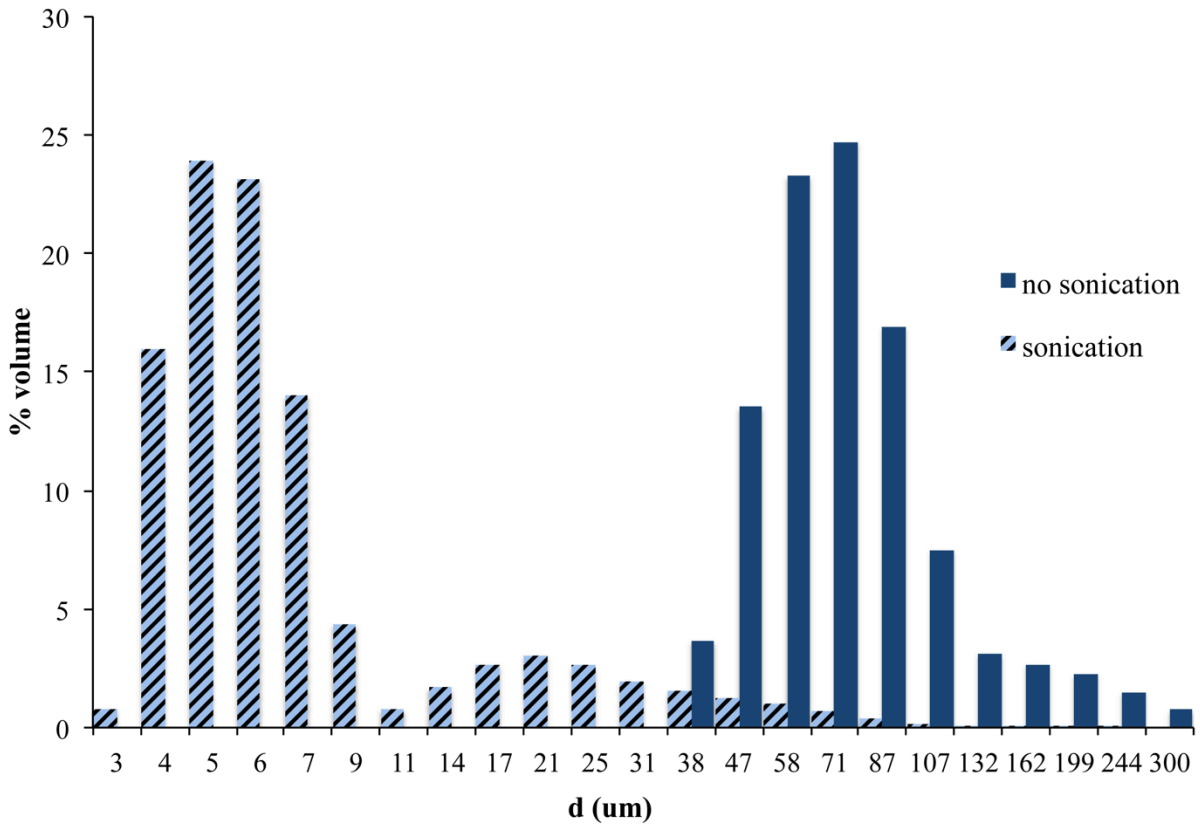

Figure 2.1 Laser diffraction results for a sample of as received dicumarol with or without prior sonication. A small amount of powder was suspended in water and for one sample the suspension was sonicated prior to performing the measurements. This figure illustrates the potential impact of sonication on the particle size results obtained by laser diffraction.

This is important because spherical particles can be described with only one dimension, their diameter, whereas needle or rod-shaped particles need two dimensions to be described. Laser diffraction is a useful technique to compare the size of particles from one batch to another, and it has the advantage of being quick and of requiring less than 1 g of sample for analysis; however, it should be combined with other size techniques such as microscopy in order to obtain a truly accurate image of the material being analyzed.

2.2.2 Microscopy

Microscopy is frequently used to assess the size of particles in solid materials, especially as an orthogonal technique to laser diffraction, and it is the only method where the individual particles can be observed and by which the morphology of the particles can be determined. Optical microscopes can be used to study the surface of objects or individual crystals depending on if they use reflected or transmitted light. Optical microscopy only requires that the sample be dispersed over a surface such as microscope slide. Particles that are too small to be imaged by optical microscopy (less than 0.5 μm) can be observed by scanning electron microscopy (SEM). SEM is also a more powerful tool to investigate the surface of a material. Electron microscopy uses focused electron beams instead of light to allow imaging of the material. The size range of particles that can be observed by SEM is 0.01-150 μm. SEM requires that the sample be coated with a conducting metal such as gold.

Atomic force microscopy (AFM) is another form of microscopy that has also been used to characterize the size and shape of particles. During AFM analyses, a probe is made to travel over the surface of the sample to obtain a topological map. The images obtained are similar to the ones obtained by SEM, with a resolution down to the nanometer range. AFM is a relatively

slow method and the sample preparation may be very involved. However, unlike SEM, it does not require coating of the material with a conductive metal.

2.2.2 Other size measurement techniques

Other particle sizing techniques were briefly used in the course of the investigation presented in this dissertation. They include dynamic light scattering (DLS) and Coulter Counter. DLS involves the measurement of fluctuation in laser intensity occurring as a result of scattering by particles moving in a Brownian motion in solution. The sensitivity of DLS instruments should be validated by size standards. The speed of the experiment and the fact that no calibration is required are some of the advantages of this technique. However, the presence of particles larger than 3 μm may skew the measurements[5]. The Coulter Counter is another popular volume-based particle sizing instrument. It measures the change in electrical impedance as particles pass between two electrodes. This change is correlated with the volume of the particle and is then converted to a particle size distribution as more particles pass through. It can be used for a similar range of sizes as laser diffraction. The analysis is fast and the results are considered highly reproducible. However, it can be difficult to characterize highly water-soluble materials using this method because the particles have to be suspended in a weak aqueous electrolyte where highly soluble compounds could dissolve.

Table 2.1 summarizes existing particle sizing methods and includes the range of sizes that can be measured by each technique. It is important to note that the size measurements obtained are very method dependent; therefore, it is crucial to combine two or more analysis methods in order to improve the accuracy of the results [5].

Table 2.1 Summary of commonly used particle size measurement techniques

Technique	Principle	Measuring range (μm)
Optical microscopy	Direct imaging	3-150
Scanning Electron Microscopy (SEM)	Direct imaging	0.01-150
Laser diffraction	Low angle diffraction rings measurement	0.5-1000
Dynamic Light Scattering (DLS)	Measurement of light intensity correlations from particles in Brownian motion	0.003-3
Coulter Counter	Change in impedance	0.6-1200

2.3 Physical form characterization techniques

As mentioned in the introduction, changes in the physical state of the solid API can occur when its particle size and particle morphology are modified during manufacturing. For this reason, it is important to characterize the physical state of the drug product. A number of physical-state characterization techniques are available, and some of the most widely used methods include thermal methods, imaging techniques, X-Ray diffraction, and spectroscopic techniques such as Raman, infrared and solid-state NMR spectroscopy (SSNMR). A combination of microscopy, X-Ray diffraction, thermal methods and SSNMR was used to characterize the physical state of the materials in most of the work presented in this dissertation. In the next section we will describe the type of information that can be provided by each of those techniques.

2.3.1 Thermal methods

Differential scanning calorimetry (DSC) is one of the most commonly used thermal methods for the physical-state characterization of solids. It involves measuring the difference in heat flow between the sample and a reference as both are heated. Phase transition events, such as melting and recrystallization, that occur as a result of the change in temperature are recorded. Melting and recrystallization events appear in a DSC thermogram as endotherms and exotherms respectively. The melting point of a material can be obtained from the melting endotherm and can be used to distinguish between polymorphs of a material that have different melting points. DSC can also be used to detect the presence of amorphous material. It is the method of choice for measuring the glass transition temperature (T_g) of amorphous materials, which represents a change in heat capacity in the material as it transitions from the glassy to the rubbery state. Figure 2.2 shows examples of thermal events that can be observed in a DSC thermogram.

A disadvantage of DSC is that it is difficult to characterize complex mixtures like formulations containing both an API and excipients using that technique because of the possible overlap of thermal events. In this dissertation, DSC was used as a complementary technique to solid-state NMR to check for the presence of amorphous material that might have been generated as a result of different pharmaceutical processes such as freeze-drying and spray-drying. More details on the operating principles of DSC and its numerous applications to the characterization of pharmaceutical of solids and other pharmaceutical systems have been outlined in a review by Clas and coworkers [6].

2.3.2 Imaging techniques

Polarized light microscopy is often used to distinguish between crystalline and amorphous material. In a birefringent microscope, the light passes through a set of polarizers. The angle of polarization of the light changes as it passes through a crystal, resulting in different colors in the image. Amorphous material appears the same color as the background. The angle at which the second polarizer is placed with respect to the first one determines the color of the crystal observed through the microscope lenses. Single crystals appear yellow or blue under polarized light microscopy, while aggregates of crystals appear green. When the stage of the microscope is rotated by 90º, the coloring of single crystals switches. Figure 2.3 shows polarized light microscopy images of a crystal of gabapentin, before and after rotating the stage of the microscope by 90 º. Polarized light microscopy is a rapid way to assess the crystallinity of a solid material; however, only a small amount of sample is imaged, and it may not be an accurate representation of the material overall.

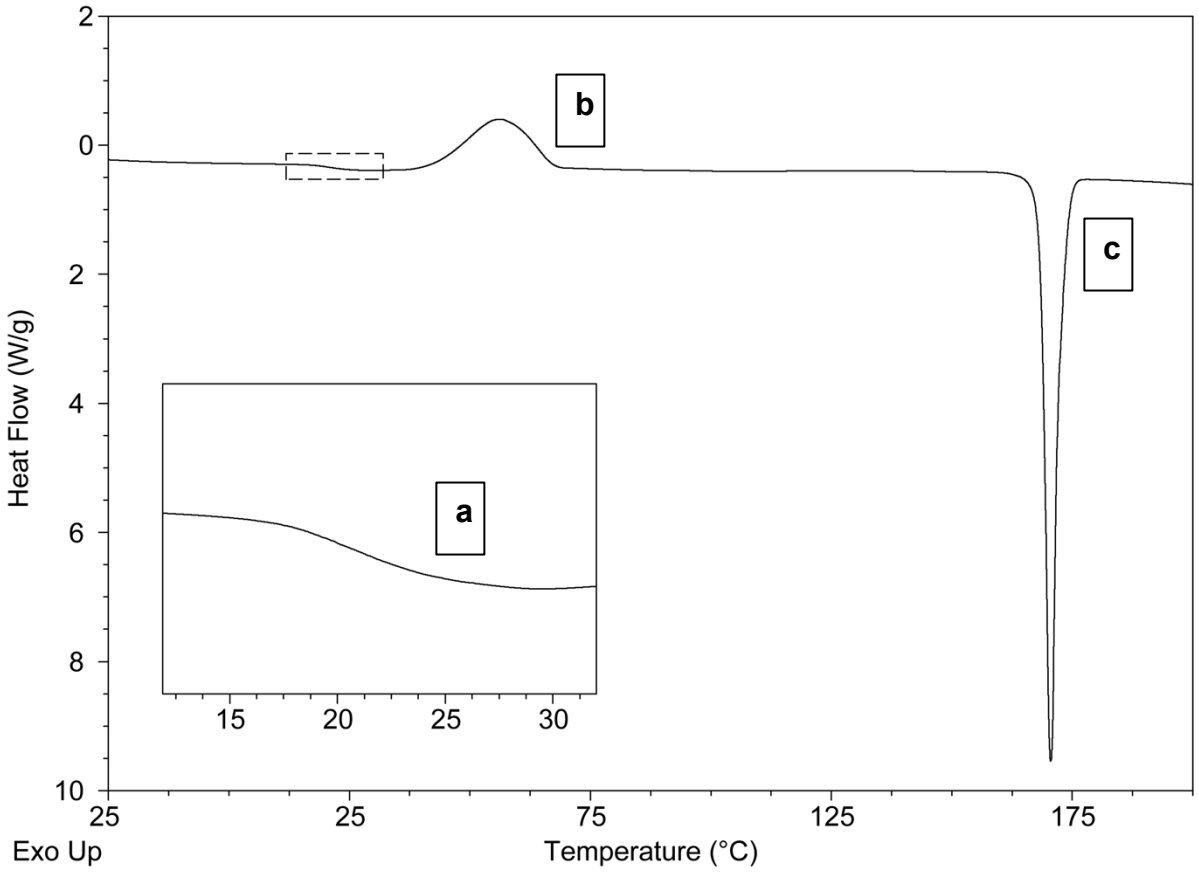

Figure 2.2. DSC thermogram of amorphous acetaminophen. This DSC contains some of the typical thermal events that can be observed by DSC. **a.** a glass transition; **b.** an endothermic peak indicating recrystallization and **c.** an endothermic peak indicating melting of the material. The thermogram was obtained using a TA Instruments DSC instrument.

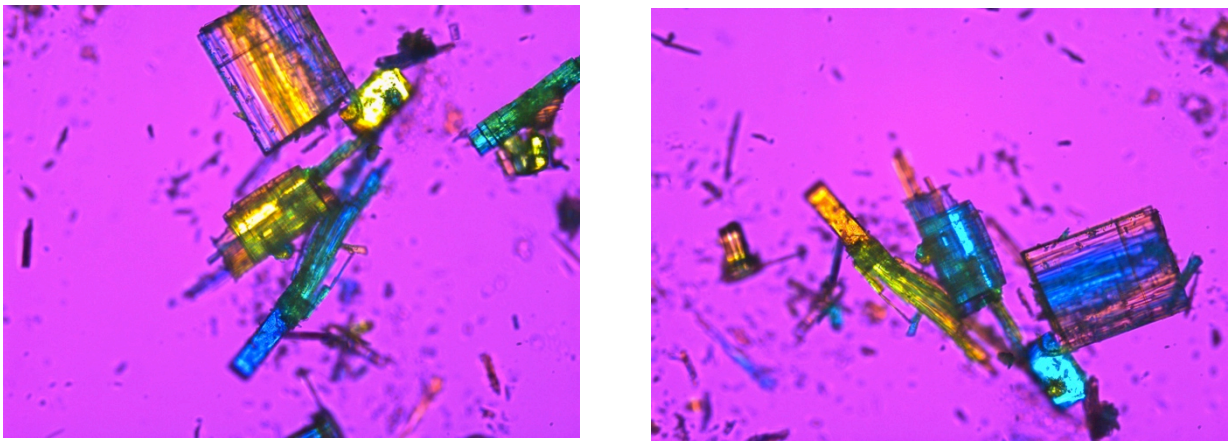

a. **b.**

Figure 2.3. Polarized light microscopy images of crystalline gabapentin Form II; **b.** was taken after rotating the stage of the microscope by 90º. The crystals appear as yellow or blue, indicating that they are single crystals. Rotating the stage of the microscope by 90º causes the colors to inverse.
The images were obtained on an Olympus microscope.

2.3.3 X-ray diffraction

X-ray diffraction techniques are based on the principle of X-rays being scattered by the atoms in a molecule to produce unique diffraction patterns. Single crystal X-ray diffraction is used for crystal structure elucidation, which is helpful when trying to understand how the molecules are packed in a given polymorph, or how spatially close reactive functional groups are to each other. When single crystals are not available, powder X-ray diffraction (PXRD) can be used to distinguish between polymorphs as well as between crystalline and amorphous materials based on the peak positions and breadth [7-9]. The PXRD patterns of crystalline peaks are characterized by sharp peaks, whereas a shapeless halo is characteristic of amorphous materials [10]. This difference exists because crystalline materials are composed of a highly ordered lattice of molecules that scatters the X-ray constructively at defined angles; conversely, amorphous material lack that order and do not produce a pattern with sharp peaks, but a halo instead. One of the advantages of PXRD is the small amount of material that is required for analysis. However, artifacts that can impact the intensity of the peaks in the diffraction pattern can arise due to the preferred orientation of crystals in a powder. This is especially true for particles with a non-spherical morphology [11,12]. Furthermore, PXRD patterns of formulations can be difficult to decipher because of the peak overlap of the different components.

2.3.4 Solid-state NMR spectroscopy

Solid-state nuclear magnetic resonance spectroscopy (SSNMR) is a non-destructive, selective and quantitative technique that is highly useful for analyzing solid pharmaceuticals [13]. The chemical shifts and linewidths of the peaks in an NMR spectrum can provide a wealth of information on a material, including information on its chemical structure, its composition, whether it is pure or a mixture, and its physical state, e.g. crystalline or amorphous. Studies have

also shown that the morphology of the particles in a crystalline sample could possibly be related back to the linewidth of the peaks in its SSNMR spectrum [14]. SSNMR relaxation times provide mobility information, and also have been related to chemical stability [15]. Because solid-state NMR is the main solid-state characterization technique used in the work presented in this dissertation, it is discussed in greater details in the following sections.

2.4 Fundamentals of Nuclear Magnetic Resonance Spectroscopy

Nuclei that have an angular momentum, and therefore a magnetic moment, are NMR active. The spin quantum number I describes the angular momentum of the spinning charge. We will only be concerned with nuclei with I=1/2, such as ^{1}H and ^{13}C, in this work because they are the most pharmaceutically relevant. In the presence of an external magnetic field B_0, these nuclei begin to precess about an axis that is at an angle of 54.7º with respect to the magnetic field B_0. The rate of precession is proportional to both the strength of B_0 and a constant specific to each nucleus called the magnetogyric ratio γ. The orientation of the nuclear spins is random in the absence of a magnetic field, but in the presence of a strong magnetic field (such as in an NMR spectrometer), nuclear spins with I=1/2 can align either parallel (α state) or anti parallel (β state) to the magnetic field B_0 (Figure 2.4). Because one of the states has a lower energy level, it contains a small population excess of nuclei. This population excess can be calculated using the Boltzmann equation:

$$\frac{N_{upper}}{N_{lower}} = e^{-\Delta E/kT} \quad (2.1)$$

where N_{upper} and N_{lower} are the populations of nuclei in the higher and lower energy state respectively; k is the Boltzmann constant, T is the absolute temperature, and ΔE is the difference in energy between the two states. ΔE can be calculated using the following equation:

$$\Delta E = \frac{\gamma h B_0}{2\pi} = h\nu_0 \quad (2.2)$$

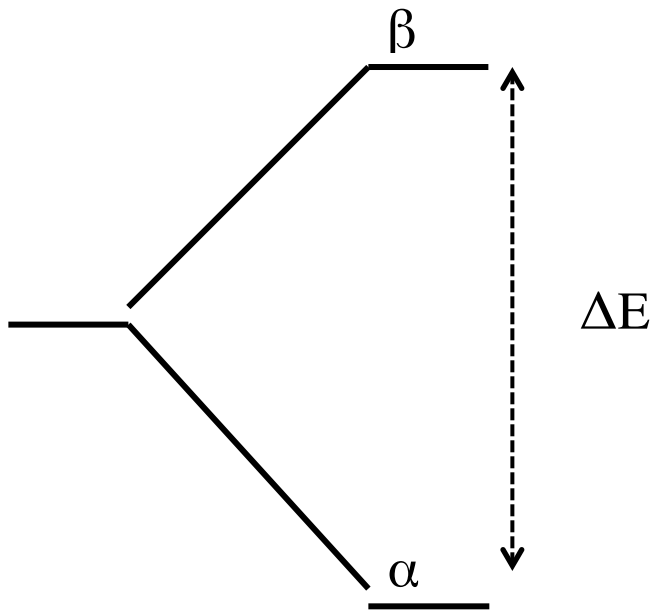

Figure 2.4. Energy diagram for the two energy levels, denoted α and β, that can be assumed by spin ½ nuclei

where γ is the magnetogyric ratio of the nucleus, h is the Planck's constant, and ν_0 is the frequency of the nucleus. When a radiofrequency (RF) pulse equal to the difference in energy (ΔE) between the two states is applied in the appropriate direction to the material, the nuclei absorb energy that causes them to transition from one energy state to the other. These nuclei are oriented with respect to one another, and the net magnetic moment of the precessing nuclei creates an alternating current signal in the NMR detection coil at a frequency of the precessing nuclei. This signal, called a free induction decay (FID), is observed during an NMR experiment. The FID is recorded in the time domain, and it is converted to the frequency domain (Hz/MHz or ppm) by a Fourier transform. The resulting spectrum contains peaks whose chemical shifts, or positions, and linewidths, or breadth, can provide us with a wealth of information about the sample. The process through which the system returns to equilibrium after the pulse is termed relaxation. Different relaxation processes exist, including spin-lattice relaxation and spin-spin relaxation. In spin-lattice relaxation, the nuclei transfer the excess magnetization acquired during the pulse in order to return to their equilibrium state. Relaxation will be discussed in more detail later in this chapter.

2.5 Solid-state NMR spectroscopy

Before we discuss how solid-state NMR chemical shifts, linewidths and relaxation measurements are used to characterize solid pharmaceuticals, it is useful to point out how solid-state and solution-state NMR differ from each other. This will be helpful in order to understand why solid-state NMR is less routinely used than its solution-state counterpart, and why it is a powerful tool to the study of solid pharmaceuticals.

In the solution state, the molecules are rapidly moving and tumbling around, causing the several interactions among the nuclei in a molecule to average to either zero or an isotropic

value. Conversely, the molecules in the solid state are held rigidly in place; therefore, this averaging does not occur. This causes the linewidths of the peaks in the SSNMR spectrum to be significantly broader than the ones present in a solution-state NMR spectrum. One interaction that causes the lines to be broad is dipolar coupling between either ^{1}H-^{1}H or ^{13}C-^{1}H. In section 2.5.1, we describe how high power decoupling is used to eliminate this cause of line broadening. Another cause of line broadening in the solid state is the chemical shift anisotropy (CSA) of the materials, which means that all the orientations assumed by the nuclei with respect to the magnetic field B_0 contribute to the chemical shift of the material observed in an NMR spectrum. While the tumbling of the molecules in solution averages all the angular-dependent orientations, this does not occur in the solid state, and the distribution of all the orientations that can be assumed by the nuclei results in a broad spectrum called a powder pattern. Figure 2.5 shows the difference between the solution and the solid-state NMR spectra of 3-methylglutaric acid. The use of a technique known as magic-angle spinning in solid-state NMR, described in section 2.5.3, eliminates the orientations that are angular dependent resulting in narrower peak linewidths. Finally, NMR active nuclei that have a low natural abundance, like ^{13}C, often have very long spin-lattice relaxation times. The consequence of this is longer NMR experiments. Transfer of magnetization from abundant nuclei such as protons to these low abundance nuclei by a process called cross polarization can be used to alleviate that issue and enhance the sensitivity, which is a factor of 4 for ^{1}H-^{13}C. Cross polarization will be discussed in section 2.5.2.

2.5.1 High power decoupling

Dipolar coupling is the through-space interaction between the dipole moment of one nuclear spin and the dipole moment of another nucleus. The strength of the dipolar coupling

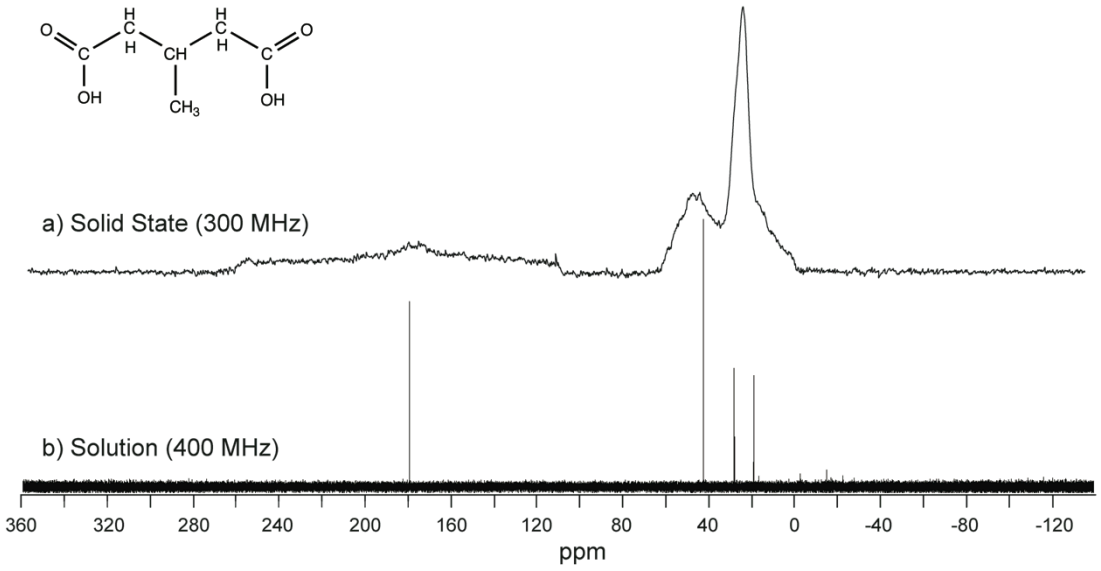

Figure 2.5 Solid-state and solution-state NMR spectra of 3-methyl glutaric acid (MGA). These specra denote the differences in linewidths obtained in solution state and solid state NMR. The solid-state spectrum is very broad and is denoted a powder pattern. The peaks in the solution NMR spectrum are very sharp by contrast.

decreases very rapidly with the cube of the distance between the two coupled nuclei according to the following equation:

$$D_{IS} = \frac{\mu_0 \hbar \gamma_I \gamma_S}{2\pi r_{IS}^3} \quad (2.3)$$

where D_{IS} is the strength of the dipolar coupling between two spins I and S, μ_0 is the vacuum permeability constant, γ_I and γ_S are the magnetogyric ratio of spins I and S, respectively and r_{IS} is the distance between the two spins. Both homonuclear and heteronuclear interactions can exist; however, with dilute nuclei such as ^{13}C (1.1% abundant), homonuclear interactions are essentially negligible because there is only a small probability for two ^{13}C nuclei to be in close proximity to each other. In contrast, ^{13}C-^{1}H and ^{1}H-^{1}H interactions are very prevalent because of the 100% natural abundance of protons. Equation 2.3 also indicates that the strength of the coupling is proportional to the magnetogyric ratio of the nucleus. The magnetogyric ratio of protons is about four times as large (26.8 x 10^{-7} $rad \cdot T^{-1} \cdot s^{-1}$) compared to that of ^{13}C (6.7 10^{-7} $rad \cdot T^{-1} \cdot s^{-1}$), which means that dipolar couplings involving protons are very strong. We will discuss in the next chapter how the strong ^{1}H-^{1}H dipolar coupling can be used for measuring distances by NMR. This strong dipolar coupling causes line broadening of the peaks in a SSNMR spectrum; high power decoupling fields on the order of 60 kHz applied at the proton resonance frequency are used to eliminate the ^{13}C-^{1}H interactions, resulting in narrower peaks.

2.5.2 Cross polarization

The use of cross-polarization allows us to take advantage of the high natural abundance of nuclei such as ^{1}H to improve the sensitivity of dilute nuclei such as ^{13}C through a magnetization transfer that takes place through dipolar coupling interactions between the two nuclei. In practice, cross-polarization is achieved by applying a 90º strong radiofrequency (RF) pulse that rotates the proton magnetization into the *x*-*y* plane. These nuclei are then held in that

place, or spin-locked, for a time period t. During that time a strong pulse is applied to the ^{13}C spins, the carbon field is then switched off, and the carbon FID is recorded. The magnitude of the fields applied to the ^{1}H and ^{13}C are chosen to satisfy the Hartmann-Hahn conditions [16]:

$$\gamma_{^1H} B_{^1H} = \gamma_{^{13}C} B_{^{13}C} \quad (2.4)$$

where $\gamma_{^1H}$ and $\gamma_{^{13}C}$ are the magnetogyric ratios of ^{1}H and ^{13}C respectively, and B is the strength of the applied frequency. When Hartmann-Hahn conditions are met, the two nuclei precess at the same rate thus allowing for efficient polarization transfer from the ^{1}H to the ^{13}C nuclei. In addition, Hartmann-Hahn cross-polarization results in shorter acquisition times for ^{13}C spectra. This is because under these conditions the relaxation rate of the material is dictated by the proton spin-lattice relaxation, which takes place significantly faster than ^{13}C spin-lattice relaxation. A gain in sensitivity of approximately four-fold per scan is also achieved.

2.5.3 Magic angle spinning

The observed chemical shift of a nucleus in a SSNMR spectrum can be defined by the equation:

$$\sigma_{obs} = \sigma_{iso} + \sigma_{aniso} (3 \cos^2 \theta - 1) \quad (2.5)$$

where σ_{obs} is the observed chemical shift, σ_{iso} is the isotropic chemical shift and σ_{aniso} is the anisotropic chemical shift. The sum of these contributions, which represents the orientations that can be assumed by the nucleus with respect to the magnetic field B_0, results in a shape referred to as a powder pattern, which may be 200 ppm wide (Figure 2.5). The anisotropic component has an angular dependence and can be eliminated through the use of magic-angle spinning (MAS), leaving the isotropic chemical shift as the only contributor. During magic-angle spinning, the sample is spun at an angle equal to 54.7 º, known as the magic angle [17,18]. At that angle, the contribution of the anisotropic component to the observed chemical shift is zero. Typical

spinning speeds range from 3000 kHz to 10,000 kHz. MAS eliminates the main anisotropic component, however a residual intensity remains in the form of spinning side bands. The spinning side bands appear on either side of a peak at a distance equivalent to the spinning speed. They can be removed with the use of a pulse sequence called TOtal Suppression of Spinning sidebands (TOSS) [19]. Spinning the sample at a speed greater than the width of the powder pattern can also eliminate the spinning sidebands. A combination of the techniques described above allows us to obtain high-quality SSNMR spectra of solid pharmaceuticals. The effect of each technique is illustrated in Figure 2.6.

2.6 Characterization of pharmaceutical solids by solid-state NMR

Solid-state NMR is recognized as a very powerful tool for the study of pharmaceuticals, and many reports of applications of SSNMR to pharmaceuticals can be found in the literature [13,20-24]. By monitoring a number of NMR parameters such as the chemical shifts of the peak in the spectrum, the linewidth of the peaks, and the relaxation rate of the material, a wealth of information on the material can be obtained. This includes information on its physical state, the existence of chemical interactions, and the amount of mobility of the sample. In the next section the information obtained from SSNMR chemical shifts, linewidths and relaxation times is summarized.

2.6.1 Chemical shifts

The chemical shifts of the peaks in a SSNMR spectrum are dependent on the electronic environment experienced by the nuclei. Functional groups can generally be assigned based on the position of their peaks in a SSNMR spectrum. In a ^{13}C SSNMR spectrum, aliphatic carbons usually appear between 10 and 40 ppm, aromatic carbons are typically found between 100 and

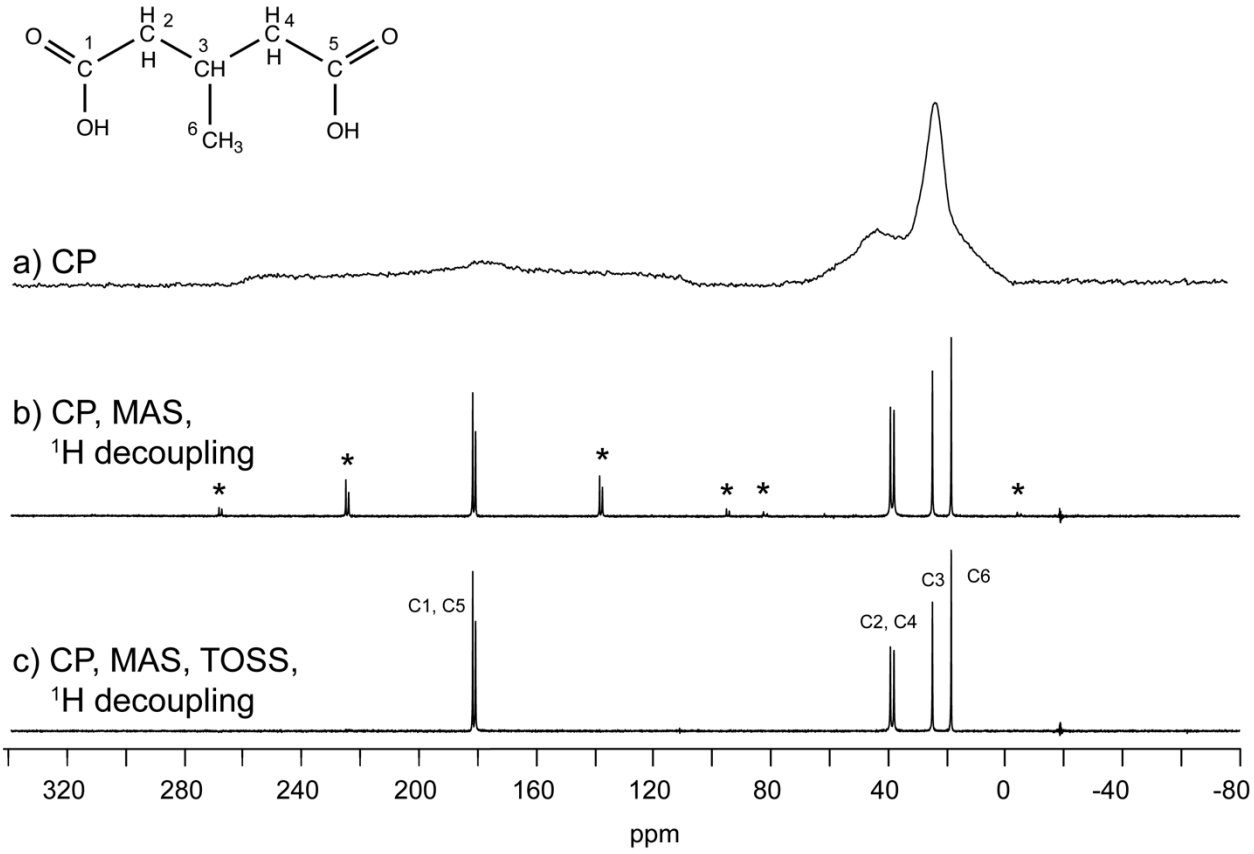

Figure 2.6 ^{13}C SSNMR spectra of 3-methyl glutaric acid illustrating the impact of the use of advanced techniques: magic angle spinning, ^{1}H decoupling and TOSS on the quality of the spectrum. The asterisks (*) in the (b) indicate spinning sidebands. The use of TOSS removes those spinning sidebands (c)

160 ppm, and peaks from carbonyl and carboxylic acid groups are generally between 160 and 180 ppm. However, unlike the solution state, these values only represent estimates and can vary dramatically based on the spatial arrangement of the molecules and the proximity of electronegative groups.

The polymorphs of a given solid have different SSNMR spectra because they differ in the conformation and/or packing arrangement of their molecules. Differences in the chemical shifts of the peaks can be used to identify the different polymorphs. Figure 2.7 shows the aliphatic region of the ^{13}C SSNMR spectra of Form II and Form III of gabapentin. Because of the significant difference in the chemical shift of the nitrogen-split peak between Form II and Form III, that peak is the most useful for form identification; its chemical shift is 39.1 ppm in Form II and 51 ppm in Form III. A large number of reports of polymorph identification by SSNMR exist in the literature [13,24].

The selectivity of SSNMR allows us to distinguish not only between polymorphs, but also between API and excipients. Common excipients, including disaccharides such as lactose and trehalose, contain substituted rings with oxygen-bonded carbons. The proximity to oxygen, an electronegative atom, causes the chemical shift of these carbons to shift to higher ppm values. Figure 2.8 shows the ^{13}C SSNMR spectrum of a mixture of ibuprofen and mannitol, another common excipient. The peaks from the mannitol appear between 50 and 100 ppm, and there is no overlap between these peaks and the ibuprofen peaks.

2.6.2 Linewidths and peak area

The linewidths of solids can be used to distinguish crystalline from amorphous materials, and the peak areas can be integrated in order to perform quantitation of the components of a mixture. The linewidths of the peaks in the SSNMR spectrum of a molecule vary with the

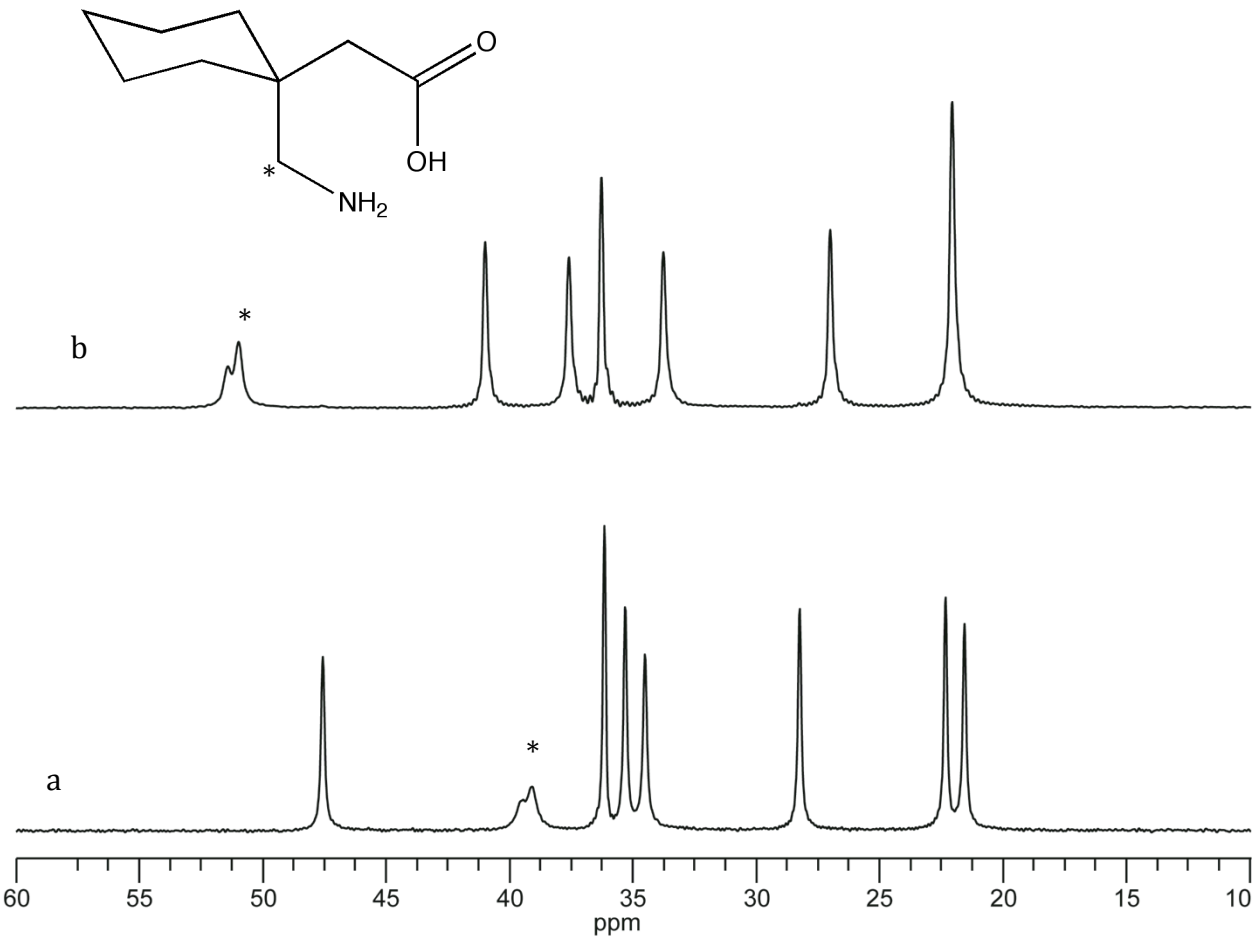

Figure 2.7 Aliphatic region of the ^{13}C SSNMR spectra of gabapentin polymorphs. a. Form II; b. Form III. The chemical shifts, or position of the peaks, in the two spectra are different, allowing the distinction of the two forms. Particularly useful in the identification is the nitrogen-split carbon peak that is indicated with an asterisk (*)

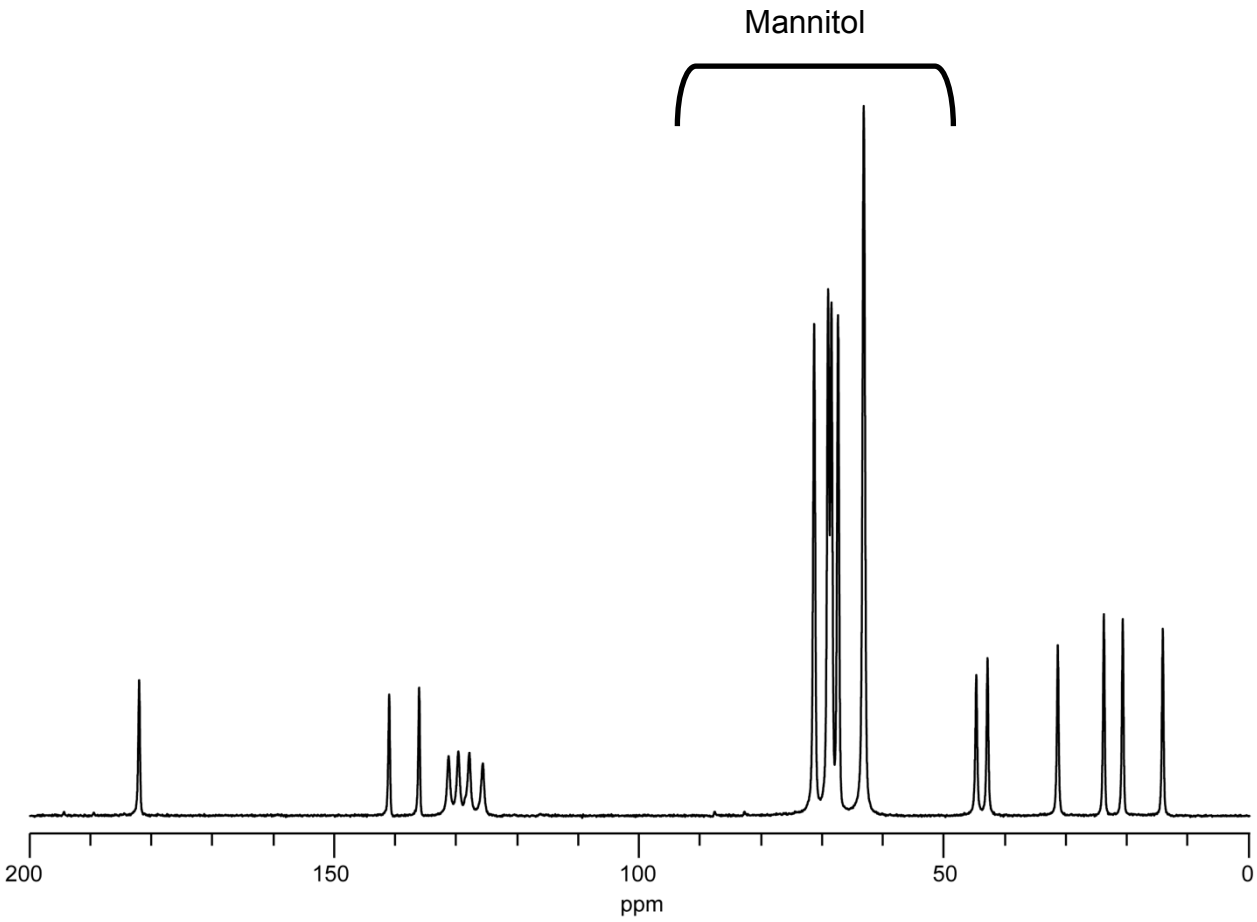

Figure 2.8. ^{13}C SSNMR spectrum of a mixture of ibuprofen and mannitol. The peaks of the API (ibuprofen) are separate from the peaks of the excipient (mannitol)

number of different conformations assumed by the molecule. Highly mobile materials such as amorphous materials have linewidths that may be ten times broader than the linewidths of rigid crystalline materials.

The crystal quality of the solid material can also impact the linewidth of the peaks in the SSNMR spectrum. Highly defective crystalline particles of ibuprofen generated by milling were shown by Barich and coworkers to have broader linewidths than as-received crystalline ibuprofen [14]. They have also shown that the presence of certain excipients, such as talc, increased the linewidth of the peaks of ibuprofen. This effect was attributed to a phenomenon known as anisotropic bulk magnetic susceptibility (ABMS).

Quantitation of the amount of each component present in mixtures by integration of peak areas in the SSNMR spectrum can be performed by SSNMR when the appropriate acquisition parameters are used. The parameters in question include the delay allowed for the material to relax and the contact time during cross-polarization. Mixtures of polymorphs have been quantified by SSNMR and limits of quantitation as low as 1% have been obtained [23,25].

2.6.3 Relaxation rates

Relaxation is the process through which a material returns to equilibrium after an NMR pulse and it occurs via various processes, including spin-lattice relaxation and spin-spin relaxation. These processes are characterized by relaxation times. NMR relaxation times are an indicator of the amount of mobility present in a material. For example highly mobile amorphous materials typically have faster relaxation rates, hence shorter relaxation times, than their highly rigid crystalline counterparts. Relaxation rates have been used to study the molecular motions in proteins [26]. The proton spin-lattice relaxation time (^{1}H T_1) is the most relevant to us in this study.

2.7 Proton spin-lattice relaxation times (^{1}H T_1)

Spin-lattice relaxation, or T_1 relaxation, refers to the transfer of energy that occurs from the excited nuclei to the surroundings; this allows the material to return to equilibrium after an RF pulse. The surroundings include other molecules in the samples and the remainder of the molecule itself containing the nucleus of interest. T_1 relaxation is an exponential process and is modeled by the following equation:

$$(N_{lower}\text{-}N_{upper}) = (N_{lower}\text{-}N_{upper})_{equil}\left(1 - e^{-\frac{\tau}{T_1}}\right) \quad (2.6)$$

where N_{lower} and N_{upper} are the nuclear populations in the lower and higher energy states respectively. The T_1 is the time that it takes for the system to return to 63% of its equilibrium value through the spin-lattice relaxation process. ^{1}H T_1 times can be measured using an experiment called a saturation recovery experiment. Figure 2.9 shows a saturation recovery pulse sequence. During saturation recovery experiments, a radiofrequency pulse is applied to the sample and the amount of time that the material is allowed to return to equilibrium, or relax, is varied. That time interval is denoted tau (τ). A designated number of spectra, usually ranging from 8 to 32, are acquired at each tau and are summed.

Figure 2.10 shows a typical ^{1}H T_1 plot, in which the intensity of the NMR signal at each τ value is plotted versus the τ value. ^{1}H T_1 times are often measured instead of ^{13}C or other nuclei because the spectra are typically acquired using cross polarization. In addition, because of their high natural abundance, protons provide a more global image of the relaxation behavior of the material, while ^{13}C times can be used to assess local motions. When using cross polarization between ^{1}H and ^{13}C, ^{1}H T_1 times can be measured from ^{13}C SSNMR spectra. This is because under cross polarization conditions the relaxation of the material is dictated by the relaxation of the abundant nucleus. ^{1}H T_1 values can range from a few seconds to thousands of seconds.

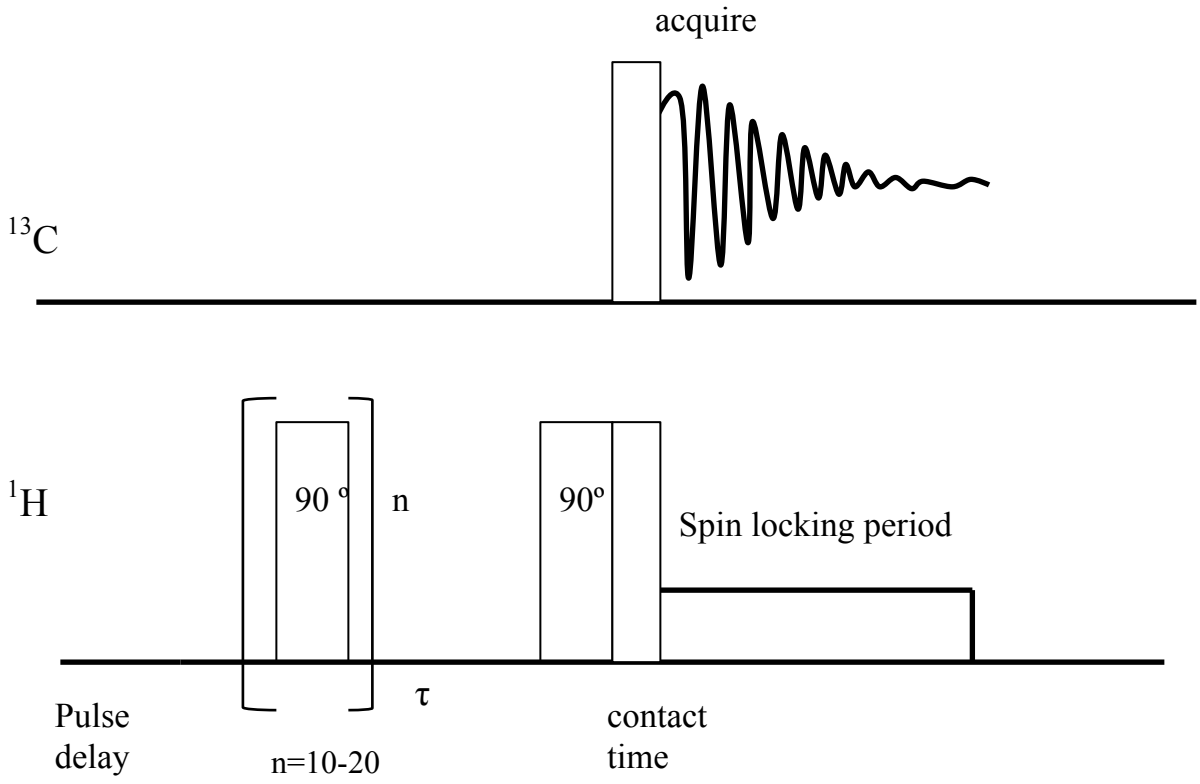

Figure 2.9 Solid-state NMR saturation recovery pulse sequence. This is a common sequence used to obtain ^{1}H T_1 times while collecting ^{13}C spectra.

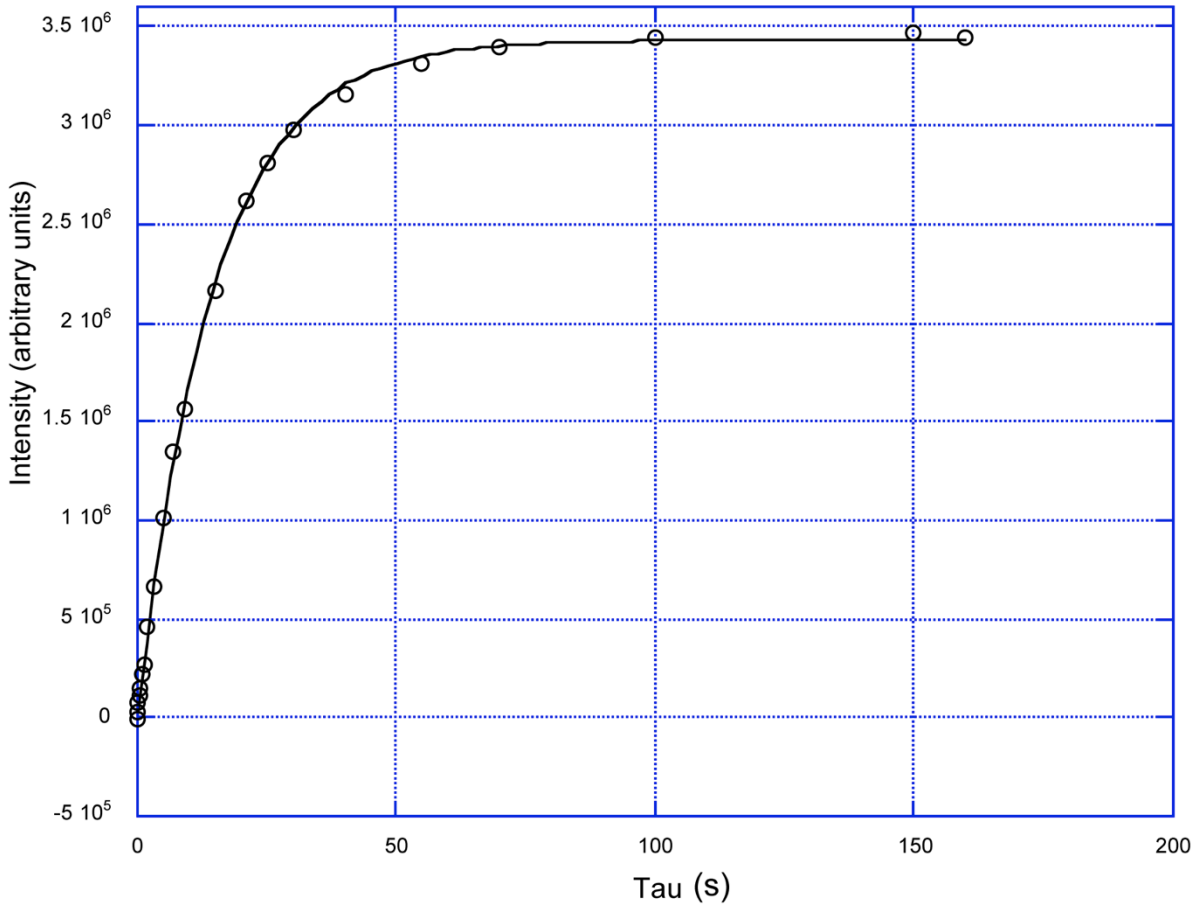

Figure 2.10 Typical T_1 relaxation plot. Plot of the intensity of the peaks in the SSNMR spectrum versus the tau time. The data (open circles) was fit to the Equation 2.6

A number of factors can affect the magnitude of the ^{1}H T_1 relaxation time measured, including the presence of relaxation sinks in the material that contribute to a decrease in ^{1}H T_1 time. Fast rotating groups such as methyl, ethyl and t-butyl groups are commonly encountered relaxation sinks. Because they are part of the chemical structure of the molecule, they are qualified as intrinsic relaxation sinks. The mobility of the material also tremendously affects the ^{1}H T_1 relaxation, with highly mobile materials such as amorphous frequently having shorter relaxation time than crystalline samples. Relaxation sinks can also be present at the bulk level. For example, a small amount of amorphous material in an otherwise crystalline material can act as a relaxation sink. Water, when it is not hydrogen-bonded, also behaves as a relaxation sink. Other factors that have been shown to impact the ^{1}H T_1 time are the presence of crystal defects, the reduction in particle size of a crystalline material, and the presence of paramagnetic oxygen [27-29].

By monitoring the ^{1}H T_1 times of mixtures, assessments of the level of miscibility of mixtures were also made [30-32]. These studies were possible because of a process known as spin diffusion that occurs with protons. Spin diffusion is a through space transfer of magnetization through dipolar coupling. As a result of spin diffusion, homogeneous solids have one ^{1}H T_1 time. Heterogeneous mixtures have more than one ^{1}H T_1 time. The spin diffusion process is also exploited for the measurement of domain sizes in solids. The ability to establish a correlation between ^{1}H T_1 times and distances is highly relevant to the work presented here and will be discussed in more detail in the next chapter.

2.6 References

1. Brittain HG 2002. Effects of mechanical processing on phase composition. Journal of Pharmaceutical Sciences 91(7):1573-1580.

2. Chan HK, Doelker E 1985. Polymorphic Transformation of Some Drugs Under Compression. Drug Development and Industrial Pharmacy 11(2-3):315-332.

3. Wardrop J, Law D, Qiu Y, Engh K, Faitsch L, Ling C 2006. Influence of solid phase and formulation processing on stability of Abbott-232 tablet formulations. Journal of Pharmaceutical Sciences 95(11):2380-2392.

4. Shekunov BY, Chattopadhyay P, Tong HHY, Chow AHL 2007. Particle Size Analysis in Pharmaceutics: Principles, Methods and Applications. Pharm Res 24:203-227.

5. Iacocca RG, Burcham CL, Hilden LR 2010. Particle engineering: A strategy for establishing drug substance physical property specifications during small molecule development. Journal of Pharmaceutical Sciences 99(1):51-75.

6. Clas S-D, Dalton CR, Hancock BC 1999. Differential scanning calorimetry: applications in drug development. Pharmaceutical Science & Technology Today 2(8):311-320.

7. Yamada H, Suryanarayanan R 2007. X-ray powder diffractometry of intact film coated tablets—An approach to monitor the physical form of the active pharmaceutical ingredient during processing and storage. Journal of Pharmaceutical Sciences 96(8):2029-2036.

8. Nunes C, Suryanarayanan R, Botez CE, Stephens PW 2004. Characterization and crystal structure of D-mannitol hemihydrate. Journal of Pharmaceutical Sciences 93(11):2800-2809.

9. Yu L 2001. Amorphous pharmaceutical solids: preparation, characterization and stabilization. Advanced Drug Delivery Reviews 48(1):27-42.

10. Bates S, Zografi G, Engers D, Morris K, Crowley K, Newman A 2006. Analysis of Amorphous and Nanocrystalline Solids from Their X-Ray Diffraction Patterns. Pharmaceutical Research 23(10):2333-2349.

11. Campbell Roberts SN, Williams AC, Grimsey IM, Booth SW 2002. Quantitative analysis of mannitol polymorphs. X-ray powder diffractometry,Äîexploring preferred orientation effects. Journal of Pharmaceutical and Biomedical Analysis 28(6):1149-1159.

12. Croker DM, Hennigan MC, Maher A, Hu Y, Ryder AG, Hodnett BK 2012. A comparative study of the use of powder X-ray diffraction, Raman and near infrared spectroscopy for quantification of binary polymorphic mixtures of piracetam. J Pharm Biomed Anal 63:80-86.

13. Harris RK 2007. Applications of solid-state NMR to pharmaceutical polymorphism and related matters*. Journal of Pharmacy and Pharmacology 59(2):225-239.

14. Barich DH, Davis JM, Schieber LJ, Zell MT, Munson EJ 2006. Investigation of solid-state NMR line widths of ibuprofen in drug formulations. Journal of Pharmaceutical Sciences 95(7):1586-1594.

15. Lubach JW. 2007. Applications of nuclear magnetic resonance spectroscopy to pharmaceutical solids. ed., United States -- Kansas: University of Kansas. p 376.

16. Pines A 1973. Proton-enhanced NMR of dilute spins in solids. J Chem Phys 59(2):569.

17. Andrew ER, Bradbury A, Eades RG 1959. Removal of Dipolar Broadening of Nuclear Magnetic Resonance Spectra of Solids by Specimen Rotation. Nature 183(4678):1802-1803.

18. Lowe IJ 1959. Free Induction Decays of Rotating Solids. Physical Review Letters 2(7):285-287.

19. Dixon WT, Schaefer J, Sefcik MD, Stejskal EO, McKay RA 1982. Total suppression of sidebands in CPMAS C-13 NMR. Journal of Magnetic Resonance (1969) 49(2):341-345.

20. Berendt RT, Sperger DM, Munson EJ, Isbester PK 2006. Solid-state NMR spectroscopy in pharmaceutical research and analysis. TrAC, Trends in Analytical Chemistry 25(10):977-984.

21. Geppi M, Mollica G, Borsacchi S, Veracini CA 2008. Solid-State NMR Studies of Pharmaceutical Systems. Appl Spectrosc Rev 43:202-302.

22. Zumbulyadis N, Antalek B, Windig W, Scaringe RP, Lanzafame AM, Blanton T, Helber M 1999. Elucidation of Polymorph Mixtures Using Solid-State 13C CP/MAS NMR Spectroscopy and Direct Exponential Curve Resolution Algorithm. Journal of the American Chemical Society 121(49):11554-11557.

23. Apperley DC, Harris RK, Larsson T, Malmstrom T 2003. Quantitative nuclear magnetic resonance analysis of solid formoterol fumarate and its dihydrate. Journal of Pharmaceutical Sciences 92(12):2487-2494.

24. Saindon PJ, Cauchon NS, Sutton PA, Chang Cj, Peck GE, Byrn SR 1993. Solid-State Nuclear Magnetic Resonance (NMR) Spectra of Pharmaceutical Dosage Forms. Pharmaceutical Research 10(2):197-203.

25. Offerdahl TJ, Salsbury JS, Dong Z, Grant DJW, Schroeder SA, Prakash I, Gorman EM, Barich DH, Munson EJ 2005. Quantitation of crystalline and amorphous forms of anhydrous neotame using 13C CPMAS NMR spectroscopy. J Pharm Sci 94(12):2591-2605.

26. Yoshioka S, Forney K, Aso Y, Pikal M 2011. Effect of Sugars on the Molecular Motion of Freeze-Dried Protein Formulations Reflected by NMR Relaxation Times. Pharmaceutical Research 28(12):3237-3247.

27. Rabbani SR, Edmonds DT 1994. Nuclear spin-lattice relaxation-time reduction in small particles. Physical Review B 50(9):6184-6188.

28. Lubach JW, Xu D, Segmuller BE, Munson EJ 2007. Investigation of the effects of pharmaceutical processing upon solid-state NMR relaxation times and implications to solid-state formulation stability. Journal of Pharmaceutical Sciences 96(4):777-787.

29. Schieber LJ. 2010. Methods for increasing sensitivity and throughput of solid-state NMR spectroscopy of pharmaceutical solids. ed., United States -- Kansas: University of Kansas. p 242.

30. Henrichs PM, Tribone J, Massa DJ, Hewitt JM 1988. Blend miscibility of bisphenol A polycarbonate and poly(ethylene terephthalate) as studied by solid-state high-resolution carbon-13 NMR spectroscopy. Macromolecules 21(5):1282-1291.

31. Schmidt-Rohr K, Clauss J, Blümich B, Spiess HW 1990. Miscibility of polymer blends investigated by ^{1}H spin diffusion and ^{13}C NMR detection. Magnetic Resonance in Chemistry 28(13):S3-S9.

32. Pham TN, Watson SA, Edwards AJ, Chavda M, Clawson JS, Strohmeier M, Vogt FG 2010. Analysis of Amorphous Solid Dispersions Using 2D Solid-State NMR and ^{1}H T_1 Relaxation Measurements. Molecular Pharmaceutics 7(5):1667-1691.

Chapter 3

Measurement of Domain Sizes using Solid-State NMR spectroscopy

3.1 Introduction

In this chapter, the use of advanced solid-state NMR techniques to measure distances is briefly reviewed, focusing on the distances that can be measured, the systems where these techniques have been applied, and the limitations of each technique. The use of spin diffusion for distance measurements by solid-state NMR is particularly emphasized because it is the most relevant in the study presented in this dissertation as it allows the measurement of longer distances. A description of the link between spin diffusion and proton spin-lattice relaxation times (^{1}H T_1) as cited in the literature will be presented. Finally, the studies previously performed in the Munson laboratory using aspirin and lactose as model compounds are summarized, where the ^{1}H T_1 times of ground and unground materials were determined. The way that they represent the starting point for the investigation presented in this dissertation will be underlined. All the SSNMR size measurement techniques that are presented are based on exploiting the dipolar coupling interactions between nuclei.

3.1.1 Dipolar coupling

Dipolar coupling is a through-space interaction between nuclei. The strength of the dipolar coupling decreases with the cube of the distance separating the two interacting nuclei according to the following relationship:

$$D_{IS} = \frac{\mu_0 \hbar \gamma_I \gamma_S}{2\pi r_{IS}^3} \quad (3.1)$$

where D_{IS} is the dipolar coupling between two spins I and S, μ_0 is the vacuum permeability constant, γ_I and γ_S are the magnetogyric ratio of spins I and S, respectively and r_{IS} is the distance between the two spins. Spin ½ nuclei with large magnetic moments such as protons have the strongest dipolar coupling. The strength of the magnetic moment of a nucleus is evident in the

magnitude of its magnetogyric ratio. All of the SSNMR distance measurement methods are based on the dipolar coupling that exists between NMR-active nuclei such as ^{13}C, ^{1}H, ^{19}Si, and ^{15}N, etc.

The distance separating two NMR active nuclei that are a few angstroms apart from each other but isolated from other nuclei can be determined directly by measuring the strength of their dipolar coupling (Figure 3.1). Nuclei that are farther apart are very weakly coupled, and therefore the distance between them cannot be measured directly because the uncertainty in measuring small dipolar couplings is too large. However, dipolar coupling interactions from the first nucleus to its nearest neighbor, with additional coupling to the final nucleus of interest can be used to measure the distance between the first and the last nuclei (Figure 3.1). This indirect way of measuring distances is the concept behind spin diffusion and is only applicable to materials containing strongly coupled nuclei that are highly abundant in the sample such as protons. Both the direct and the indirect size measurement approaches will be discussed here.

3.2 Direct distance measurements

A number of NMR pulse sequences have been developed in order to take advantage of the dipolar coupling between two nuclei that are in close proximity to each other to measure the distance between them. REDOR (Rotational Echo DOuble Resonance), TEDOR (Transferred-Echo DOuble Resonance), DRAWS (Dipolar Decoupling With A Windowless Sequence), and RFDR (Radio Frequency-Driven Recoupling) are of some of these sequences [1-3]. They have been applied to measure distances between atoms in biomolecules, biological membranes, and inorganic and organic solid materials [1,4,5]. Distances probed by REDOR are on the order of a few angstroms. Since the accuracy of the measurement is dependent on the strength of the dipolar

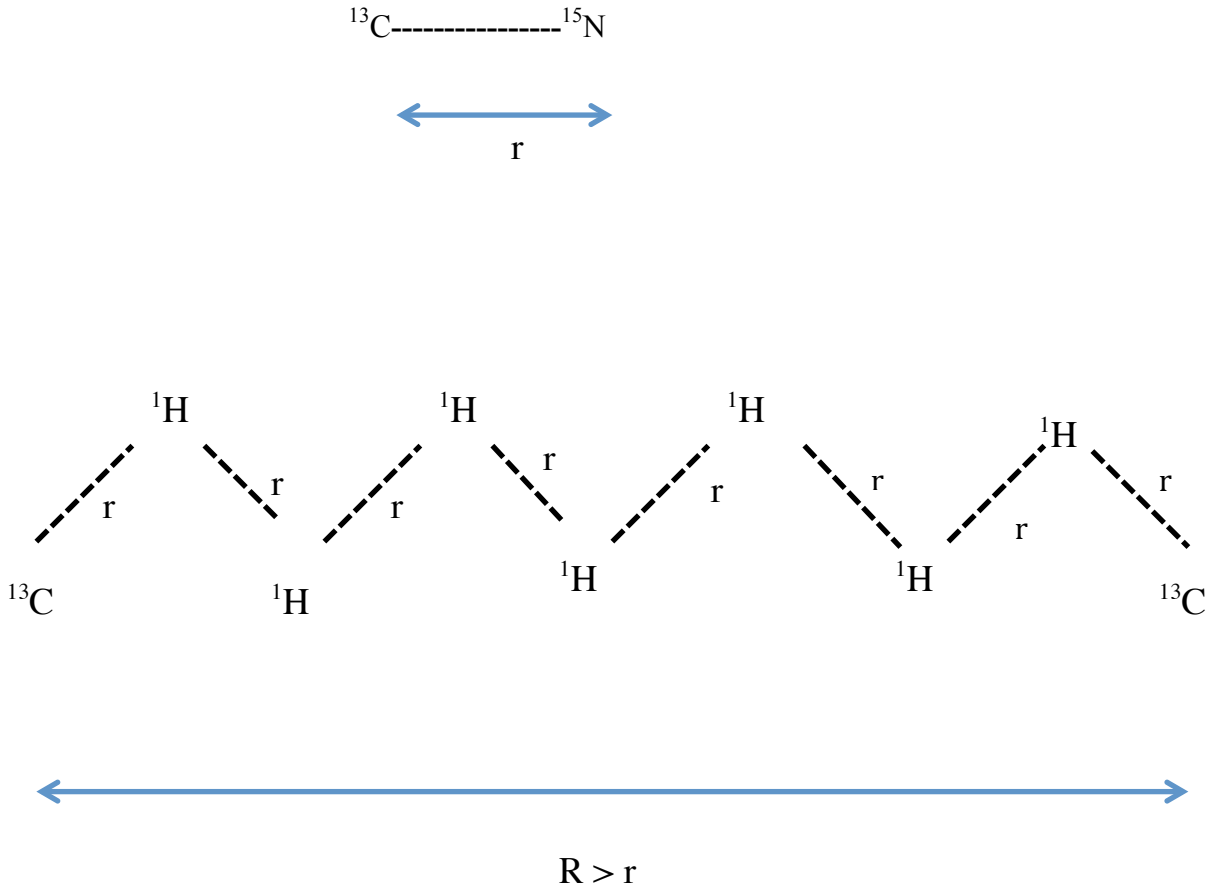

Figure 3.1. The dashed line represents the dipolar coupling between two nuclei and r the distance separating them. Longer distances are accessible through spin diffusion through numerous dipolar couplings (bottom figure) than through direct measurement from one dipolar coupling

coupling between the nuclei as shown in Equation 3.1, the distances measured are dependent on the pair of nuclei studied. ^{13}C-^{15}N distances below 5Å are usually considered reliable. REDOR experiments typically require that the atoms of interest be isotopically labeled, which is one of the limitations of this technique.

Cross polarization experiments are another popular means of directly measuring the distance separating two close nuclei. In the previous chapter, it was mentioned that cross-polarization allows us to take advantage of the high natural abundance of nuclei such as ^{1}H to more rapidly obtain spectra of dilute nuclei such as ^{13}C [6]. Experiments that measure the growth in intensity during the cross-polarization time between heteronuclei can be employed to measure interatomic distances between them [7,8]. During cross-polarization experiments, the nuclei are allowed to exchange magnetization with one another for a given amount of time denoted the contact time, and an NMR signal is subsequently acquired. The contact time is varied and the NMR signal is collected after each contact time. The efficiency of the magnetization transfer between the two nuclei is reflected in the intensity of the NMR signal recorded and is indicative of the strength of the dipolar coupling between the two nuclei and, as a result, is also indicative of the distance separating them. Equation 3.1 is then used to calculate the distance between the two nuclei.

The techniques mentioned so far provide direct distance measurements that are only a few angstroms in length; and are only applicable to the measurement of interatomic distances. One way to measure longer distances by SSNMR is to take advantage of the strong dipolar coupling of protons and their high natural abundance.

3.3 Indirect distance measurements - Spin diffusion

Spin diffusion is the transfer of magnetization between protons through homonuclear dipolar coupling. Because protons are 100% abundant and strongly coupled due to their high magnetogyric ratio, this magnetization transfer occurs over longer overall distances than the heteronuclear couplings discussed earlier. Through SSNMR spin-diffusion experiments, distances as small as 0.5-50 nm have been estimated; this is below the resolution of electron microscopy [9]. Similar distances can be assessed by small angle X-Ray scattering (SAXS) and comparison between distances obtained by that technique and SSNMR spin diffusion measurements have been performed. Jack and coworkers compared domain size measurements of polystyrene-polyisoprene block copolymers obtained by NMR and SAXS. The domains ranged from 2 nm to 10 nm in size [10]. The authors found that the values for domain sizes obtained by both techniques were in very good agreement. Because spin diffusion experiments allow such small distances to be characterized, they have been widely employed to measure the domain sizes of the components of polymeric blends and other systems including biomolecules [11-16].

3.3.1 Spin diffusion experiments

Spin diffusion experiments consist of monitoring the transfer of magnetization from a magnetization-dense region, or source, to a magnetization-poor region, or sink, where it is released. The time that it takes for this transfer to occur is dependent on the distance separating the source of the magnetization and the sink, and on the speed of the spin diffusion process. The transfer of magnetization from one region to the other is assessed by the intensity of the NMR signal collected. Therefore, if the rate of the spin diffusion is known, one can estimate the distance travelled by the magnetization and the size of the domain by monitoring how the

intensity of the NMR signal changes with time. Spin diffusion experiments were first initiated by Goldman and Shen on an inorganic material [17].

Typical spin diffusion experiments include a selection, a mixing, and a detection period. One of the components of the material studied is excited during the selection period, while the other one is devoid of magnetization. The magnetization is then allowed to travel from that magnetization-excess region to a low-magnetization region, and finally the amount of magnetization present in the second region is detected in terms of signal intensity. Ideally, each component can be easily identified in the NMR spectrum of the mixture by a particular peak (Figure 3.2). The detection consists in monitoring the gain, or loss, of intensity of the distinguishable peaks. The rate at which the spin diffusion is taking place is given by the spin-diffusion coefficient. For a given spin diffusion coefficient, the transfer of magnetization will be completed more rapidly over smaller distances than over larger distances. The correlation between the intensity of the NMR signal and the amount of time that the magnetization is allowed to propagate is depicted by build-up curves that are plots of the intensity versus the square root of the time. Typical build-up curves are presented in Figure 3.3. The equation correlating the intensity of the NMR signal to the duration of the diffusion has been derived from the point diffusion out of a sphere, thus explaining the dependency on the square root of the time [18].

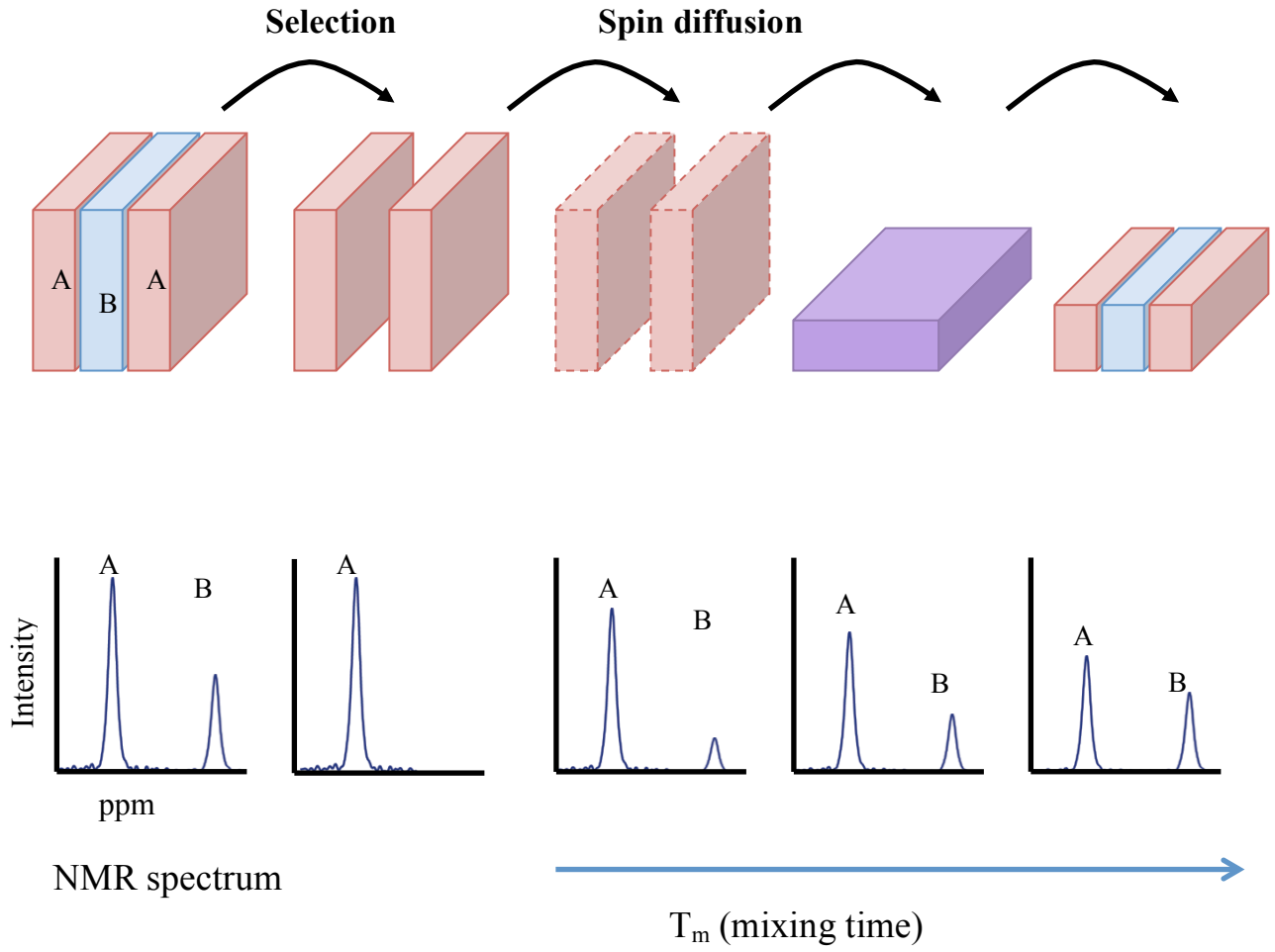

Figure 3.2 Schematics describing basic spin-diffusion experiment. Modified from (19). Two polymers A and B are in a blend. Polymer A is selected during the selection portion of the spin diffusion experiment, and the intensity of the peaks of A and B in the NMR spectrum is monitored as the mixing time is varied and spin diffusion occurs.

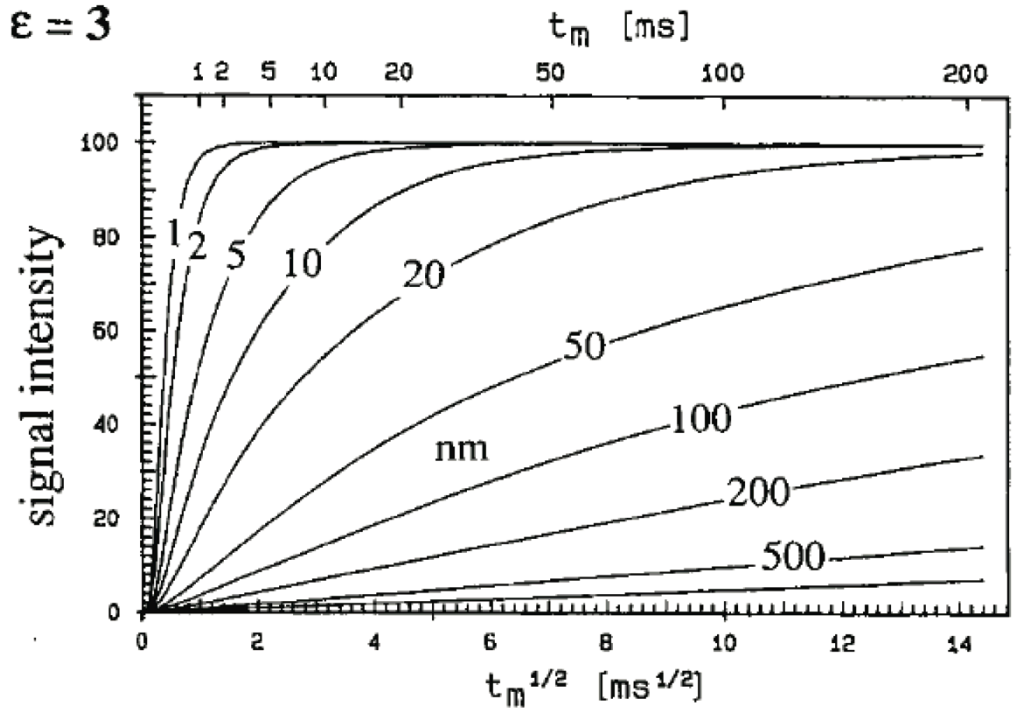

Figure 3.3 Typical intensity vs √time spin diffusion build up curves. The numbers by the curves represent the distance d between the source of the magnetization and the sink.

Reproduced from [19] with permission

In practice, the experimental data obtained from the magnetization exchange experiments are fitted and a build-up curve is obtained. The spin diffusion coefficient must be known in order to perform the simulation. The time at which the magnetization would reach a 100% is then extrapolated and plugged into the following equation in order to obtain the size of the domain [18-20].

$$< d^2 >= 6Dt \qquad (3.2)$$

where $<d^2>$ is the mean square displacement, t is the time and D is the spin diffusion coefficient. The value of the integer in Equation 3.2 varies slightly depending on the morphology of the domains in the materials studied [9,18].

3.3.2 Limitations of spin diffusion experiments

The spin diffusion coefficients must be known in order to obtain domain sizes. The spin diffusion coefficients of a variety of polymers have been measured experimentally. The values obtained ranged from 0.2-0.8 nm^2/ms, depending on the rigidity of the material and the method used to perform the measurements [19,21]. The less rigid the material is the smaller the spin diffusion coefficient.

One of the limits of the size measurements performed through SSNMR spin diffusion experiment is the proton spin-lattice relaxation rate of the material. During spin-lattice relaxation, magnetization is also transferred to a sink. Spin diffusion and spin-lattice relaxation occur concurrently. However, if the spin diffusion does not process faster than the spin-lattice relaxation, then there are limitations on the size of the domains that can be measured. That is because the intensity of the NMR signal collected during the spin diffusion experiment is no longer solely dependent on the rate of spin diffusion, but also incorporates spin-lattice relaxation. Therefore the maximum domain size that can be measured through spin diffusion is dictated by

the magnitude of the ^{1}H T_1 time of the material analyzed [19]. The majority of polymers are amorphous or semi-crystalline; as a result they have very short proton spin lattice relaxation times, on the order of a few seconds. The longer distances that have been measured for polymers are on the order of 100-200 nm [20,22].

When spin diffusion occurs faster than the spin-lattice relaxation, it is believed to be responsible for the observation of a single proton spin-lattice relaxation time in homogeneous solids [23,24]. This averaged common relaxation time is specific to protons. For example, all the ^{13}C nuclei in a molecule are expected to have different spin-lattice relaxation rates since spin diffusion does not occur among ^{13}C. Because of the spin diffusion process, proton spin-lattice relaxation times are highly dependent on domain sizes as well. This dependency is exploited for the study of the miscibility of polymer blends and pharmaceutical amorphous solid dispersions [23,24].

Unlike amorphous polymers, crystalline organic materials can have very long proton spin-lattice relaxation times due to their rigidity, and the size of some crystalline solids has been shown to impact their ^{1}H T_1 times. However, the ability of SSNMR to measure domain sizes of crystalline materials has never been investigated although changes in ^{1}H T_1 times of crystalline materials have been reported.

3.4 Changes in ^{1}H T_1 times of crystalline solids

Schieber has shown that the ^{1}H T_1 time of ground crystalline aspirin decreased from 55.5 s to 8.6 s when the material was exposed to high levels of oxygen [25]. This was a reversible effect, and purging the oxygen out of the materials using N_2 gas caused the ^{1}H T_1 to return to close to its original value. The presence of oxygen had no effect on the ^{1}H T_1 time of unground aspirin. Schieber hypothesized that, due to the smaller size of the ground aspirin particles and the likely

presence of defects created by the grinding process, the relaxation occurs faster in the ground sample because the paramagnetic oxygen, which is a relaxation sink, can penetrate through the defects and speed up the relaxation of the material.

A study by Rabbani and Edmonds indicated that reducing the size of particles of small organic materials by grinding led to a decrease in relaxation time of the materials [26]. The sole objective of the study was to introduce an alternative to the use of paramagnetic impurities to reduce the length of SSNMR experiments. Spin diffusion was believed to be responsible for the transport of magnetization, referred to as "heat" in the article, from the molecules in the center of the particles to the ones on the surface that have a faster relaxation rate, hence a shorter relaxation time. Small organic materials were used as models in the study and a mathematical model describing the mechanism through which the relaxation occurred was proposed. Several reasons why the model and the experimental results did not fully agree were pointed out. They include the fact that the particles in the samples produced by ball milling are likely not spherical, nor uniform in size or morphology. The authors also pointed out that the "grains possess dislocations" that contribute to increasing the surface area of the particles. As a result, there is a larger amount of surface molecules than the one calculated by assuming that particles are perfect spheres. These dislocations, like any other imperfections in crystals, are commonly referred to as crystal defects. The authors concluded that using their model one could obtain an order of magnitude calculation of the size of the grains (particles).

Finally, previous work in the Munson laboratory has shown that a decrease in relaxation time occurred in lactose monohydrate when it was cryoground [27]. In that study, Lubach and coworkers cryoground crystalline α-lactose monohydrate for different lengths of times and obtained ^{1}H T_1 times and ^{13}C SSNMR spectra of all the samples. They found that at longer

grinding times, crystalline lactose converted to amorphous lactose. This was obvious by the significantly broader peaks observed in the SSNMR spectra. Lactose ground for 2 min remained crystalline, yet its ^{1}H T_1 relaxation times was an order of magnitude shorter than that of the unground material. Similarly to lactose, a decrease in ^{1}H T_1 times was observed with increasing grinding time when aspirin was cryoground [28]. However, unlike lactose, aspirin remained crystalline regardless of the length of grinding. The reduction in ^{1}H T_1 magnitude observed in both lactose and aspirin was hypothesized to be due to the creation of crystal defects or the reduction in particle size both caused by grinding. These conclusions and the Rabbani study, suggest the existence of a correlation between the ^{1}H T_1 magnitude of a crystalline material and the crystallites size.

3.5 Conclusion

In this chapter, ways that solid-state NMR was employed to measure distances and domain sizes in a variety of systems have been presented. The size of the majority of the systems that have been studied is in the angstrom or nanometer range. Spin diffusion experiments allow the measurements of longer distances and domain sizes, and studies suggesting a relationship between spin diffusion, the magnitude of the proton spin-lattice relaxation (^{1}H T_1) time of a material, and the domain size of the material were discussed. In the remainder of this dissertation an investigation of the correlation between particle size and ^{1}H T_1 time will be presented.

3.6 References

1. Leppert J, Ohlenschläger O, Görlach M, Ramachandran R 2004. RFDR with Adiabatic Inversion Pulses: Application to Internuclear Distance Measurements. Journal of Biomolecular NMR 28(3):229-233.

2. Gullion T, Schaefer J 1989. Rotational-echo double-resonance NMR. Journal of Magnetic Resonance (1969) 81(1):196-200.

3. Isbester PK, Jr. 1999. Development of an isolated flow variable-temperature magic-angle spinning (MAS) nuclear magnetic resonance (NMR) probe for heterogeneous catalysis studies and high-temperature high-speed 19F MAS NMR techniques applied to fluoropolymers. ed., United States -- Minnesota: University of Minnesota. p 179-179 p.

4. Lane Gilchrist Jr M, Monde K, Tomita Y, Iwashita T, Nakanishi K, McDermott AE 2001. Measurement of Interfluorine Distances in Solids. Journal of Magnetic Resonance 152(1):1-6.

5. Fyfe CA, Lewis AR, Chezeau J-M 1999. A comparison of NMR distance determinations in the solid state by cross polarization, REDOR, and TEDOR techniques. Can J Chem 77(Copyright (C) 2012 American Chemical Society (ACS). All Rights Reserved.):1984-1993.

6. Pines A 1973. Proton-enhanced NMR of dilute spins in solids. J Chem Phys 59(2):569.

7. Hayashi S, Akiba E 1994. Interatomic distances in layered silicates and their intercalation compounds as studied by cross polarization NMR. Chem Phys Lett 226(Copyright (C) 2012 American Chemical Society (ACS). All Rights Reserved.):495-500.

8. Klein Douwel CH, Maas WEJR, Veeman WS, Werumeus Buning GH, Vankan JMJ 1990. Miscibility in PMMA/poly(vinylidene fluoride) blends, studied by fluorine-19-enhanced carbon 13 CPMAS NMR. Macromolecules 23(2):406-412.

9. Chen Q, Schmidt-Rohr K 2006. Measurement of the local 1H spin-diffusion coefficient in polymers. Solid State Nuclear Magnetic Resonance 29(1-3):142-152.

10. Jack KS, Wang J, Natansohn A, Register RA 1998. Characterization of the microdomain structure in polystyrene-polyisoprene block copolymers by 1H spin diffusion and small-angle x-ray scattering methods. Macromolecules 31(Copyright (C) 2012 American Chemical Society (ACS). All Rights Reserved.):3282-3291.

11. Huster D, Yao X, Hong M 2002. Membrane Protein Topology Probed by 1H Spin Diffusion from Lipids Using Solid-State NMR Spectroscopy. Journal of the American Chemical Society 124(5):874-883.

12. Krushelnitsky A, Brauniger T, Reichert D 2006. 15N spin diffusion rate in solid-state NMR of totally enriched proteins: The magic angle spinning frequency effect. Journal of Magnetic Resonance 182(2):339-342.

13. Kumashiro KK, Schmidt-Rohr K, Murphy OJ, Ouellette KL, Cramer WA, Thompson LK 1998. A Novel Tool for Probing Membrane Protein Structure:,Solid-State NMR with Proton Spin Diffusion and X-Nucleus Detection. Journal of the American Chemical Society 120(20):5043-5051.

14. Buda A, Demco DE, Bertmer M, Blümich B, Reining B, Keul H, Höcker H 2003. Domain sizes in heterogeneous polymers by spin diffusion using single-quantum and double-quantum dipolar filters. Solid State Nuclear Magnetic Resonance 24(1):39-67.

15. Mauri M, Thomann Y, Schneider H, Saalwächter K 2008. Spin-diffusion NMR at low field for the study of multiphase solids. Solid State Nuclear Magnetic Resonance 34(1-2):125-141.

16. Traaseth NJ, Gopinath T, Veglia G 2010. On the Performance of Spin Diffusion NMR Techniques in Oriented Solids: Prospects for Resonance Assignments and Distance Measurements from Separated Local Field Experiments. The Journal of Physical Chemistry B 114(43):13872-13880.

17. Goldman M, Shen L 1966. Spin-Spin Relaxation in LaF_{3}. Physical Review 144(1):321-331.

18. Henrichs PM, Tribone J, Massa DJ, Hewitt JM 1988. Blend miscibility of bisphenol A polycarbonate and poly(ethylene terephthalate) as studied by solid-state high-resolution carbon-13 NMR spectroscopy. Macromolecules 21(5):1282-1291.

19. Clauss J, Schmidt-Rohr K, Spiess HW 1993. Determination of domain sizes in heterogeneous polymers by solid-state NMR. Acta Polymerica 44(1):1-17.

20. Schmidt-Rohr K, Spiess H.W. 1994. Multidimensional solid-state NMR and polymers. ed.: Academic Press.

21. Spiegel S, Schmidt-Rohr K, Boeffel C, Spiess HW 1993. 1H spin diffusion coefficients of highly mobile polymers. Polymer 34(21):4566-4569.

22. Demco DE, Johansson A, Tegenfeldt J 1995. Proton spin diffusion for spatial heterogeneity and morphology investigations of polymers. Solid State Nucl Magn Reson 4(Copyright (C) 2012 U.S. National Library of Medicine.):13-38.

23. Schantz S, Ljungqvist N 1993. Structure and dynamics in polymer blends: a carbon-13 CPMAS NMR study of poly(3-octylthiophene)/poly(phenylene oxide). Macromolecules 26(24):6517-6524.

24. Pham TN, Watson SA, Edwards AJ, Chavda M, Clawson JS, Strohmeier M, Vogt FG 2010. Analysis of Amorphous Solid Dispersions Using 2D Solid-State NMR and 1H T1 Relaxation Measurements. Molecular Pharmaceutics 7(5):1667-1691.

25. Schieber LJ. 2010. Methods for increasing sensitivity and throughput of solid-state NMR spectroscopy of pharmaceutical solids. ed., United States -- Kansas: University of Kansas. p 242.

26. Rabbani SR, Edmonds DT 1994. Nuclear spin-lattice relaxation-time reduction in small particles. Physical Review B 50(9):6184-6188.

27. Lubach JW, Xu D, Segmuller BE, Munson EJ 2007. Investigation of the effects of pharmaceutical processing upon solid-state NMR relaxation times and implications to solid-state formulation stability. Journal of Pharmaceutical Sciences 96(4):777-787.

28. Lubach JW. 2007. Applications of nuclear magnetic resonance spectroscopy to pharmaceutical solids. ed., United States -- Kansas: University of Kansas. p 376.

Chapter 4

Selection and Characterization of Model Compounds

4.1 Introduction

The objective of the work presented in this chapter was to investigate quantitatively the correlation between particle size and ^{1}H T_1 relaxation time using model compounds. In the previous chapter the use of SSNMR to measure distances was discussed. In particular, the process of spin diffusion and its utility when measuring distances on the order of hundreds of nanometers was shown. Also mentioned at the end of the previous chapter were previous studies performed in the Munson laboratory that found that the proton spin-lattice relaxation times (^{1}H T_1) of both lactose monohydrate and aspirin decreased with the length of time that the material were cryoground [1,2]. A few hypotheses were proposed to explain the change in ^{1}H T_1 time observed including the presence of crystal defects created by the grinding process and the decrease in particle size of the materials. Here, particles in the μm to nm size range were studied because they are more and more commonly encountered during the pharmaceutical drug development as particle size reduction is often employed in the pharmaceutical industry during manufacturing and is also becoming a means to increase the dissolution rate of poorly soluble compounds [3].

Four specific aims were identified:

- Identify the desired characteristics of a pharmaceutically relevant model compound and choose a suitable compound.
- Prepare uniformly sized particles of our model compound(s), ranging from a few nanometers to a few micrometers in size, with a particle size distribution as narrow as possible.
- Measure the size of the particles in the samples prepared using common particle sizing methods such as scanning electron microscopy (SEM).

- Characterize the prepared and the as-received materials by solid-state NMR and investigate the correlation between ^{1}H T_1 and particle size.

Certain characteristics of lactose and aspirin made it necessary to find other model compounds. First, lactose becomes amorphous when processed, and it would not be possible to separate the effect of the presence of amorphous material on the ^{1}H T_1 time of the material from that of any change in particle size. We were also interested in preparing and characterizing nanoparticles in this study, and a large number of the nanoparticles preparation techniques involve suspending the solid in water, which would not be possible with lactose since it is water soluble. Aspirin remained crystalline when ground; however, it is known to undergo hydrolysis to salicylic acid and acetic acid, therefore similarly to lactose, sample preparation methods requiring the solid to be suspended in water would likely not be an option since aspirin could degrade during sample preparation. It is unclear how the presence of salicylic acid in the sample would affect the ^{1}H T_1 times. Moreover the ^{1}H T_1 time of aspirin is still fairly short (60 s); as a result it could be difficult to confidently identify small changes in its magnitude as being real, as opposed to being within experimental error.

Based on our experience with lactose and aspirin we have identified the properties desired in a model compound for this study. This chapter presents the first two specific aims of the study: the model compound selection, and the sample preparation. Both of these aims involved the physical state characterization of the as-received and prepared materials. The next chapter will present the last two specific aims of this investigation: the size and ^{1}H T_1 characterization and the correlation between the two parameters.

4.1.1 Desired properties of a model compound

An ideal model compound for this study will have the following properties.

- Has a long ^{1}H T_1 relaxation time. Even a small change in magnitude would be easily detected with a compound that has a long ^{1}H T_1 time (> 500 s), and less likely to be within the error margin of the ^{1}H T_1 time measurements. The absence of highly mobile groups such as methyl or t-butyl groups in the structure of a material, and the presence of rigid groups such as benzene rings are good indicators that it is likely to have a long ^{1}H T_1 time.
- No polymorphism. This is to prevent complicating the system with possible polymorphic conversions during sample preparation, and to ensure that any change in ^{1}H T_1 NMR relaxation time detected is due to the change in particle size of the material, and not the presence of another form.
- Remains crystalline during processing. This is based on the above-mentioned study where lactose monohydrate was used as a model compound to study the impact of pharmaceutical processing on ^{1}H T_1 relaxation times. Lubach and coworkers found that the relaxation time of lactose decreased as they increased the grinding time however lactose also became amorphous upon grinding [2]. Since amorphous lactose was known to have a short relaxation time, its presence alone could have been responsible for the decrease in ^{1}H T_1 time observed. Therefore no firm conclusion could be drawn on the possible impact of particle size on the ^{1}H T_1 time.
- Poorly water-soluble. The objective of the work presented in this dissertation is to correlate the size of the particles in a crystalline material to its proton spin lattice relaxation time (^{1}H T_1), and specifically to engineer particles of the model compound in the 100 nm-100 μm size range to correlate them to the ^{1}H T_1 time. A number of size reduction techniques exist, and the majority of them are best suited for use with

poorly soluble compounds. This is because they were developed as a way to increase the bioavailability of poorly water-soluble compounds such as BCS Class II and IV compounds. As a result, a model compound for this study would most likely be poorly water-soluble.

- Inexpensive. About 200-300 mg of material is needed to fill a 7 mm NMR rotor. Considering this relatively large amount of material, a cheap model compound would be more economical.
- Non-toxic. A safe compound is preferred in order to minimize the exposure of the students in the laboratory to highly toxic chemicals.

Once a model compound was chosen, methods to prepare particles ranging from hundreds of nanometers to hundred of micrometers were identified. A number of particle size reduction methods exist, a brief summary of which is presented in the next section.

4.1.2 Particle size reduction techniques

Two main particle size reduction strategies exist: top-down and bottom-up [4]. In the bottom-up approach, the drug is dissolved in a solvent, and precipitated in an anti-solvent in a controlled fashion. Surfactants are often used in order to prevent the particles formed from agglomerating. Typical surfactants include block co-polymers such as Pluronics and other polymers such as hydroxypropyl methylcellulose (HPMC). Both the type of polymer and the ratio of polymer to API are often chosen by trial and error. The difference between the ability of different surfactants to stabilize the same materials has been investigated numerous times [4,5]. Supercritical fluid precipitation and solvent-anti-solvent precipitation are two examples of bottom-up methods [6]. The suspensions produced are often freeze-dried or otherwise dried to obtain a solid final product [7]. Several studies evaluated the effect of the preparation method and

the influence of different surfactants and stabilizers on the size of the particles obtained, and on the physical stability in terms of conservation of the size of particles in the final product [4,8]. Still, the conclusions appear to be very compound-specific and much remains to be understood in order to obtain complete control over the size engineering of particles.

The top-down approach consists of mechanically reducing the size of larger particles to obtain smaller ones. Grinding, high-pressure homogenization and media milling are examples of top-down methods. During media milling, the solid is suspended in a non-solvent, usually water, and circulated through a chamber where it is milled by small polymeric or ceramic beads. The size of the beads and the length of milling can be varied in order to obtain particles of different sizes. Top-down size reduction techniques such as milling are often used during manufacturing of solid pharmaceuticals in order to increase the powder flow properties of the material.

Some groups have investigated which of the particle size reduction approach, top-down or bottom-up, presents an advantage over the other [4]. However, it seems that the best technique to use is highly dependent on the material whose size is being reduced as well as on the desired final size therefore in this dissertation, a combination of top-down and bottom-up techniques was used to prepare particles of the model compounds selected.

4.2 Materials and Methods

4.2.1 Materials

Salicylic acid, and dicumarol were purchased from Sigma Aldrich (St Louis, MO) and used as-received.

4.2.2 Sample preparation

Cryogrinding

About 1.5 g of salicylic acid or dicumarol was placed in a vessel and ground while immersed in liquid nitrogen after a 15 min precooling period with alternating cycles of 2 min of cooling and 2 min of grinding (SPEX SamplePrep 6770 Freezer/Mill, SamplePrep, Inc., Metuchen, NJ). The rate of grinding was 10 counts per second. The total grinding time was 60 min for salicylic acid and 30 min for dicumarol.

Sieving

850, 710, 600, 425, 300, 125 and 75 μm sieves were used to separate the particles in as-received salicylic acid based on size (USA Standard Sieve 3"). The sieves were shaken for 15 min on a sieve shaker (Gilson company, Inc. Performer III Model SS-3, Lewis Center, OH) set at an amplitude of 5. The powder remaining on top of each sieve was then collected, weighed, and stored over dessicant at ambient conditions.

Spray drying

A 5% (w/v) solution of salicylic acid in methanol was spray dried in a Buchi mini spray-dryer (Mini Spray-Dryer B-290, Buchi Corporation, New Castle, DE) using the conditions presented in Table 4.1.

Anti-solvent precipitation

In all cases the API was dissolved in a solvent and added to water, or to an aqueous solution of surfactant, under sonication (Fisher brand sonic dismembrator, Fisher Scientific, Pittsburgh, PA). A Fisher brand injector and a 5mL syringe with a 20-gauge needle (Popper deflected non coring septum 20 x 8", Popper & Sons, Hyde Park, NY) were used for the injections. The suspensions

were then lyophilized in a Virtis freeze- dryer (Advantage 2.0 Benchtop Freeze Dryer, SP Scientific, Gardiner, NY).

Salicylic acid- Salicylic acid was dissolved in either acetonitrile or acetone and precipitated in aqueous solutions of polyvinyl acetate (PVA) (BASF), Pluronics F 68 (PF 68) (Sigma), or hydroxypropyl methylcellulose (HPMC) (Sigma). The ratio of salicylic acid to surfactant was always 10:1 and the injection rate was 30 mL/h. The suspensions were then lyophilized. The precipitation conditions are summarized in Table 4.2 and the lyophilization cycles used were variations of the following cycle: hold at -45 ºC for 360 min; ramp to at -25 ºC and 100 mTorr in 120 min, ramp to -10 ºC in 480 min at 100 mTorr, hold at -10 ºC and 100 mTorr for 480 min, ramp to -5 ºC at 110 mTorr in 240 min, hold at -5 ºC and 100 mTorr for 240 min, hold at 0 ºC and 100 mTorr for 360 min, hold at 5 ºC and 100 mTorr for 360 min, hold at 10 ºC and 10 mTorr for 60 min.

Dicumarol-A suspension of dicumarol in dimethyl sulfoxide (DMSO) was stirred and heated to at least 100 ºC overnight to obtain a 1mg/mL solution. The solution was then injected into water under sonication. The sonication amplitude was 20% for all the samples. Table 4.3 summarizes the ratios of DMSO to water, as well as the injection speed employed for each lot prepared. 10-15 vials were prepared using each set of parameters. After injection, the suspensions were freeze-dried using the following cycle: hold at -70 ºC for 120 min, extra freezing at -50 ºC for 60 min; hold at -5 ºC and 100 mTorr for 1320 min, ramp to 15 ºC in 300 min at 100 mTorr, hold at 15 ºC and 100 mTorr for 600 min, ramp to 30 ºC at 50 mTorr for 300 min, hold at 60 ºC and 10 mTorr for 60 min. The vials were held at 25 ºC and 200 mTorr until they were removed from the lyophilizer.

4.2.3 Sample characterization

Differential scanning calorimetry (DSC)

1-4 mg of sample was weighed in a standard, hermetic or T-Zero normal TA aluminum pan. Samples were heated from -10ºC to 250 ºC or 300ºC using a 10ºC/min ramp (DSC Q200 or DSC Q2000, TA Instruments, New Castle, DE).

Solid-State Nuclear Magnetic Resonance (SSNMR) spectroscopy

All the samples were packed under ambient conditions in 7 mm zirconia rotors (Revolution NMR, Fort Collins, CO). ^{13}C SSNMR spectra were collected using either a Chemagnetics CMX300 (Varian, Palo Alto, CA) or a Tecmag Appolo (Tecmag, Inc., Houston, TX) spectrometer both operating at a ^{13}C frequency of ~75 MHz. 3-methylglutaric acid was used as an external standard, with the methyl peak referenced at 18.84 ppm [9]. All spectra were acquired using cross-polarization and magic angle spinning (CP/MAS) [10-13]. The magic angle spinning frequency was 4 kHz. A SPINAL-64 decoupling pulse sequence was used, and the spinning sidebands were suppressed using total sideband suppression (TOSS) [14]. A contact time of 1 ms was used both for salicylic acid and dicumarol. A ^{1}H decoupling field of 70-80 kHz was used. The number of acquisition points was 1024 for both salicylic acid and dicumarol. ^{1}H T_1 relaxation times were measured by saturation recovery.

Table 4.1. Salicylic acid spray-drying conditions

Concentration	50mg/mL
Inlet temperature	150 ºC
Pump rate	15 mL/min
Aspirator	100%
Flow rate	50
Outlet temperature	54 ºC

Table 4.2. Conditions employed for anti-solvent precipitation of salicylic acid

Parameters	**1**	**2**	**3**
Solvent	Acetonitrile	Acetone	Acetone
Surfactant or polymer	HPMC	PVA	Pluronic F 68
Salicylic acid: surfactant (w/w)	5:1	5:1	2:1
Solvent: water (v/v)	1:10	1:10	1:10
Injection speed	30 mL/h	30 mL/h	30 mL/h

Table 4.3. Conditions used to generate the different lots of dicumarol by anti-solvent precipitation of a solution of dicumarol in DMSO into water

Lot	**Ratio DMSO: H_2O**	**Injection speed**
A	1: 9	60 mL/h
B	1: 9	30 mL/h
C	1:1	40 mL/h
D	1:1	60 mL/h
E	2:1	40 mL/h

4.3 Results and Discussion

4.3.1 Selection process

Salicylic acid and dicumarol were identified as model compound candidates based on the requirements for a model compound discussed in the introduction. Salicylic acid was considered for this study because it has a small rigid structure and lacks mobile groups such as methyl or ethyl groups that cause fast relaxation; therefore, it was expected to be a slow relaxer and have a much longer ^{1}H T_1 relaxation time than aspirin (Figure 4.1a). Salicylic acid is a commonly used anti-acne medicine and is therefore safe and cheap, and it has only one known polymorph. Similarly, dicumarol is a natural product with only one known polymorph that was used as an anticoagulant until it was replaced by warfarin. It has two sets of fused rings in its structure and no relaxation sinks; therefore, its ^{1}H T_1 relaxation time was anticipated to be fairly long (Figure 4.1b). Dicumarol is very poorly water soluble while salicylic acid is not. The comparatively high solubility of salicylic acid in water was believed to impact our ability to prepare nanoparticles of that material. The first step in the selection process was to confirm that the compounds chosen for this study would behave similarly to aspirin when ground, i.e. remain crystalline while their ^{1}H T_1 time decreases. Therefore we cryoground both compounds and characterized the physical state and the ^{1}H T_1 times of the ground materials.

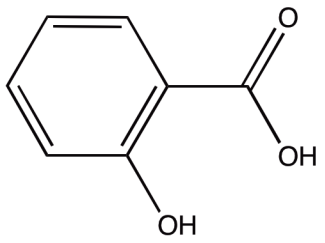

a.

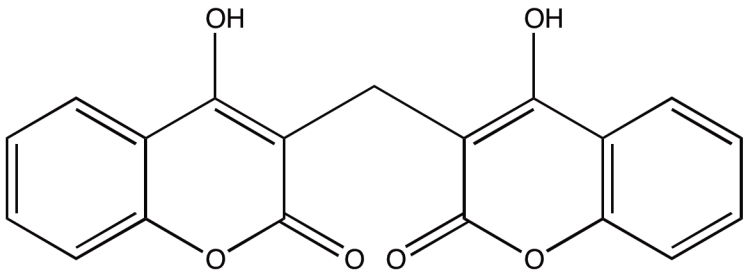

b.

Figure 4.1. Chemical structure of **a.** salicylic acid; **b.** dicumarol

4.3.2 Effect of cryogrinding on the physical state of the model compound candidates

DSC and SSNMR were used to characterize the physical state of the materials in order to verify that no new polymorph was created, and that no crystalline to amorphous conversion occurred as a result of grinding. Figure 4.2 is an overlay of the DSC thermograms of as-received salicylic acid and cryoground salicylic acid. An endotherm showing the melting of salicylic acid around 160 ºC, the expected melting point of salicylic acid, is present in both thermograms, suggesting that ground salicylic acid is crystalline. Other events such as endotherm or glass transition that would indicate recrystallization and the presence of amorphous material respectively are absent from the thermograms. Small differences in the shape of the endothermic peaks can be seen; such differences between the DSC thermograms of a given materials, and the presence of shoulders can be attributed to differences in particle morphology and/or particle size distribution[15,16]. Although such differences become relevant when DSC is used to perform quantitative studies, here they do not require much concern as DSC is only used as a qualitative tool to assess the physical state of material. The ^{13}C SSNMR spectra of as-received salicylic acid and salicylic acid cryoground for 60 min are shown in Figure 4.3. No change in chemical shift occurred, however the peaks of the ground materials are significantly broader than those of the as-received salicylic acid. Fractures and other defects created by grinding can cause line broadening because they decrease the homogeneity of the material.

Figure 4.4 shows an overlay of the DSC thermograms of as-received and 30 min cryoground dicumarol, and the ^{13}C SSNMR spectra of the same materials. An endotherm indicative of the melting of dicumarol around 290 ºC is the only thermal event present. Again the small differences between the two thermograms are likely due to particle size or morphology differences. Therefore the DSC results suggest that dicumarol remained crystalline upon being

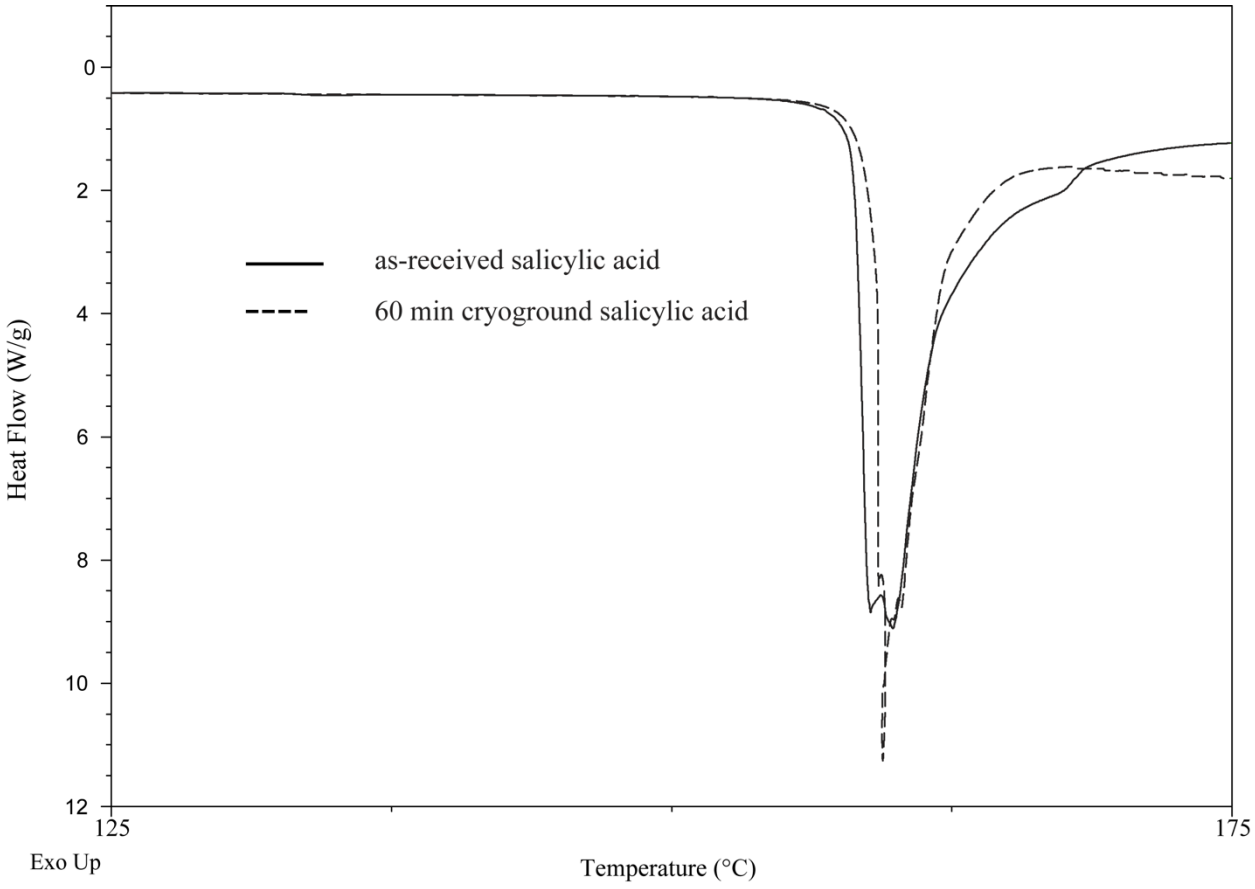

Figure 4.2. DSC thermograms of as-received salicylic acid and 60 min cryoground salicylic acid

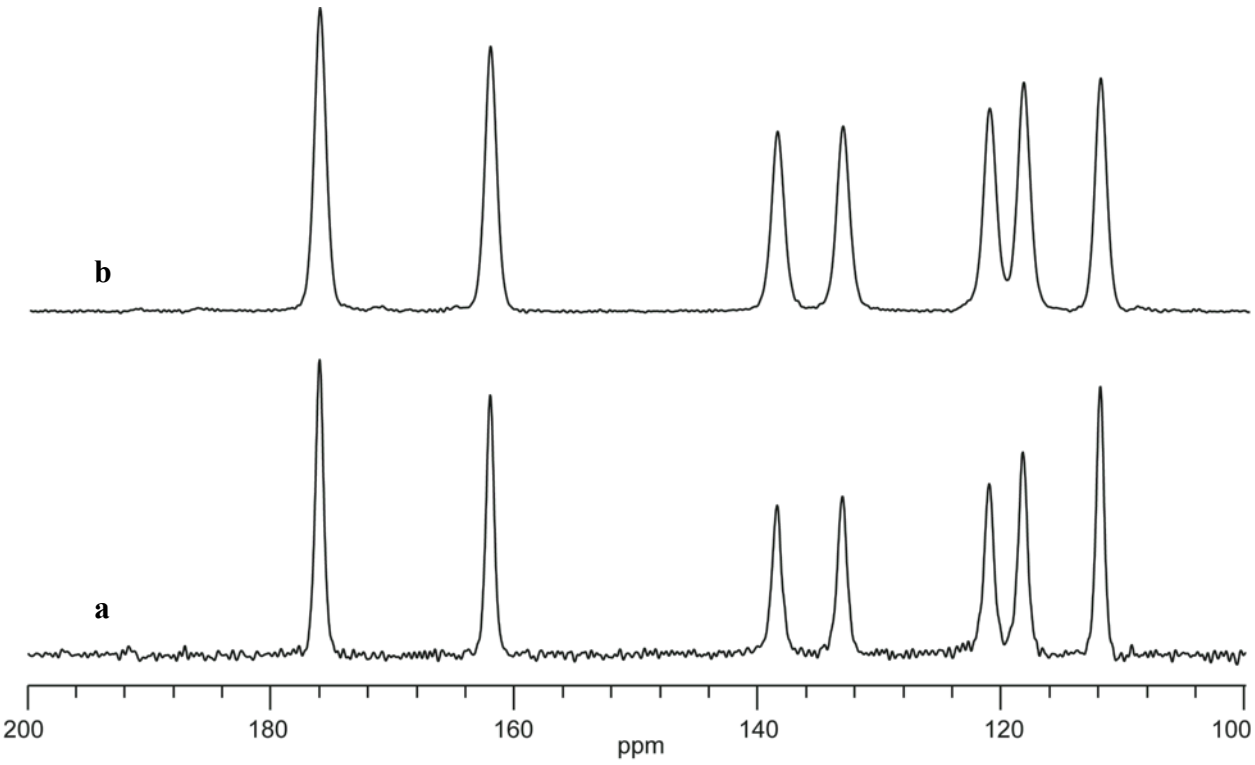

Figure 4.3. ^{13}C SSNMR spectra of **a**. as-received salicylic acid; **b**. 60 min cryoground salicylic acid

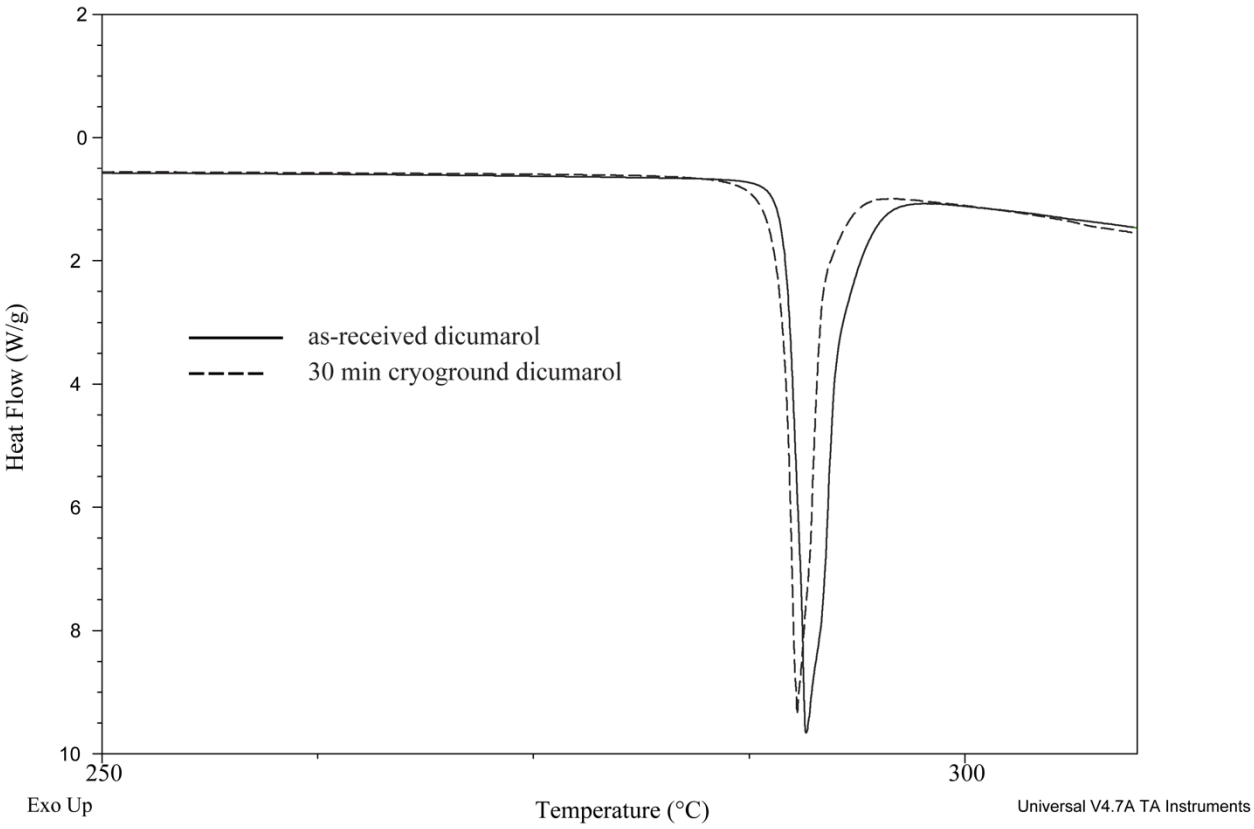

Figure 4.4. DSC thermograms of as-received and 30 min cryoground dicumarol

milled. The ^{13}C SSNMR spectra of as-received and 30 min cryoground dicumarol are shown in Figure 4.5. The two SSNMR spectra contain the same number of peaks at the same chemical shifts, indicating that no polymorphic conversion occurred upon milling. The linewidths of the peaks in the three spectra are also very similar, although the peaks of the cryoground samples are slightly broader than the ones of the as-received material, as best evidenced by the loss of resolution of the split peak at 115 ppm. Similarly to salicylic acid, this is likely due to a decrease in sample homogeneity due to grinding.

4.3.3 Effect of grinding on the ^{1}H T_1 relaxation time of salicylic acid and dicumarol

The ^{1}H T_1 time of as-received salicylic acid is approximately 3900 s. The ^{1}H T_1 value of salicylic acid cryoground for 60 min is 59 s. This represents a decrease in the ^{1}H T_1 time of nearly two orders of magnitude. Similarly the ^{1}H T_1 time of as-received dicumarol is 1500 s, and that of dicumarol cryoground for 30 min is 15 s. The SSNMR results demonstrate that grinding caused the ^{1}H T_1 times of both salicylic acid and dicumarol to decrease, while the materials remained crystalline after grinding. Based on the results of the grinding experiments, salicylic acid and dicumarol were retained as a model compound for this study.

Grinding is a quick and efficient way of reducing particle size, and can be employed to prepare a large amount of material. However, the particles produced by grinding are not always uniform in size. For example, the cryoground salicylic acid particles are uneven chunks with rough edges (Figure 4.6a). Although it is obvious they are a few micrometers in size, the lack of size uniformity in the cryoground material makes it difficult to accurately estimate the size of the particles. Also grinding is known to produce defect-containing particles due to the mechanical stress and the heat that it usually generates [17]. These defects can contribute to the enhancement of the relaxation rate of crystalline materials. One additional limitation of grinding is that it often

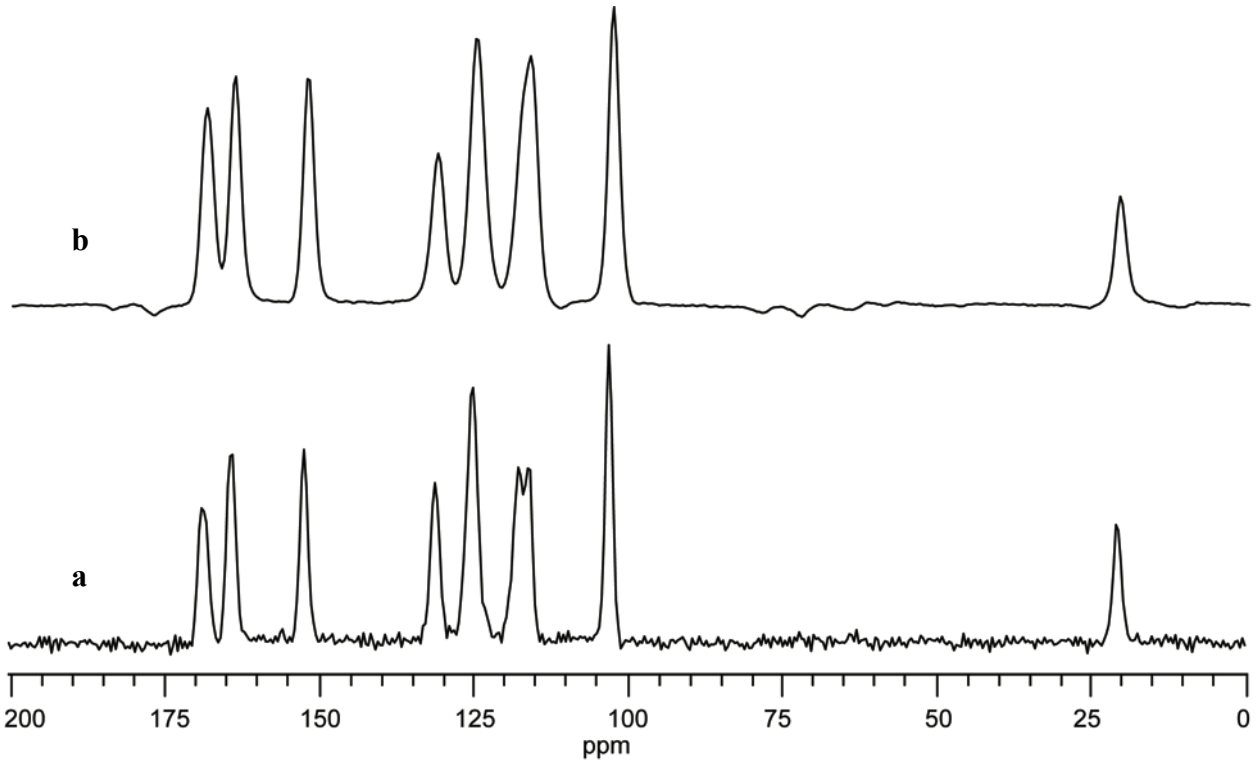

Figure 4.5. ^{13}C SSNMR spectra of **a**. as-received dicumarol; **b**. 30 min croground dicumarol

b.

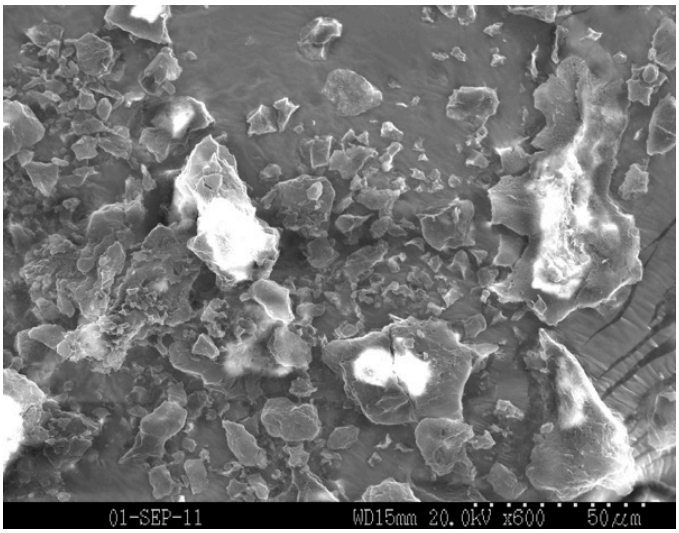

a.

Figure 4.6. SEM micrograph of **a.** salicylic acid cryoground for 60 min; **b.** as received salicylic acid

does not allow the generation of nanometer-size particles. For these reasons grinding was not used to generate the samples that would be used for the study of the correlation between particle size and ^{1}H T_1 time. For the purpose of this study and in order to generate particles in the nanometer size range, the ideal size reduction method would generate uniform particles without producing crystal defects.

4.3.4 Preparing uniformly sized particles of salicylic acid over a wide particle-size range

We wanted to prepare a variety of particle sizes of salicylic acid ranging from larger than 100 μm to below 1 μm that are uniformly distributed. Thus anti-solvent precipitation, spray-drying, and sieving were identified as three techniques that could be used to generate particles with sizes ≤ 5 μm, 5-100 μm and >100 μm, respectively. In addition, for our study it was important that the preparation process not alter the crystalline state of the materials prepared. The particles of as-received salicylic acid appear non-uniform in size even to the naked eye, so sieving was anticipated to be a good method to separate the particles based on their size (Figure 4.6b). Table 4.4 summarizes the sizes of the sieve fraction of salicylic acid obtained and the relative amounts by weight of material in each sieve fraction.

The parameters used to perform spray drying, including the solvent, concentration, and temperature, were chosen empirically. Since one of the disadvantages of spray drying is the loss of material encountered during the process, the conditions used to spray dry salicylic acid were chosen both to maximize the yield and to generate particles of the smallest size possible; the conditions are presented in Table 4.1. Methanol is a commonly-used solvent for spray-drying and was used here as well. The spray-dryer manufacturers indicated that the concentration of the solid in solution has a significant influence on the size of the particles in the final product: the lower the concentration the smaller the size of the particles obtained. Because spray-drying is

Table 4.4. Sieve fractions obtained from sieving as-received salicylic acid.

Sieve fraction	% of total (weight)
> 850 µm	19.5 %
710-850µm	5.4 %
600-710 µm	6.8 %
425-600 µm	14.5 %
300-425 µm	40.6 %
180-300 µm	11.0 %
125-180 µm	1.2 %
<125 µm	1.06 %

known to generate amorphous material, it was important to characterize the physical state of the material prepared [18].

Anti-solvent precipitation of salicylic acid was attempted using a variety of solvent-antisolvent combinations in order to generate smaller size particles. However, all the attempts were unsuccessful as the materials produced were not uniform in size. Figure 4.7 shows scanning electron microscopy images of salicylic acid samples obtained by anti-solvent preparation. The SEM of the samples also suggest that they are not crystalline. The high solubility of salicylic acid in water is a possible explanation for our unsuccessful attempts. In all cases, a polymer or a surfactant was used in order to stabilize the salicylic acid particles that were generated. Still, instead of precipitating, salicylic acid might have been dissolving in the water, and then recrystallizing or complexing with the polymer during freeze drying.

4.3.5 Physical state characterization of the prepared salicylic acid samples

Sieving is not expected to change the physical state of the material, and the melting endotherms of salicylic acid in the sieved fractions all overlap within 1-2 ºC with the melting endotherm of the as received material, as shown by the DSC thermograms in Figure 4.8. The DSC thermograms (Figure 4.9) and SSNMR spectra (Figure 4.10) of the spray-dried salicylic acid samples indicated that they are crystalline. An endotherm showing the melting of salicylic acid is present in the spray-dried samples at the same temperature as the endotherm in the as-received material around 160ºC. The onset of melting, as well as the shape of the endotherm, is also the same in all three materials. Differences in the DSC thermograms of a given materials, such as the presence of shoulders has also been attributed to difference in particle morphology[15].

All the peaks in the SSNMR spectra of the spray-dried samples are narrow and at the same chemical shifts as the peaks of the as-received material, confirming the crystallinity of the

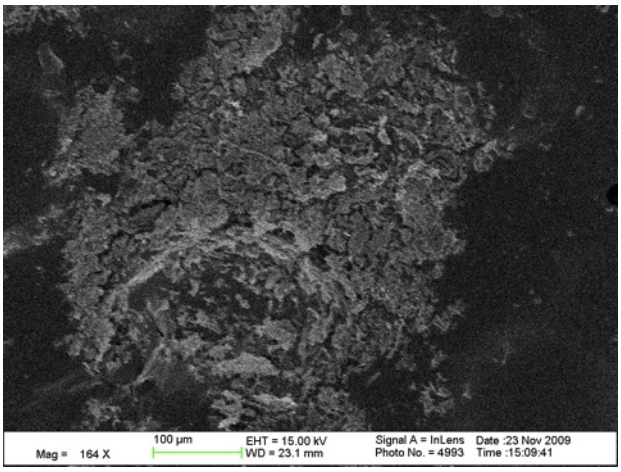

a.

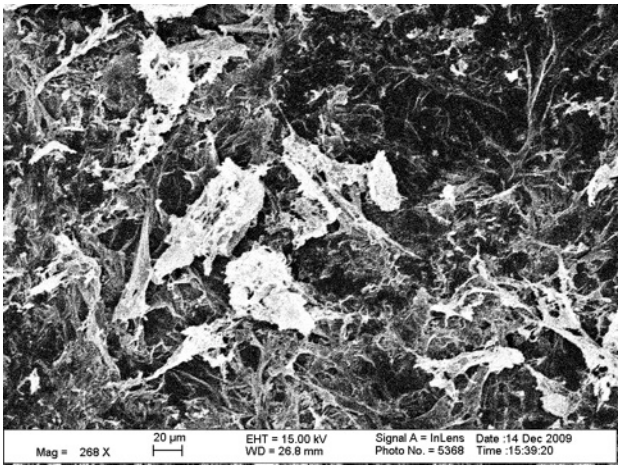

b.

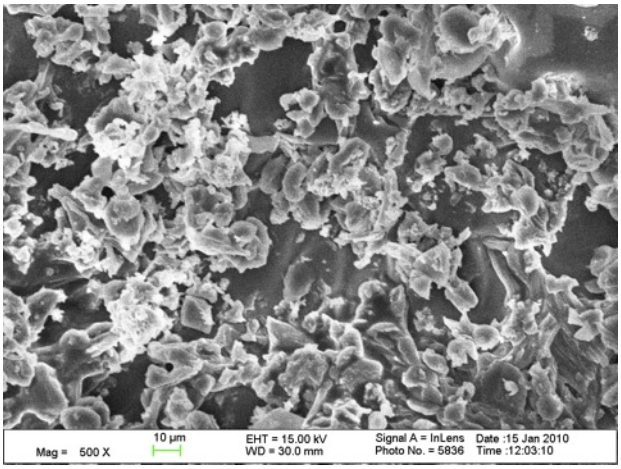

c.

Figure 4.7. SEM micrograph of salicylic acid prepared by anti-solvent precipitation. The samples differe by the kind of surfactant or polymer used as well as the ratio of salicylic acid to polymer or surfactant. **a**. salicylic acid : HPMC 5:1; **b**. salicylic acid : PVA 5:1; **c**. salicylic acid : Pluronic F 68 2 :1

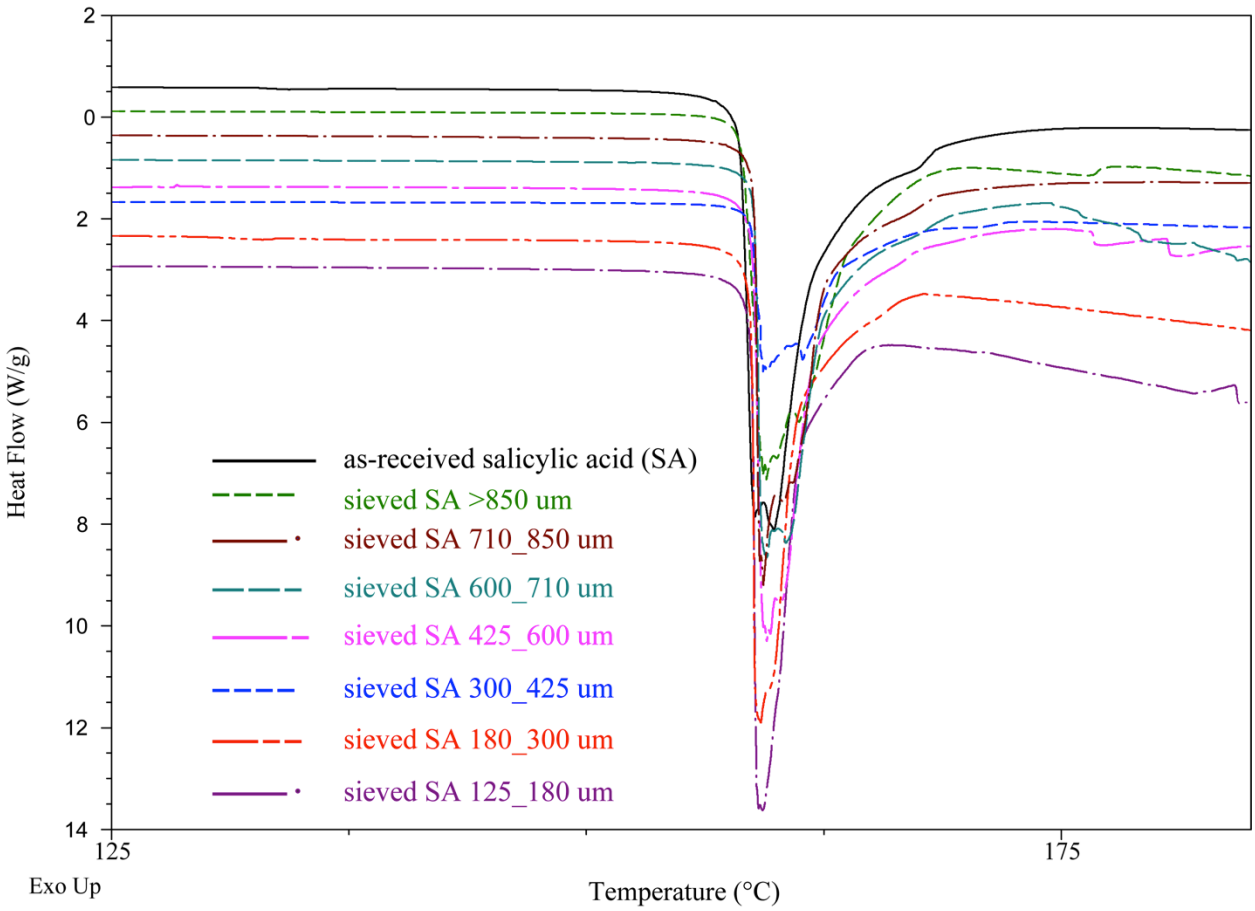

Figure 4.8 DSC thermograms of as-received and sieved fractions of salicylic acid

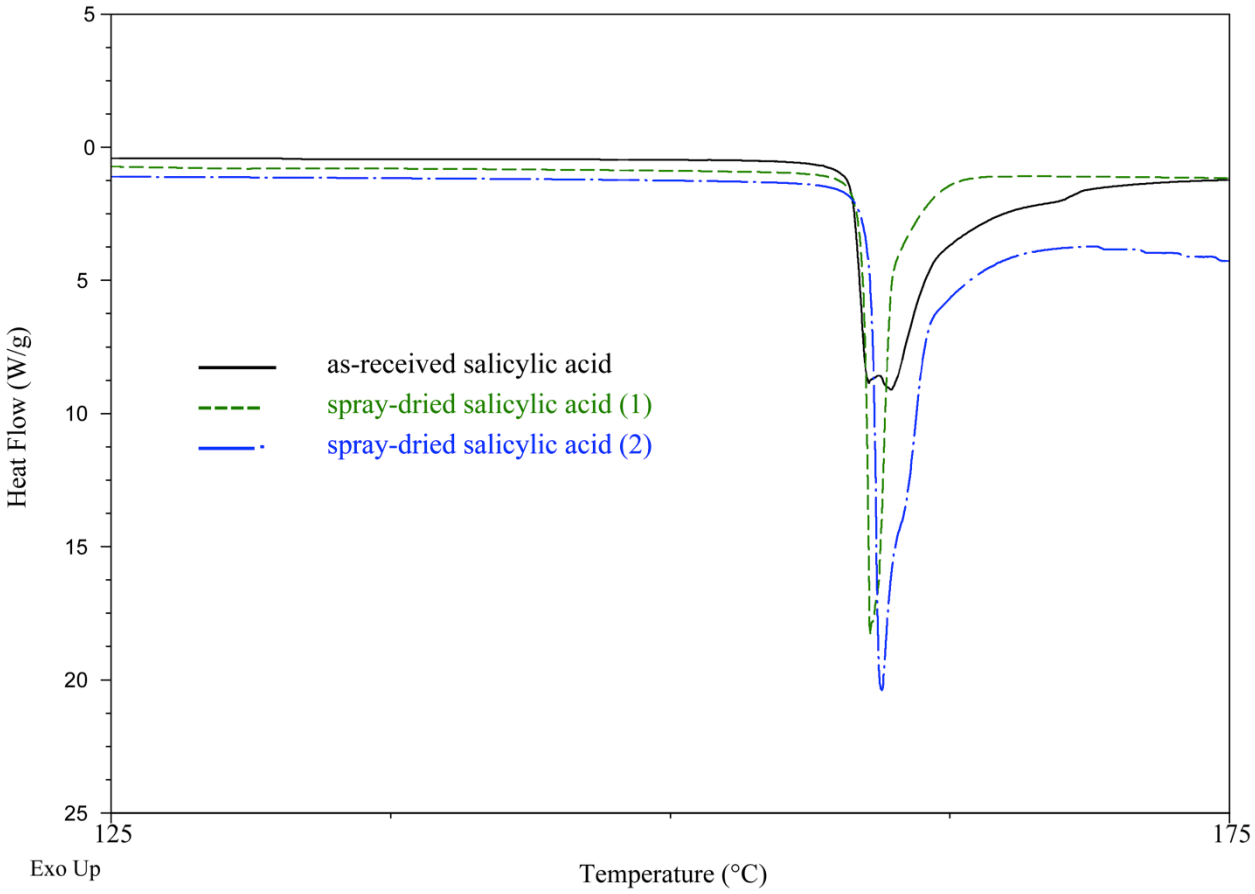

Figure 4.9 DSC thermograms of as-received and spray-dried salicylic acid

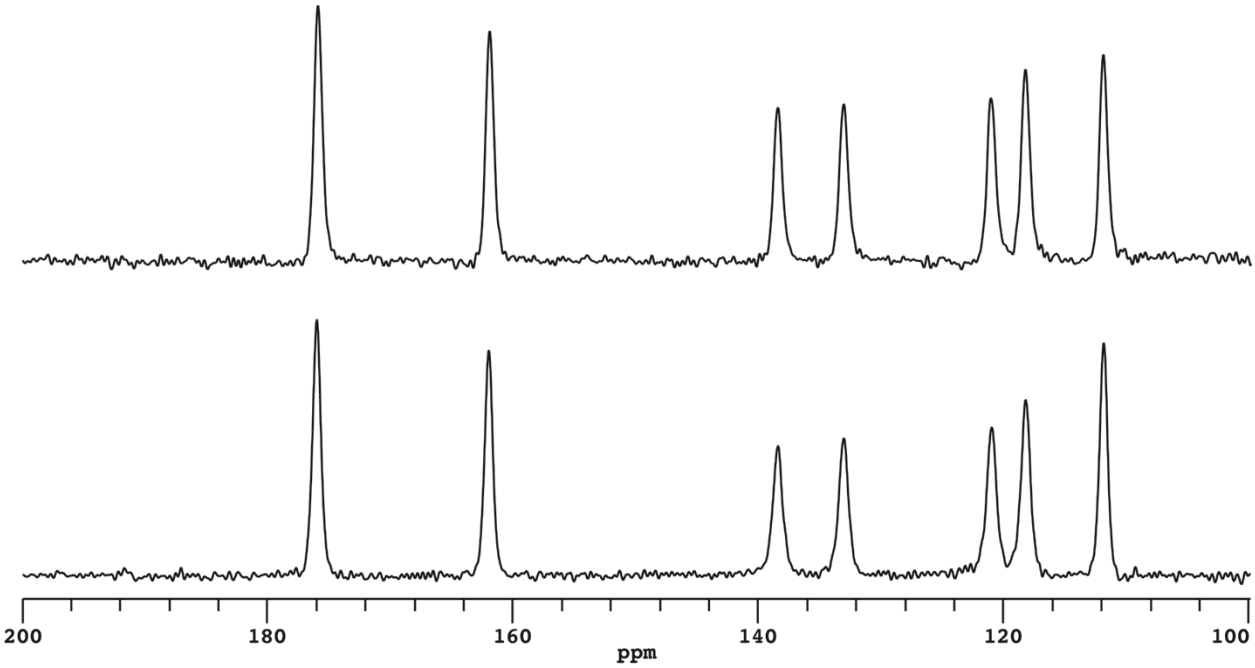

Figure 4.10 ^{13}C SSNMR spectra of **a**. as-received salicylic acid; **b**. spray-dried salicylic acid

spray dried materials.

4.3.6 Dicumarol samples preparation

A similar approach to sample preparation as with salicylic acid was attempted with dicumarol. However, the size particles of as-received dicumarol (~50 μm) were already below the smallest size sieve fraction that we had (75 μm), therefore sieving could not be used. We were unable to dissolve dicumarol in solvents that are typically used for spray-drying, such as methanol and dichloromethane. Therefore anti-solvent precipitation was used to prepare particles of dicumarol of a micrometer and less in size. Although anti-solvent precipitation did not allow us to produce particles of salicylic acid in our desired size range, that technique was still attempted as a preparation technique for dicumarol.

Dicumarol is less soluble than salicylic acid in water, which was considered to be an advantage for anti-solvent precipitation. However, the precipitation conditions used with salicylic acid could not be applied to dicumarol, so a new set of conditions was tried. Table 4.3 summarizes the precipitation conditions used for dicumarol. DMSO was chosen as a solvent because it is the only solvent in which dicumarol could be dissolved. The concentration of dicumarol in DMSO was 10 mg/mL in all cases. The solution had to be heated (100º C) and stirred for more than an hour in order to ensure complete dissolution. This step was also observed by others as being necessary in order to dissolve dicumarol in DMSO (18). Decreasing the temperature caused the API to precipitate out of solution, so more concentrated dicumarol solutions were not used since they would be even less stable. The sonication amplitude used during injection of dicumarol into DMSO was also kept constant at 20% for all samples. This is because sonication causes the solution to heat. We wanted to avoid re-dissolving of the drug in solution, and a more acceptable alternative was a low sonication amplitude. The parameters that

were modified from one sample to the other were the speed of the injection of the dicumarol solution into water and the ratio of DMSO to water. The rate of injection of the solvent into the anti-solvent has been shown to impact the size of the final particles obtained for a number of pharmaceutical compounds [8]. Faster injection rates usually yield to larger particles. While only the preparation and physical state characterization of the materials are presented in this chapter, the ultimate goal was to generate particles of a variety of sizes.

The ratio of solvent to anti-solvent was also varied. This was done for two reasons: first that ratio impacts the size of the particles generated by changing the degree of supersaturation in the final solution; and second a large amount of material (200-300 mg) is needed for solid-state NMR analysis, and using larger volumes of the dicumarol solutions would yield more product. Surfactants were not used because their effect on the ^{1}H T_1 relaxation rate of dicumarol is unknown. The absence of surfactant would likely cause the particles prepared to agglomerate, which is acceptable in this study since the primary focus is not the drug delivery and dissolution properties of our material but rather its physical state.

All of the suspensions were lyophilized following precipitation in order to obtain a solid product. Lyophilization was chosen other drying methods such as spray-drying because it does not cause any loss of material. Although there are reports of lyophilization from DMSO, no report on freeze-drying from mixtures of DMSO and water was found [19]. However, a study published in 1966 warned against significant lower freezing point of mixtures of DMSO and water at certain ratios, compared to the individual components [20]. The authors found that mixtures with a 0.2-0.4 mole ratio of DMSO froze below -100ºC. However, such low temperatures were not needed in order to freeze the samples prepared here. Moreover, in order to test the efficiency of the cycle at removing all of the liquid phase, mixtures of DMSO and water

in the ratios used during the precipitation were freeze-dried. All the vials were empty to the naked eye at the end of the cycle, as a result the cycle was considered acceptable and was used to freeze-dry all the dicumarol suspensions.

4.3.7 Physical state characterization of the prepared dicumarol samples

The DSC thermograms of the precipitated samples showed that dicumarol in the precipitated lots melted a few degrees lower than the bulk material (Figure 4.11). This is likely due to the significant particle size difference between the bulk and the precipitated materials. The onset of melting was also slightly different for all the materials, and the melting endotherms of the precipitated lots with an early melting onset are broader than the endotherms of the other materials.

The ^{13}C SSNMR spectra of the precipitated materials are shown in Figure 4.12. All the peaks in the spectra of the precipitated lots have a similar linewidths to the as-received material, confirming that they are crystalline. The peaks in the spectra also have the same chemical shifts as the as-received dicumarol, indicating that no apparent polymorphic conversion occurred. The spectra of the five precipitated lots presented in Figure 4.13 have poor signal to noise ratio because they were extracted from the ^{1}H T_1 relaxation data sets, which were collected with a small number of acquisitions. That poor signal to noise ratio could explain the differences in resolution observed between samples. The difference is most obvious in the splitting of the peak at 123 ppm. The splitting is not apparent in Lots A, C, D and E, whereas it is easily seen in lot B and the as-received material.

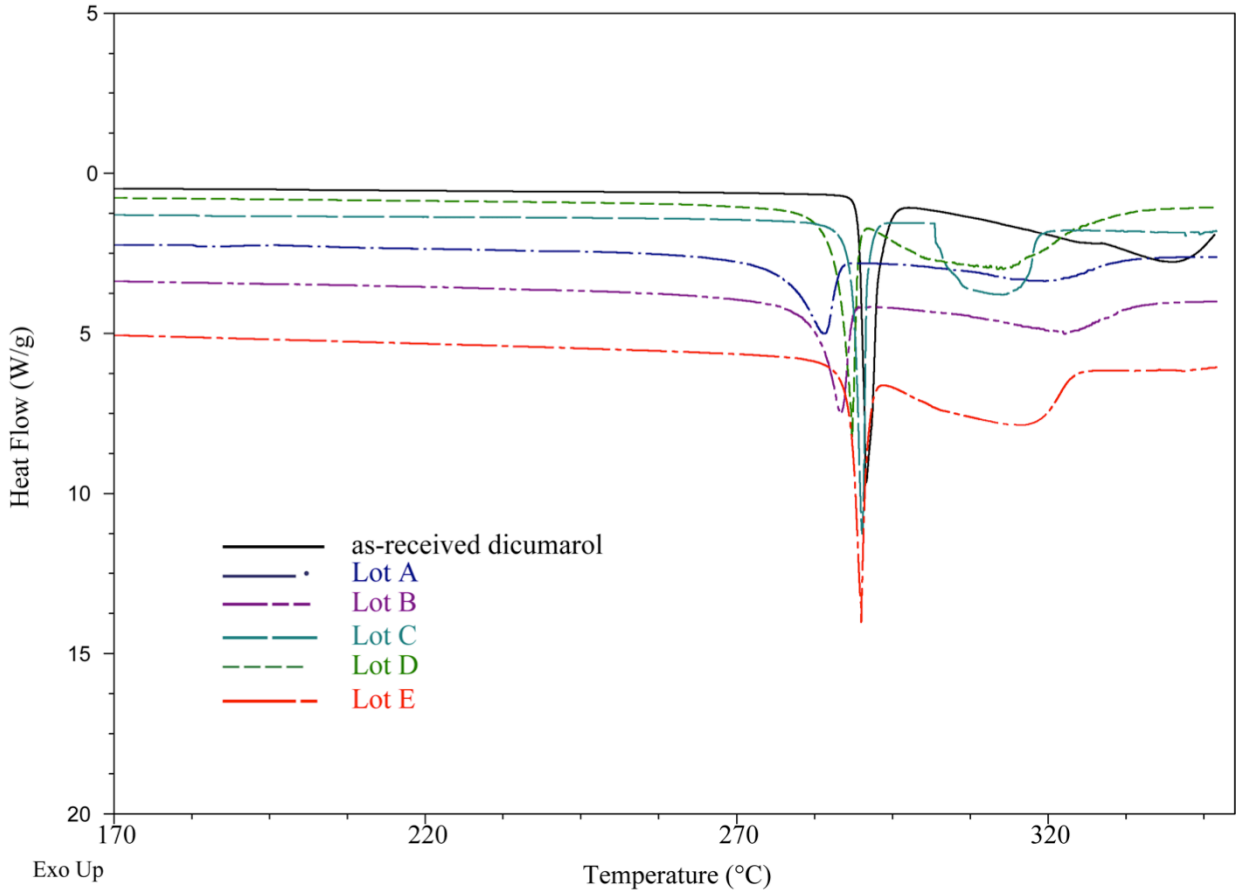

Figure 4.11 DSC thermograms of precipitated samples of dicumarol

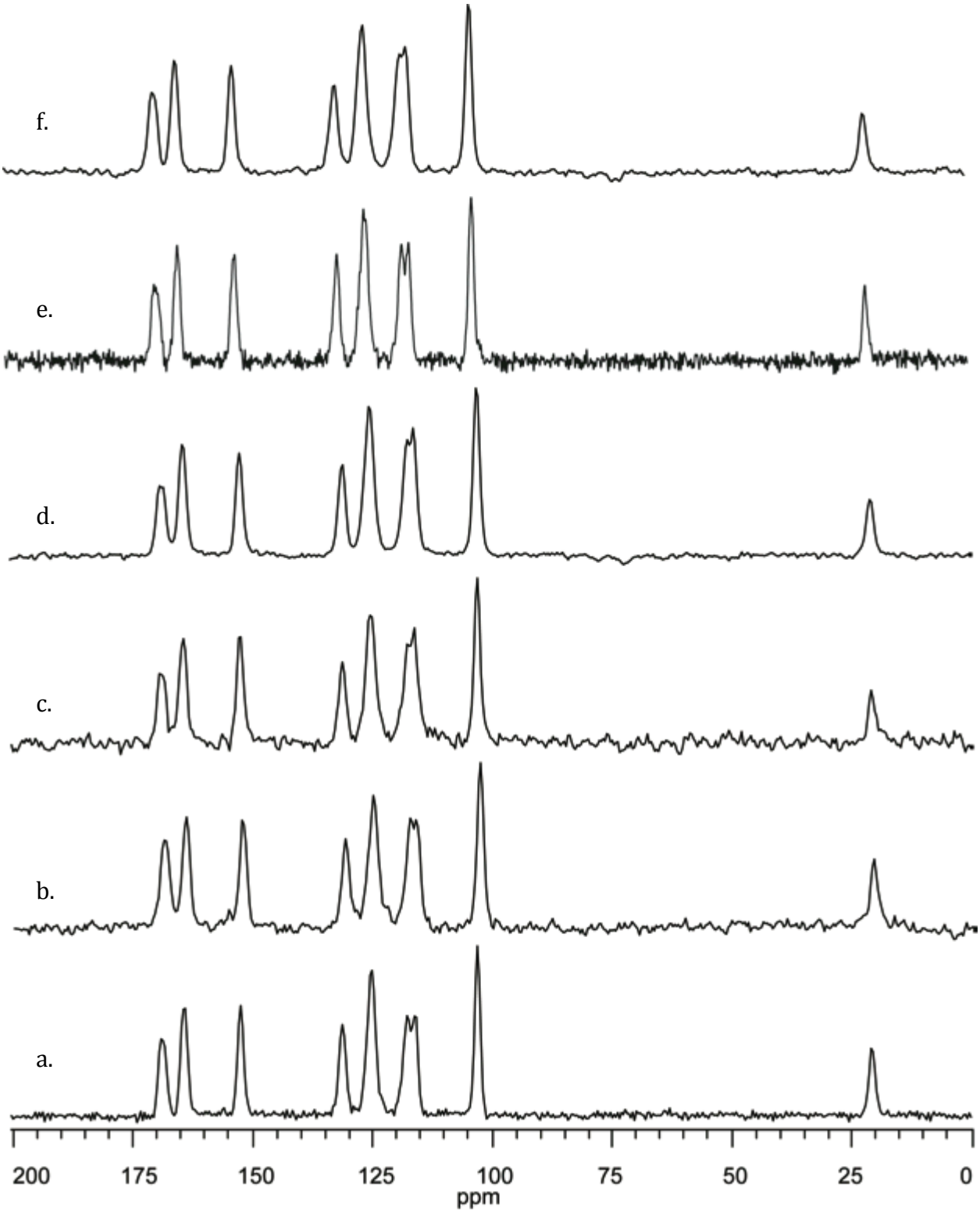

Figure 4.12 ^{13}C SSNMR spectra of **a.** as-received dicumarol, **b.** Lot A, **c.** Lot B, **d.** Lot C, **e.** Lot D, **f.** Lot E

4.4 Conclusions

Salicylic acid and dicumarol were chosen as model compounds for the rest of this study based on the fact that they both have long ^{1}H T_1 times, 3900 s and 1500s, respectively, that decreased upon grinding. Sieving was used to prepare crystalline particles of salicylic acid greater than 100 μm. Anti-solvent precipitation of dicumarol from a DMSO solution into water generated crystalline particles in the micrometer and nanometer size ranges. The materials prepared and characterized here were used in order to investigate the correlation between particle size and ^{1}H T_1 relaxation time as described in the next chapter.

4.5 References

1. Lubach JW. 2007. Applications of nuclear magnetic resonance spectroscopy to pharmaceutical solids. ed., United States -- Kansas: University of Kansas. p 376.

2. Lubach JW, Xu D, Segmuller BE, Munson EJ 2007. Investigation of the effects of pharmaceutical processing upon solid-state NMR relaxation times and implications to solid-state formulation stability. Journal of Pharmaceutical Sciences 96(4):777-787.

3. Kesisoglou F, Panmai S, Wu Y 2007. Nanosizing -- Oral formulation development and biopharmaceutical evaluation. Advanced Drug Delivery Reviews 59(7):631-644.

4. Verma S, Gokhale R, Burgess DJ 2009. A comparative study of top-down and bottom-up approaches for the preparation of micro/nanosuspensions. International Journal of Pharmaceutics 380(1-2):216-222.

5. Ain-Ai A, Gupta PK 2008. Effect of arginine hydrochloride and hydroxypropyl cellulose as stabilizers on the physical stability of high drug loading nanosuspensions of a poorly soluble compound. International Journal of Pharmaceutics 351(1-2):282-288.

6. Shekunov B, Chattopadhyay P, Seitzinger J, Huff R 2006. Nanoparticles of Poorly Water-Soluble Drugs Prepared by Supercritical Fluid Extraction of Emulsions. Pharmaceutical Research 23(1):196-204.

7. Abdelwahed W, Degobert G, Stainmesse S, Fessi H 2006. Freeze-drying of nanoparticles: Formulation, process and storage considerations. Advanced Drug Delivery Reviews 58(15):1688-1713.

8. Dong Y, Ng WK, Shen S, Kim S, Tan RBH 2009. Preparation and characterization of spironolactone nanoparticles by antisolvent precipitation. International Journal of Pharmaceutics 375(1-2):84-88.

9. Barich DH, Gorman EM, Zell MT, Munson EJ 2006. 3-Methylglutaric acid as a 13C solid-state NMR standard. Solid State Nuclear Magnetic Resonance 30(3-4):125-129.

10. Pines A 1973. Proton-enhanced NMR of dilute spins in solids. J Chem Phys 59(2):569.

11. Pines A, Gibby MG, Waugh JS 1972. Proton-enhanced nuclear induction spectroscopy 13C chemical shielding anisotropy in some organic solids. Chemical Physics Letters 15(3):373-376.

12. Andrew ER, Bradbury A, Eades RG 1959. Removal of Dipolar Broadening of Nuclear Magnetic Resonance Spectra of Solids by Specimen Rotation. Nature 183(4678):1802-1803.

13. Lowe IJ 1959. Free Induction Decays of Rotating Solids. Physical Review Letters 2(7):285-287.

14. Dixon WT, Schaefer J, Sefcik MD, Stejskal EO, McKay RA 1982. Total suppression of sidebands in CPMAS C-13 NMR. Journal of Magnetic Resonance (1969) 49(2):341-345.

15. Sussich F, Cesàro A 2000. Transitions and Phenomenology of α,α-trehalose Polymorphs Inter-conversion. Journal of Thermal Analysis and Calorimetry 62(3):757-768.

16. Van Dooren AA, Müller BW 1982. Effects of heating rate and particle size on temperatures and specific enthalpies in quantitative differential scanning calorimetry. Thermochimica Acta 54(1–2):115-129.

17. Wildfong PLD, Hancock BC, Moore MD, Morris KR 2006. Towards an understanding of the structurally based potential for mechanically activated disordering of small molecule organic crystals. Journal of Pharmaceutical Sciences 95(12):2645-2656.

18. Yu L 2001. Amorphous pharmaceutical solids: preparation, characterization and stabilization. Advanced Drug Delivery Reviews 48(1):27-42.

19. Den Brok MWJ, Nuijen B, Lutz C, Opitz H-G, Beijnen JH 2005. Pharmaceutical development of a lyophilised dosage form for the investigational anticancer agent Imexon using dimethyl sulfoxide as solubilising and stabilising agent. Journal of Pharmaceutical Sciences 94(5):1101-1114.

20. Havemeyer RN 1966. Freezing point curve of dimethyl sulfoxide—water solutions. Journal of Pharmaceutical Sciences 55(8):851-853.

Chapter 5

Investigation of the relationship between crystallite size and proton spin-lattice relaxation (^{1}H T_1) times of salicylic acid and dicumarol

5.1 Introduction

In this chapter, the correlation between the size of crystalline particles of salicylic acid and dicumarol and their proton spin-lattice relaxation (^{1}H T_1) times was investigated. The theoretical relationship between the two parameters is first discussed, followed by the characterization of the particle size and ^{1}H T_1 times of the materials. Finally, the relationship between the two parameters in the model systems was compared to the theoretical model. The samples whose ^{1}H T_1 times measurements and particle size characterization are presented in this chapter were prepared as described in the previous chapter. Their physical state characterization was also described in the previous chapter.

5.2 Materials and Methods

5.2.1 Sample preparation

The preparation of both dicumarol and salicylic acid samples by anti-solvent precipitation, sieving and spray-drying were presented in Chapter 4 in §4.2.2.

5.2.1 Sample characterization

Laser diffraction. Laser diffraction measurements were performed by Dr. Joseph Lubach at Genentech. A Malvern 2000 Mastersizer was used. The powders were suspended in hexane and sonicated for 2 min in the measuring chamber before each measurement. The refractive index of dicumarol was calculated using the ACD Labs software.

Scanning electron microscopy (SEM). The samples were mounted on an SEM stage line with carbon tape, and coated with approximately 30 nm of gold or 15 nm of a gold-palladium mixture. The samples were imaged on a Hitachi-S3200-N scanning electron microscope (Hitachi High

Technologies America, Inc., Schaumburg, IL). The size of the particles imaged by SEM was estimated using a ruler and the scale of the images.

Solid-State NMR spectroscopy. All the samples were packed under ambient conditions in 7 mm zirconia rotors (Revolution NMR, Fort Collins, CO). ^{13}C SSNMR spectra were collected using either a Chemagnetics CMX300 (Varian, Palo Alto, CA) or a Tecmag Apollo (Tecmag, Inc., Houston, TX) spectrometer both operating at a ^{13}C frequency of ~75 MHz. 3-methylglutaric acid was used as an external standard, with the methyl peak referenced at 18.84 ppm [1]. ^{1}H T_1 relaxation times were measured by saturation recovery. All spectra were acquired using cross-polarization and magic angle spinning (CP/MAS)[2-4]. The magic angle spinning frequency was 4 kHz. A SPINAL-64 decoupling pulse sequence with total sideband suppression (TOSS) was used [5]. A contact time of 1 ms was used and a ^{1}H decoupling field of 70-80 kHz were used. The number of acquisition points was 1024 for both dicumarol and salicylic acid.

5.3 Results and Discussion

5.3.1 Particle size-proton spin-lattice relaxation (^{1}H T_1) time correlation--theory

In Chapter 3, the relationship between spin-lattice relaxation times and spin diffusion of nuclear magnetization was described. As shown previously, spin diffusion is the mechanism through which nuclear magnetization is transferred through the sample to reach relaxation sinks. The following equation can be written to describe the rate of spin diffusion [6,7]:

$$\langle d^2 \rangle = 6Dt \quad (5.1)$$

where d is the maximum path length of the magnetization, D is the spin diffusion coefficient and t is the time during which the diffusion process occurs. The distance d in Equation 5.1 can also

be described as the maximum distance from the source of magnetization to the relaxation sink (Figure 5.1). The relationship described in Equation 5.1 has been employed to measure domain sizes up to 200 nm of polymers in blends of different polymers. In those systems, the magnetization is traveling from one polymer in the blend to the other, where the latter constitutes the relaxation sink. In rigid systems with long proton spin-lattice relaxation (^{1}H T_1) times (> 10s), the time t in Equation 5.1 would correspond to the spin-lattice relaxation time [8,9]. Dicumarol and salicylic acid are such systems with relaxation times of 1500 s and 3900 s, respectively. In samples containing crystalline particles of only pure dicumarol or salicylic acid, the relaxation sink is expected to be the surface of the particles, and therefore the distance d in equation 5.1 would correspond to the size of the particles, and smaller particles would be expected to have shorter ^{1}H T_1 times (Figure 5.1). Assuming a diffusion coefficient of 0.2 nm^2/ms, which is the value that is expected for rigid polymers and should be applicable to rigid crystalline organic compounds, a log-log plot of the square root of the ^{1}H T_1 time versus the size of the particles can be constructed using Equation 5.1 (Figure 5.2) [6]. In such a plot, the slope describing the correlation between ^{1}H T_1 time and particle size is 1 and the y-intercept is 1.46. The following equations describe the mathematics involved to arrive to that conclusion.

$$\langle d^2 \rangle = 6D(^1\text{H } T_1)$$

$$(^1\text{H } T_1) = \langle d^2 \rangle / 6D$$

$$(\sqrt{}^1\text{H } T_1) = d / \sqrt{(6D)}$$

$$\text{Log } (\sqrt{}^1\text{H } T_1) = \log d - \log (\sqrt{6D}) \quad (5.2)$$

The implication of this slope and y-intercept is that single crystal, or crystallite, sizes of approximately 100 nm would have a ^{1}H T_1 time of approximately 8 s. Particle sizes of 1 μm are

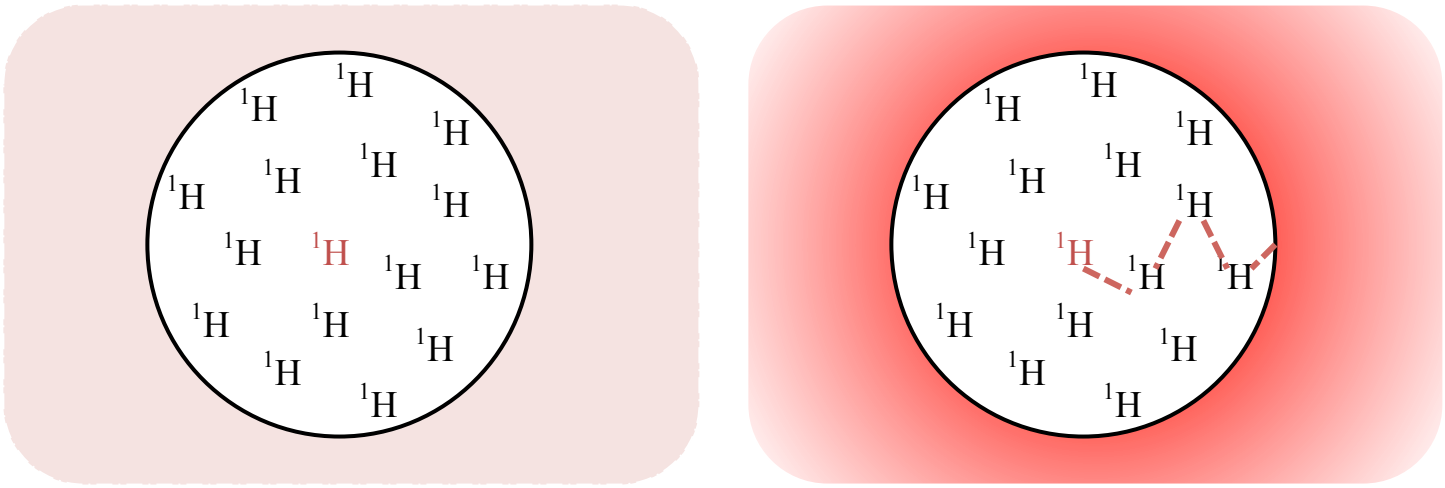

Figure 5.1 Schematics depicting spin-diffusion as a spin-lattice relaxation mechanism inside a crystalline particle. The nucleus in red is an excited nucleus carrying excess magnetization. That excess magnetization is being carried to a relaxation sink via proton-hopping mechanism or spin-diffusion (red dashes). For larger particles (a) the distance d from the source to the relaxation sink is longer than it is for smaller particles (b)

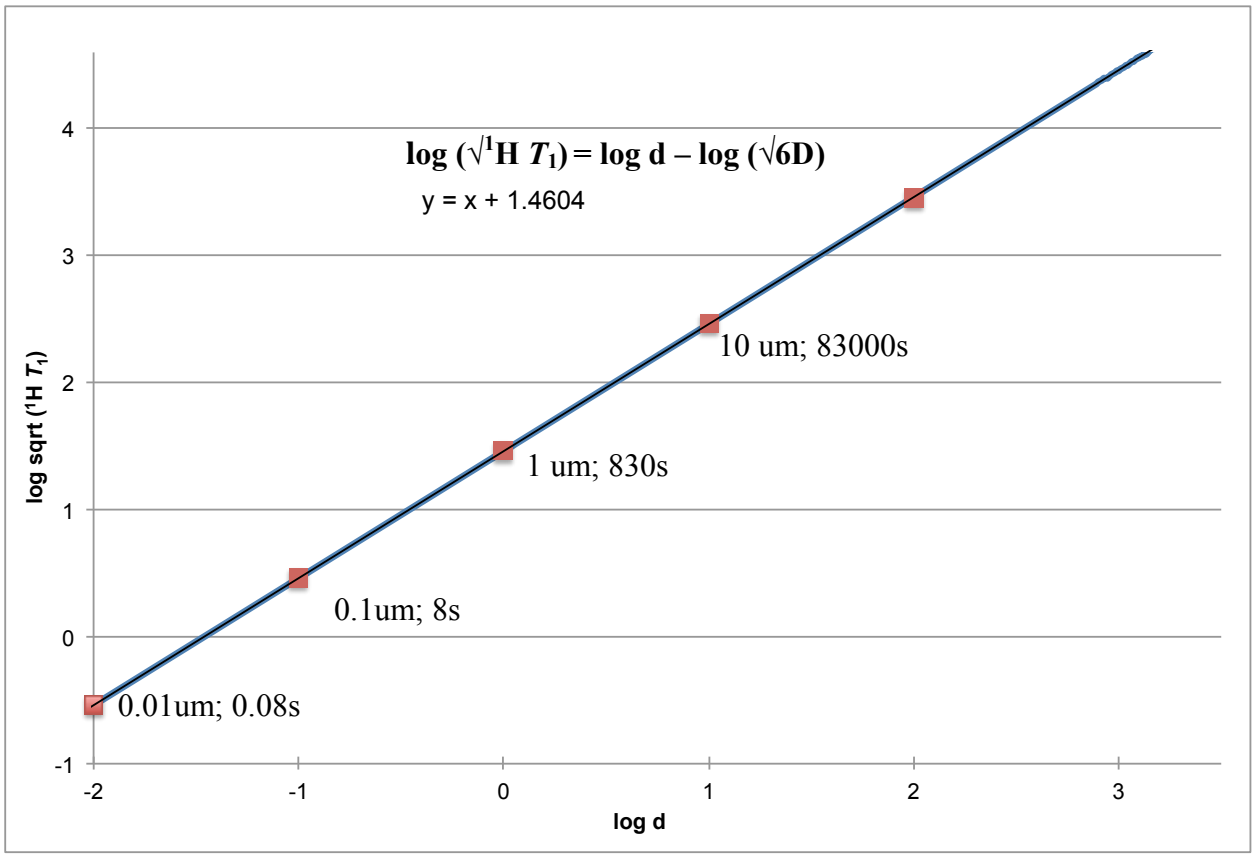

Figure 5.2 Theoretical log-log plot of $\sqrt{}^{1}H$ T_1 vs particle size, assuming a diffusion coefficient D of 0.2 nm^2/ms

expected to have a ^{1}H T_1 time of 830 s and particles of 10 μm in size would have a ^{1}H T_1 time of 83000 s. Since to the best of our knowledge no crystalline organic compound has ever been observed to have a ^{1}H T_1 time of 83000 s, it is likely that this correlation does not hold for particle sizes greater than 10 μm. In the next sections, the results obtained with salicylic acid and dicumarol and the way that they differ from the above-described model will be presented.

5.3.2 Particle size characterization of precipitated dicumarol using SEM and laser diffraction

SEM images of the five lots of precipitated dicumarol samples prepared as described in Table 5.1 are presented in Figure 5.3. Using the scale on the images, the approximate size of the particles in the materials was calculated and the results are summarized in Table 5.3. The size of the majority of the particles in the precipitated materials as estimated by SEM ranges from 0.5 to 1 μm. However, larger particles estimated to be 2 μm and 8 μm can be seen in the micrographs of lot C and lot D. The as-received dicumarol particles measure approximately 50 μm. The size of the particles in Lot B could not be estimated as well as the size of the particles in the other samples due to the poor resolution of the SEM micrograph, however it is obvious that the particles measure less than 5 μm. The poor resolution could be due to a non-uniform coating of the material before SEM analysis.

Laser diffraction data for all the samples are also presented in Table 5.3. As discussed in Chapter 2, the d 0.1, d 0.5 and d 0.9 values represent the size below which 10 %, 50 % and 90 % of the sample lies (by volume), respectively. The d 0.5 values range from about 3 μm to approximately 5 μm for the precipitated materials. The laser diffraction particle size values are significantly larger than the ones obtained from SEM. One possible reason for the lack of agreement between the two techniques is that laser diffraction analysis actually measured the

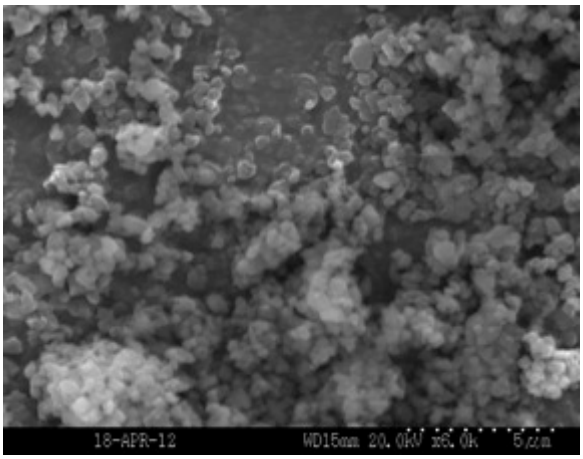

Lot A

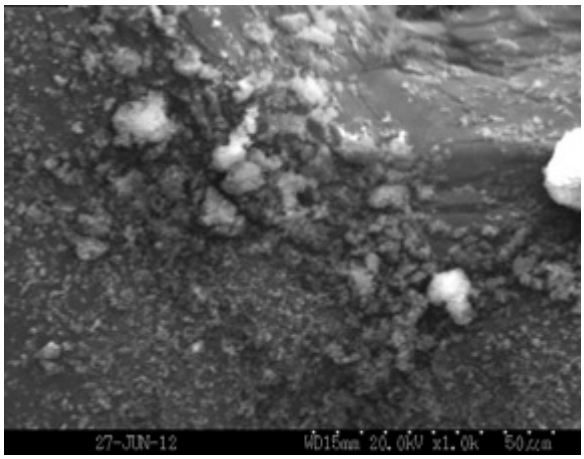

Lot B

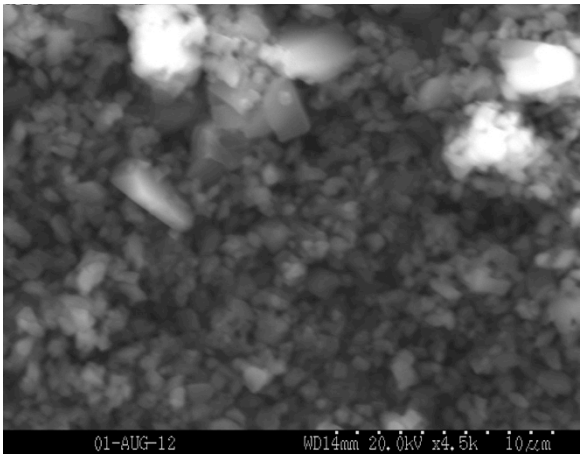

Lot C

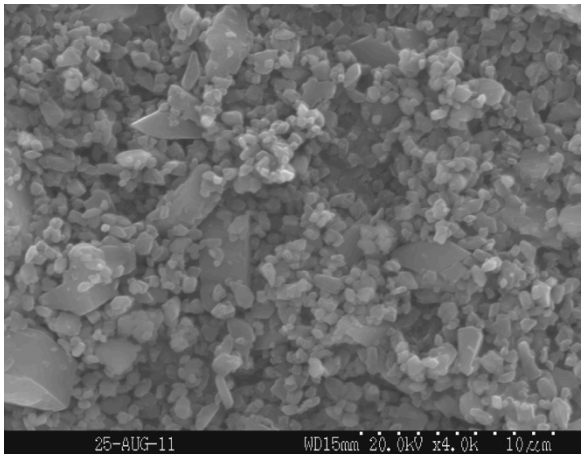

Lot D

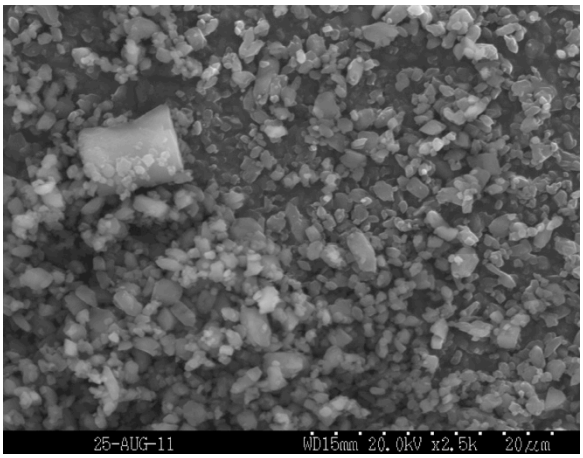

Lot E

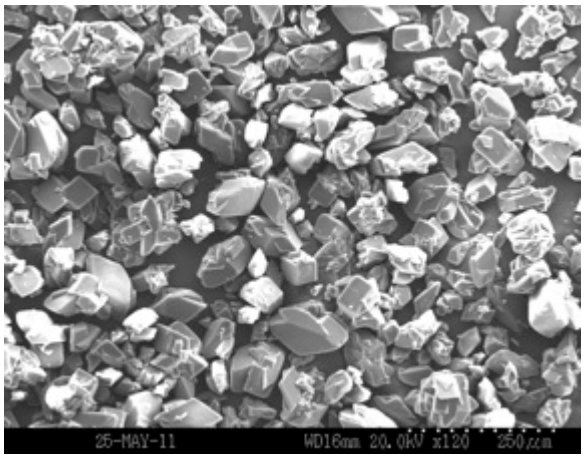

As-received

Figure 5.3 SEM images of as-received and precipitated dicumarol denoted Lots A through E

Table 5.3 Mean particle sizes of as-received and precipitated dicumarol obtained by SEM and laser diffraction

	SEM	Laser Diffraction		
		d 0.1	**d 0.5**	**d 0.9**
Lot A	0.5 μm	1.6 μm	4.9 μm	18.0 μm
Lot B	N/A	0.9 μm	4.8 μm	19.0 μm
Lot C	2 μm 0.5 μm	0.9 μm	2.8 μm	20.0 μm
Lot D	0.7 μm 8 μm	1.2 μm	3.8 μm	16.5 μm
Lot E	1 μm	1.0 μm	3.3 μm	13.3 μm
As-received	50 μm	10.9 μm	23.8 μm	43.3 μm

size of the agglomerates rather than the size of the individual particles. As seen in the SEM micrographs (Figure 5.3), most of the dicumarol particles in the precipitated samples are agglomerated. That is likely due to the fact that no surfactant was used during precipitation. All of the materials were sonicated for 2 min before laser diffraction measurements; however, it is possible that this step did not break down all of the agglomerates. Another possible reason for the discrepancy in particle size measurements between laser diffraction and SEM is the non-uniformity in particle size distribution of the samples. As already mentioned, two of the precipitated lots (lots C and D) contain particles both larger and smaller than 1 μm. The presence of both big and small particles in a sample is known to skew the results of laser diffraction measurements and this is illustrated by the obvious disagreement between the particle size distribution of lots C and D and the d 0.5 values (Figure 5.4) [10]. Both materials present a bimodal size distribution with the smaller range of particle sizes constituting the majority of the sample, and therefore cannot be accurately represented with just one particle size. Since the results obtained by laser diffraction did not accurately reflect the size of the particles of dicumarol, SEM was the only particle sizing technique used henceforth.

5.3.3 Particle size characterization of salicylic acid samples

Samples of salicylic acid were prepared using spray-drying and particles of saclicylic acid were separated sieving. The particles generated by spray-drying were smaller than the ones obtained by sieving, and as a result, the samples prepared required analysis by SEM. SEM micrographs of the spray-dried salicylic acid samples are shown in Figure 5.5. The particles have an irregular morphology, which makes it difficult to accurately estimate their size. Nonetheless they can be estimated at 5 μm for the smaller particles and 20 μm for the larger ones.The sieved particles of salicylic acid ranged from less than 125 μm to larger than 850 μm in size as shown in

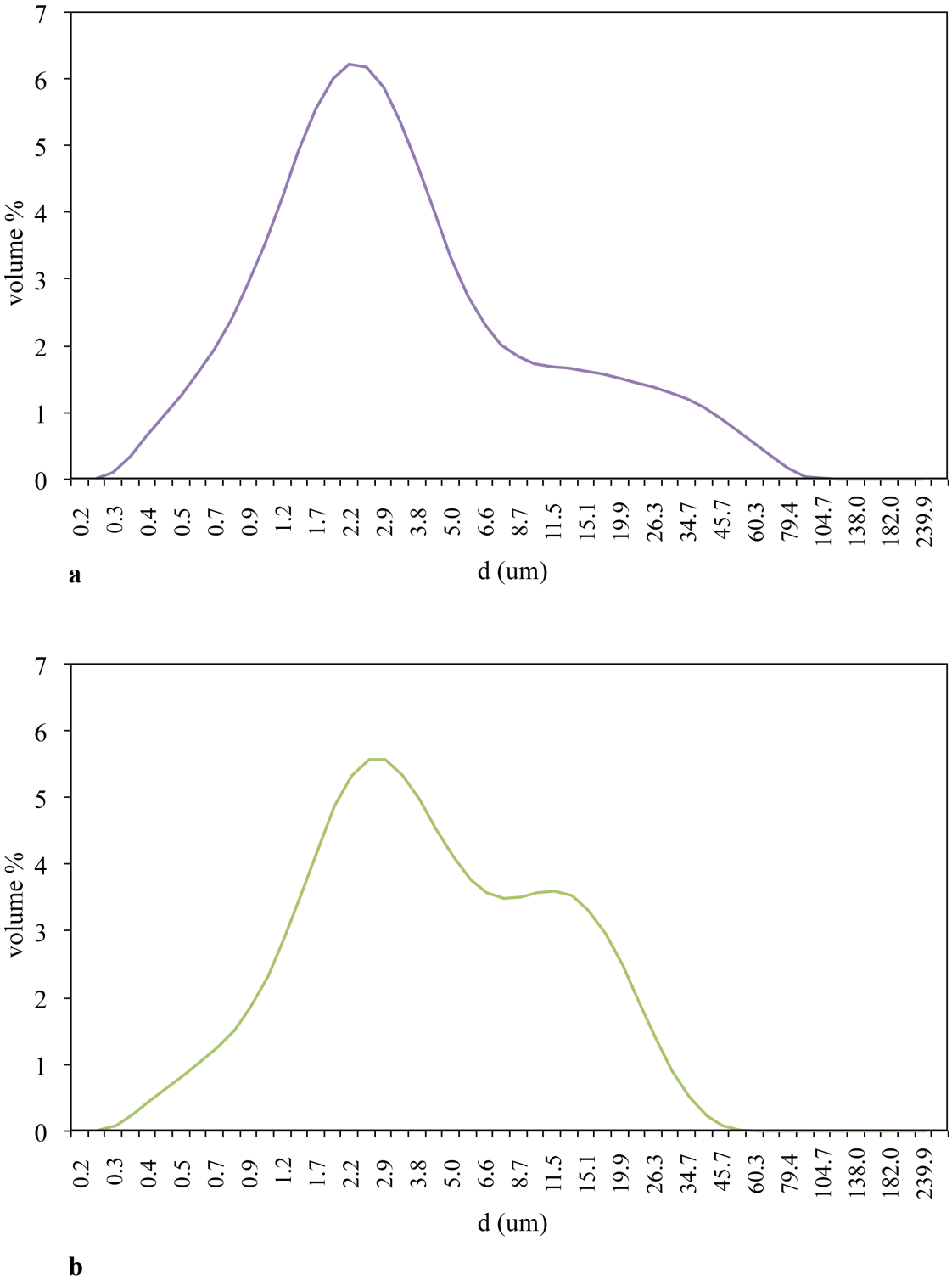

Figure 5.4 Laser diffraction curves of two samples of precipitated dicumarol: **a.** Lot C; **b**. Lot D

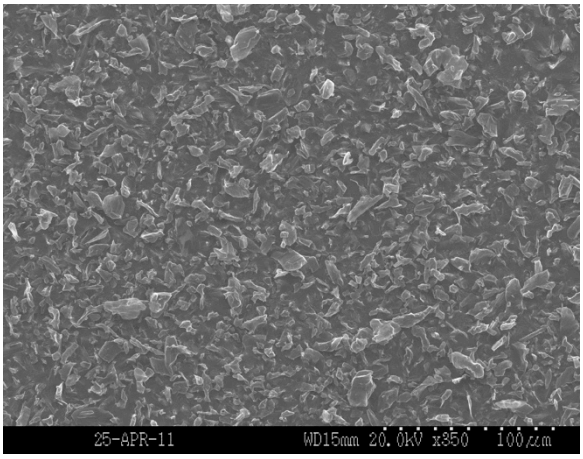

1.

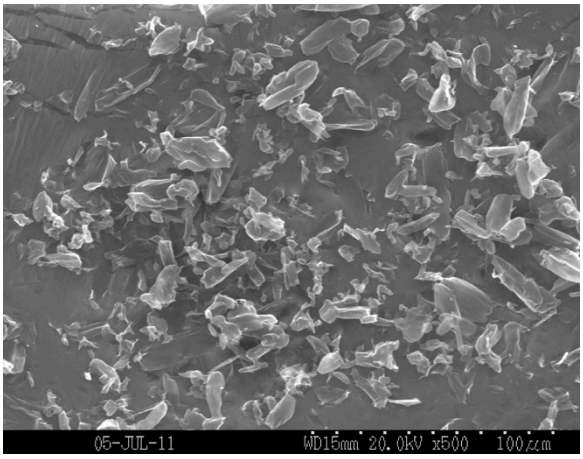

2.

Figure 5.5 SEM micrographs of spray-dried salicylic acid. The numbers below the pictures indicate samples (1) and (2) of spray dried salicylic acid

Table 5.4 Sieved salicylic acid fractions. The median of each sieved fraction was obtained and used to construct the plot presented in Figure 5.6

Sieved samples	Median
75-125 µm	100 µm
125-300 µm	212.5 µm
180-300 µm	240 µm
300-425 µm	362.5 µm
425-600 µm	512.5 µm
600-710 µm	655 µm
> 850 µm	850 µm

Table 5.4. The size of the particles obtained was limited both by the mesh sizes available and the size of the particles in the starting material.

5.3.4 ^1H T_1 times of dicumarol and salicylic acid materials

The ^{1}H T_1 times of precipitated lots A-E of dicumarol were measured and are summarized in Table 5.5. The ^{1}H T_1 times of all the samples prepared by precipitation are shorter than the ^{1}H T_1 time of as-received dicumarol (1500 s), which is consistent with the expectation that the ^{1}H T_1 time of crystalline materials decreases with particle size. More specifically, the ^{1}H T_1 times of the precipitated samples range from 16 s to 520 s. Two samples, lots C and D, had two distinct ^{1}H T_1 times. That is because the relaxation of these materials is not uniform; instead, two relaxation profiles are present and they are each characterized by a distinct ^{1}H T_1 time. It is important to note that these two samples were also the one whose particle size distribution was bimodal as shown by laser diffraction; the detection of two ^{1}H T_1 times is consistent with this distribution.

The ^{1}H T_1 times of the sieved fractions of as-received and spray-dried salicylic acid samples were measured and are summarized in Tables 5.6 and 5.7. The ^{1}H T_1 time of salicylic acid mostly increased as the size of the sieve fraction increased. The ^{1}H T_1 time of the largest fraction (> 850 μm) is 6100 s while the ^{1}H T_1 time of the smallest fraction (75-125 μm) is 3300 s. Two ^{1}H T_1 times were detected for each of the spray-dried materials: for the first spray-dried sample ^{1}H T_1 times of 1000 s and 65 s were measured, and for the other one the values obtained were 620 s and 100 s.

Table 5.5 ^{1}H T_1 times of dicumarol- The percentages in parenthesis after the relaxation time represent the amount of material having that relaxation time in the sample. For Lots C and D the longer ^{1}H T_1 value detected was assigned to the larger particle size present in the material. This was done based on the assumption that ^{1}H T_1 time decreases with particle size.

	size (SEM)	**^{1}H T_1**	**$\sqrt{}$^{1}H T_1**
Lot A	0.5 μm	20 s ± 2	4.5
Lot B	N/A	20 s ± 3	4.5
Lot C	0.5 μm 2 μm	16 s ± 3 (40 %) 68 s ± 8 (60 %)	4.0 8.2
Lot D	0.7 μm 8 μm	49 s ± 6 (76 %) 520 s ± 280 (24 %)	7.0 22.8
Lot E	1 μm	80 s ± 7	8.9
As-received	50 μm	1500 s	38.7

Table 5.6 ^{1}H T_1 times of sieved salicylic acid. The errors indicated are the errors of the fit

Sieved samples	**^{1}H T_1 (s)**	**$\sqrt{}^{1}$H T_1**
75-125 µm	3300s ± 430	57.4
125-300 µm	3900s ± 270	62.4
180-300 µm	4000s ± 300	63.2
300-425 µm	3700s ± 300	60.8
425-600 µm	5300s ± 510	72.8
600-710 µm	5900s ± 400	76.8
> 850 µm	6100s ± 550	78.1

Table 5.7. ^{1}H T_1 times of spray-dried salicylic acid. The percentages in parenthesis after the relaxation time represent the amount of material having that relaxation time.

	Size (SEM)	**^{1}H T_1**
1	20 μm 5 μm	620 ± 51s (69%) 65 ± 10 s (31%)
2	20 μm 5 μm	1000 ± 250s (70%) 100 ± 38 s (30%)

5.3.5 ^1H T_1 times- particle size correlation—salicylic acid

Figure 5.6 shows a log-log plot of the square root of the ^{1}H T_1 times of the salicylic acid samples versus the size of the particles and includes both the spray-dried and the sieved samples. The median size of the sieve fraction was used for plotting the sieved salicylic acid samples except for the greater than 850 μm fraction. From the shape of the plot it is difficult to determine the kind of correlation that exists between the ^{1}H T_1 times and the particle size. It appears to be a two-regime linear relationship, and indeed each set of data can be described by a linear trend line. The slope and the y-intercept of the trend line describing this correlation are 0.14 and 1.5 for the sieved salicylic acid, and 0.82 and 0.38 for the spray-dried samples, respectively. Because the plot of the spray-dried salicylic acid contains only two samples, these samples will not be included in the remainder of the discussion, although the results are consistent with later conclusions drawn in this chapter.

5.3.6 ^1H T_1 times- particle size correlation—dicumarol

Figure 5.7 is a log-log plot of the square root of the ^{1}H T_1 times of dicumarol versus the size of the particles. Because the results obtained from laser diffraction were not believed to accurately represent the size of the particles in the dicumarol materials, the particle size obtained by SEM were used to construct the plot. The dicumarol plot was constructed using both the precipitated samples and the as-received material. For the two lots that presented two ^{1}H T_1 times, the larger particles seen in the SEM micrographs were assigned to the longer ^{1}H T_1 time and the smaller ones to the shorter ^{1}H T_1 time. The data can be described with a linear trend line whose slope is 0.46 and y-intercept is 0.87.

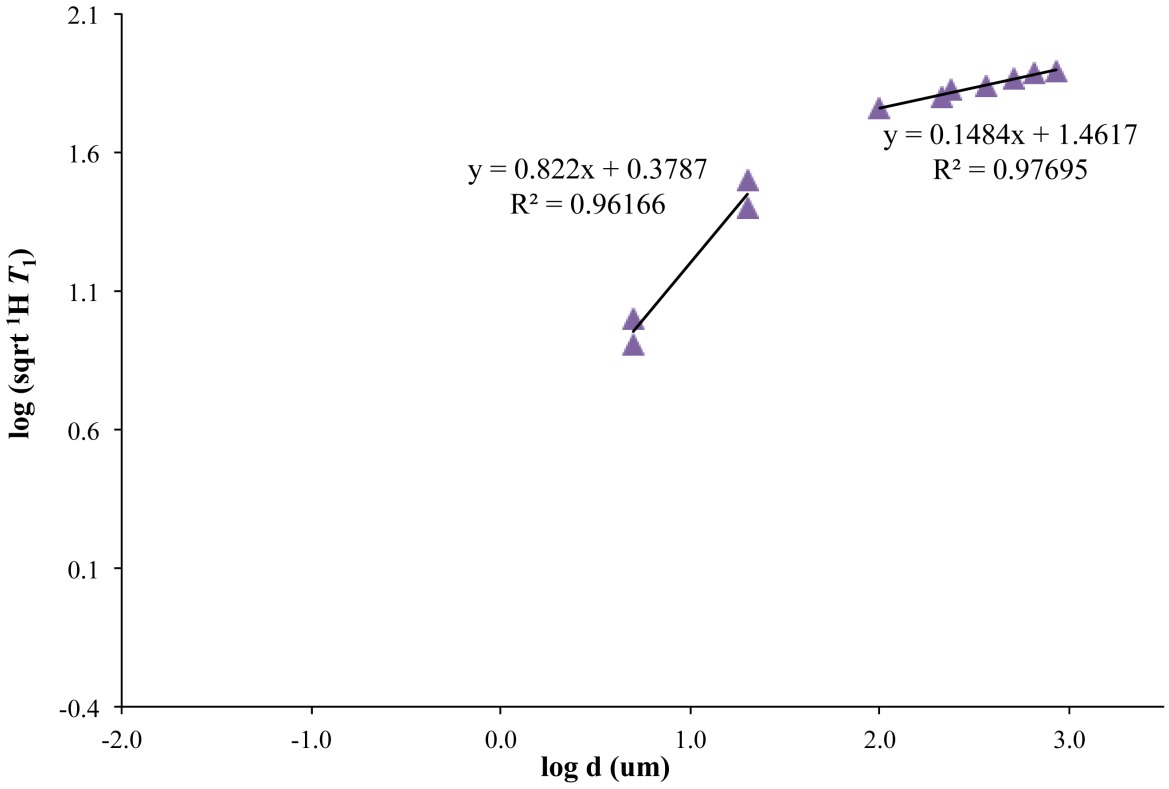

Figure 5.6. Log-log plot of the square root of the ^{1}H T_1 time of salicylic acid versus the size of the particles

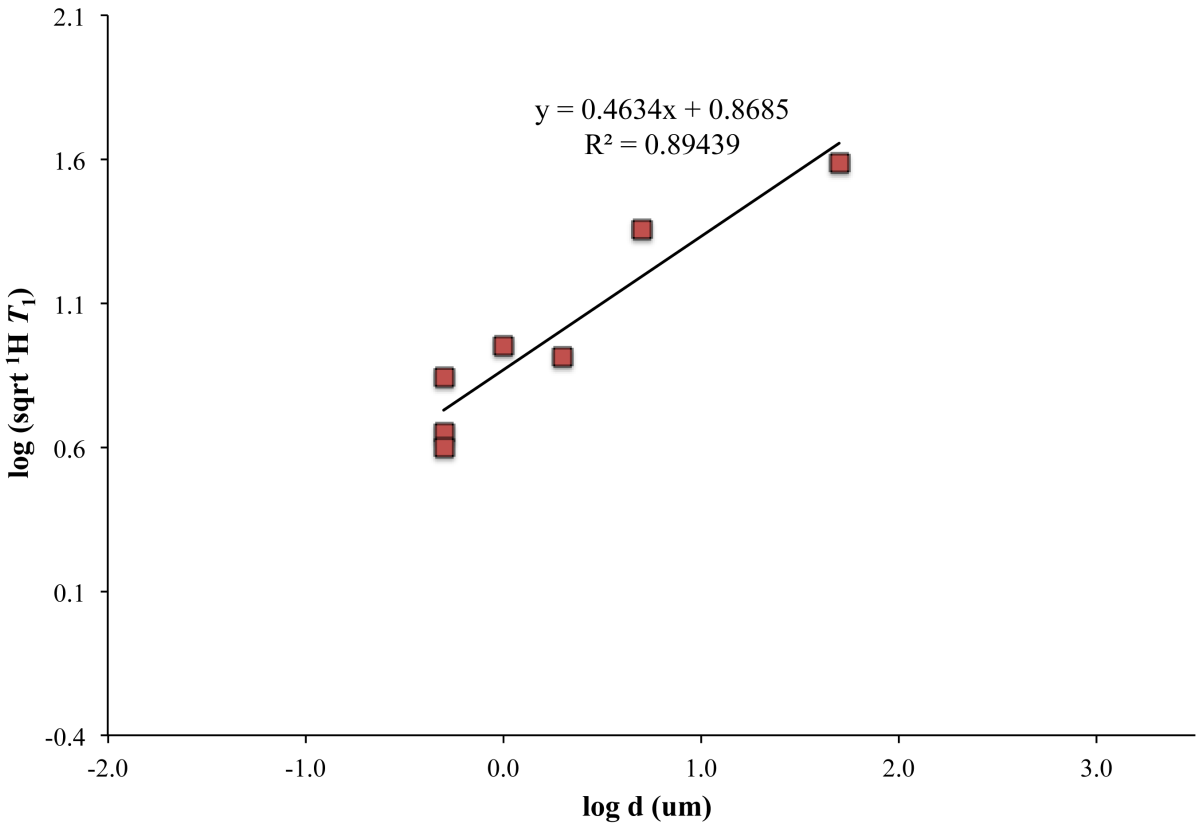

Figure 5.7 Log-log plot of the square root of the ^{1}H T_1 time of dicumarol versus the size of the particles

5.3.7 Comparison between theoretical model and experimental results of dicumarol and salicylic acid

In order to visualize how the results obtained with our samples compare with the theory, a log-log plot of the square root of the ^{1}H T_1 time versus particle size that includes the theory and our data was constructed (Figure 5.8). The experimental data are below the theoretical description of the spin diffusion, indicating that the relaxation times of our samples are shorter than predicted by the theory. In addition, the slopes of the data are also different from each other and from the theoretical slope of 1: for dicumarol, the slope of the line is close to 0.5, and for sieved salicylic acid the slope is close to 0.15. This means that for our model compounds, the ^{1}H T_1 times increase more slowly with the size of the particles than predicted by the model.

We suspect that in the dicumarol and salicylic acid particles, relaxation sinks other than the surface of the crystals exist. These relaxation sinks may be crystal defects such as grain boundaries or line defects [11]. As the spin diffusion process occurs, the diffusing magnetization will begin to interact with these defect sites before it reaches the surface; this leads to a faster relaxation rate and shorter relaxation time than predicted. In dicumarol, the density of the relaxation sinks is not believed to be very high, and the resulting spin diffusion rate corresponds to the distance, or particle size, being proportional to relaxation time instead of the square root of relaxation time. If the distance is proportional to the relaxation time instead of the square root of the relaxation time the slope is expected to be 0.5; this is consistent with the dicumarol data that

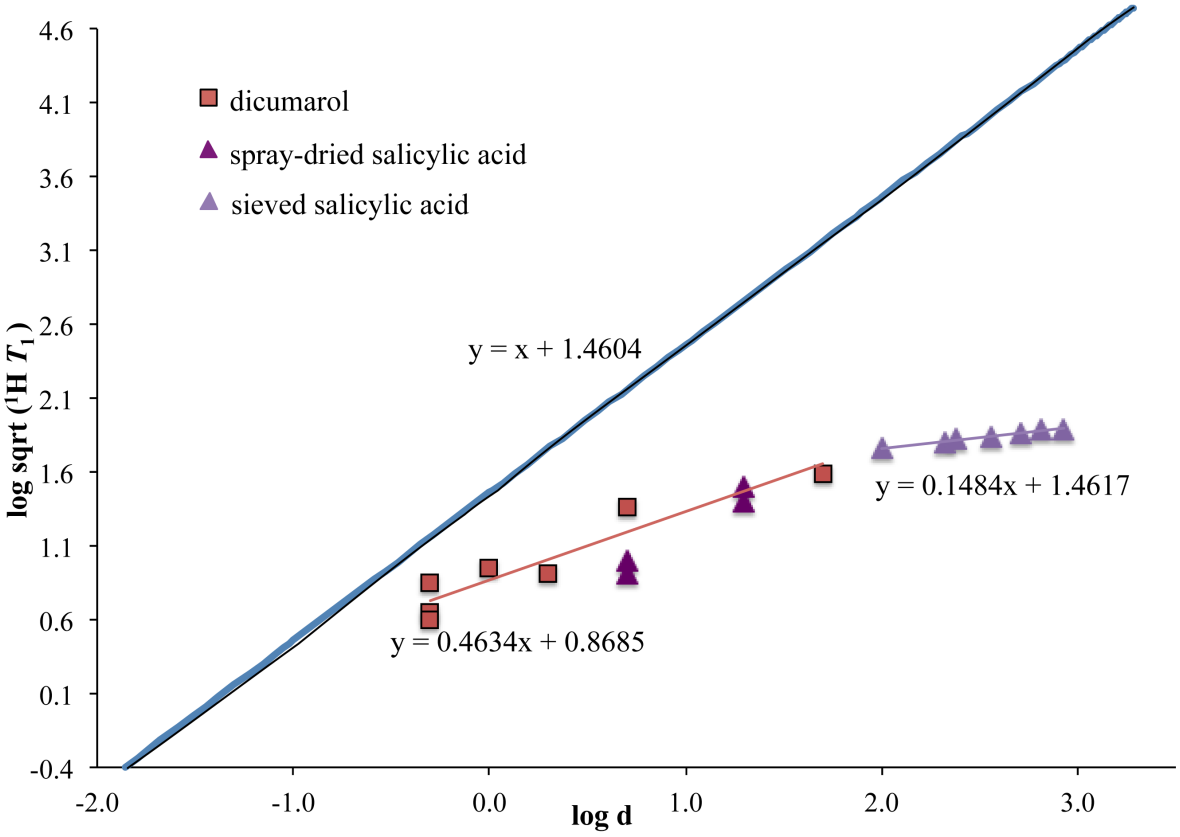

Figure 5.8 Log-log plots of the square root of the ^{1}H T_1 time versus particle size. The spin diffusion-based theoretical line (blue) as well as the dicumarol and salicylic acid data are present on the plot.

have slope of 0.46. In salicylic acid, however, there might be more defects and the distance, or particle size, is closer to being proportional to the cube of the relaxation time; this would correspond to a slope of 0.16. The slope obtained with the salicylic acid data is 0.14.

Considering the difference between our experimental data and the spin-diffusion based theory of the correlation between particle size and ^{1}H T_1 times, it is useful to investigate the possible role of other relaxation mechanisms in dicumarol and salicylic acid that could be responsible for the changes in the ^{1}H T_1 times observed.

5.3.8 Understanding the spin-lattice relaxation of dicumarol and salicylic acid particles

Factors that can cause decreases in ^{1}H T_1 times include the presence of relaxation sinks, such as solvent molecules that are not hydrogen-bonded to the solid molecules or amorphous material. Although increases in temperature can also cause decrease in ^{1}H T_1 times, NMR data for all the as-received and processed samples were obtained under the same conditions; therefore temperature is most likely not the reason for the reduction in ^{1}H T_1 time observed. Moreover, the increase in temperature that occurs as a sample is spun at 4 kHz in the NMR spectrometer was shown to be very small [12]. The physical state characterization of the materials presented in Chapter 4, specifically the DSC data (Figures 4.9, 4.10 and 4.12), revealed that no amorphous material was present in either the salicylic acid or dicumarol materials. Also, thermogravimetric analysis of the materials did not indicate the presence of any significant amount of residual solvent in the samples; lots A and B seemed to have a little more than the other samples of dicumarol (~5-10%), and for these two lots it is possible that water played a small role in the decrease in ^{1}H T_1 time (Figure 5.9).

Crystal defects are also believed to act as relaxation sinks. Therefore high-quality single crystals are anticipated to have significantly longer proton spin-lattice relaxation times than defect-

containing crystals. Salicylic acid was recrystallized from ethanol in order to obtain high quality single crystals and compare their ^{1}H T_1 times to the value obtained for the as- received and sieved samples of salicylic acid. Recrystallization was not performed with dicumarol because it is insoluble in the majority of commonly used organic solvents. The recrystallized crystals of salicylic acid appear to be single crystals under polarized light and have a needle morphology. They measure 500 μm or longer as seen on the SEM images of the particles (Figure 5.10). Compared to the sieved salicylic acid samples, the crystals of salicylic acid obtained by recrystallization from ethanol are more uniformly sized and shaped; they are also larger in size. The ^{1}H T_1 time of the recrystallized sample was best described with two ^{1}H T_1 times: 2700 ± 300 s and 710 ± 50 s versus 4900 s for the larger than 850 μm sieve fraction of salicylic acid. The ^{1}H T_1 times of recrystallized salicylic acid are lower than expected if we argue that crystal quality plays a significant role in the proton spin-lattice relaxation of the material and that higher quality crystals should have a longer ^{1}H T_1 time. It is possible that the needle morphology of the recrystallized salicylic acid has a significant impact on the proton spin-lattice relaxation of the material: if the surface is the only relaxation sink present, the relaxation can reach that sink in both the longer and the shorter dimension of the crystal. Therefore when comparing the size of the crystals, it may be that the smaller dimension of the needles is the most relevant. Unfortunately we were not able to measure the size of the smaller dimension of the particles even by SEM.

In order to further investigate the presence and role of crystal defects on the spin-lattice relaxation of the salicylic acid materials, a surface analysis of the sieved salicylic acid was performed using a BET surface analyzer with the expectation that the presence of defects could potentially increase the surface area of the materials. Table 5.8 summarizes the BET results.

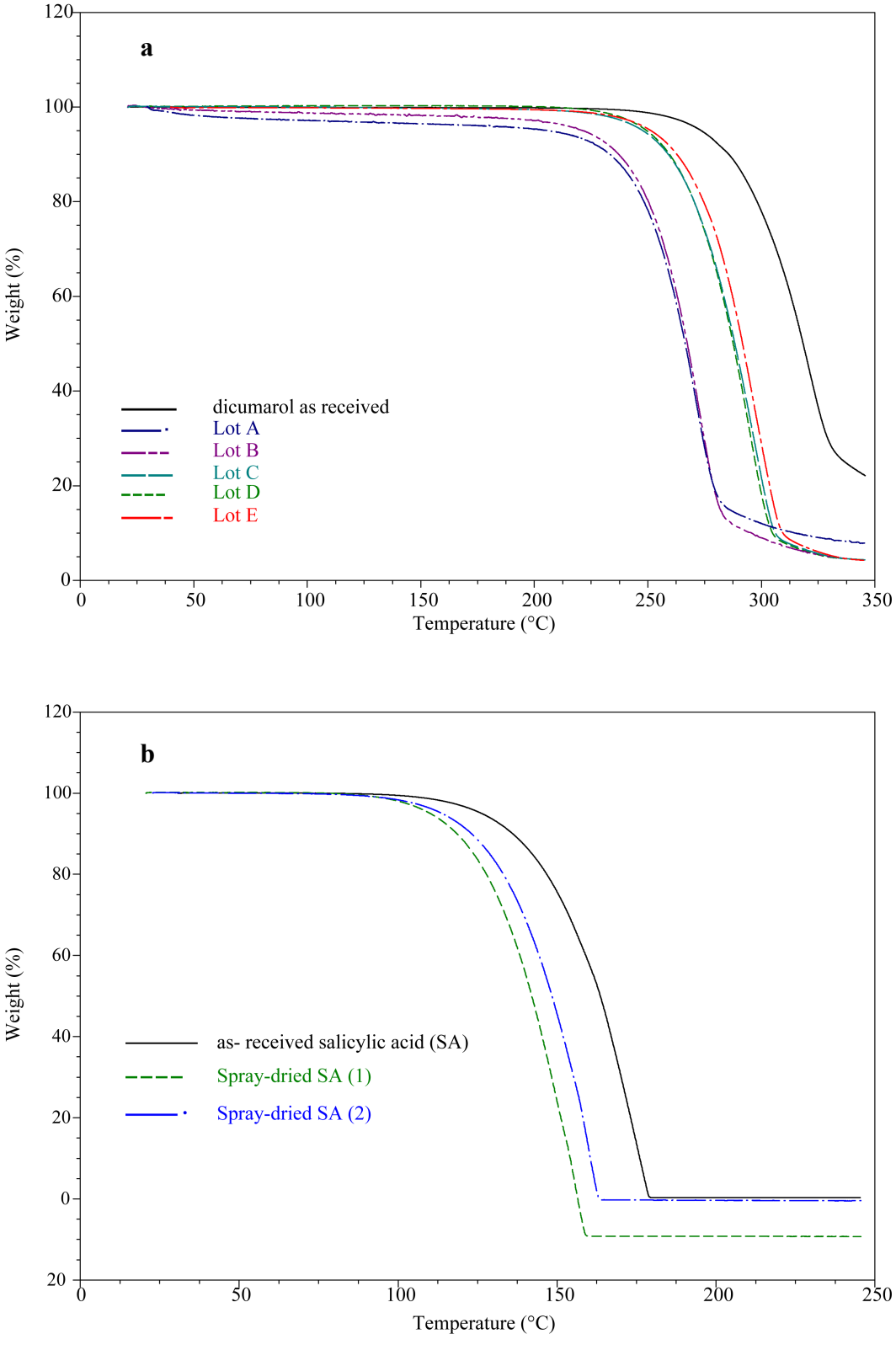

Figure 5.9 Thermogravimetric analysis thermogram of **a.** dicumarol samples, **b.** spray-dried salicylic acid

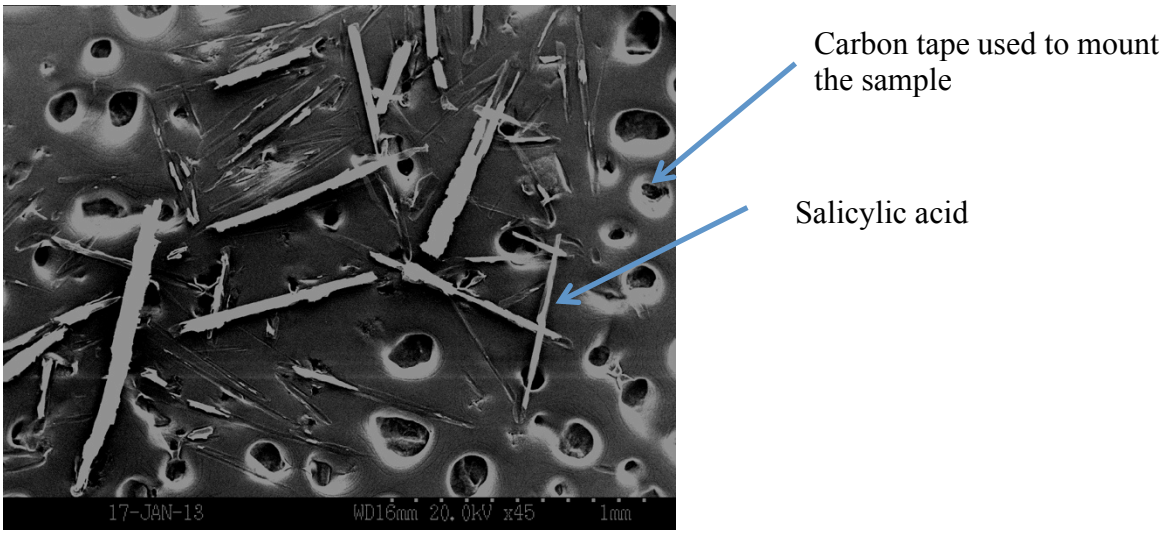

Figure 5.10 SEM of recrystallized salicylic acid

Table 5.8 BET surface analysis results of sieved salicylic acid

Sieved samples	BET surface area
< 125 µm	0.3 ± 0.05 m^2/g
300-425 µm	0.0 ± 0.0 m^2/g
425-600 µm	0.0 ± 0.0 m^2/g
600-850 µm	0.0 ± 0.0 m^2/g
> 850 µm	0.0 ± 0.0 m^2/g

Except for the < 125 μm sieve fraction, the surface area obtained was zero. This might be because of a combination of not enough material being used to perform the measurements and the small surface area of the particles in the larger sieve fractions. This result suggests that if defects are present, they do not cause a significant increase in surface area. There are four different kinds of defects that can exist in crystals: point defects, line defects, planar defects or volume defects [13]. It is possible that point defects are the kind of defects present in the salicylic acid particles. BET analysis was not performed with the precipitated dicumarol materials because of lack of material.

Other possible reasons for the decrease in ^{1}H T_1 time, such as the presence of paramagnetic oxygen, were investigated with dicumarol [14]. Oxygen is believed to act as a surface relaxation mechanism, by behaving as a relaxation sink for the excited spins that are at the surface: once the excess magnetization is carried through the material to the surface by spin diffusion, it is possible that the oxygen then absorbs the excess magnetization and allows the material to relax. However, the ability of oxygen to enhance the spin-lattice relaxation of a solid is limited by the material's internal relaxation mechanisms. In other words, if there are enough internal crystal defects or mobility, then the relaxation time will be unaffected by the presence of surface oxygen. That is the reason why Schieber saw little to no decrease in ^{1}H T_1 time when as-received crystalline aspirin was purged with oxygen [14]. The rate at which the magnetization reaches the surface or other relaxation sinks is dictated by the rigidity of the material and the efficiency of spin diffusion. In order to determine how the level of oxygen affects the spin-lattice relaxation of dicumarol, a rotor packed with as-received dicumarol was purged with pure oxygen and the ^{1}H T_1 time of the material was measured. The ^{1}H T_1 time was the same as as-received dicumarol packed under ambient oxygen conditions. The ^{1}H T_1 time of dicumarol cryoground for

8 min was also measured after the material was purged with oxygen. Under these conditions the ^{1}H T_1 time of the material was the same as under ambient oxygen conditions (8 s). These results suggest that the mechanisms of internal relaxation are dominant when it comes to the spin-lattice relaxation of dicumarol.

Experiments were performed in order to estimate the impact of the spin-diffusion rate on the spin-lattice relaxation of dicumarol and salicylic acid. First the ^{1}H T_1 time of a sample of dicumarol was measured at several magic angle spinning speeds. Because salicylic acid already has such a long ^{1}H T_1 time, spinning speed experiments were performed only using dicumarol. At faster spinning speeds, the dipolar coupling interactions are weaker, and as a result the efficiency of the spin diffusion is expected to decrease and the spin lattice relaxation time would increase [15]. However, it should be noted that at higher spinning speeds the temperature of the sample is expected to be higher, and this could also cause longer spin-lattice relaxation times. Tables 5.9 summarizes the ^{1}H T_1 times of a sample of dicumarol prepared by precipitation obtained using at 4, 8 and 10 kHz magic angle spinning speeds. The material was only packed once and the same rotor was used at all spinning speeds. The ^{1}H T_1 times of the dicumarol sample range from 34 s to 45 s. However, the longer ^{1}H T_1 time, 45 s, was not obtained at the highest spinning speed but at 8 KHz. Nonetheless the ^{1}H T_1 times obtained at 8 and 10 KHz are both longer, by at least 2 s, than the ^{1}H T_1 time obtained when the sample was spun at 4KHz.

Magnetic field strength can also impact the spin-diffusion rate. The ^{1}H T_1 time of a rigid crystalline material is expected to increase a small amount with field strengths because the field strength affects the resonance frequency between two nuclei. This is illustrated in the larger chemical shift differences between nuclei in a sample at higher fields. The ^{1}H T_1 time of a rigid material at 400 MHz is expected to be larger than at 300 MHz [16]. The ^{1}H T_1 times obtained for

Table 5.9 Precipitated dicumarol ^{1}H T_1 times measured at three different magic angle spinning speeds

5 mg/mL dicumarol precipitated	
Spinning speed	**^{1}H T_1**
4 KHz	34 s ± 5
8 KHz	45 s ± 3
10 KHz	37 s ± 5

three fractions of sieved salicylic acid using a 400 MHz spectrometer are slightly longer (1.1-1.2x) than the ones obtained on the 300 MHz spectrometer (Table 5.10). This is consistent with the spin diffusion model, where the relaxation times would be slightly longer at higher fields.

5.3.9 Proposed model

The results obtained with dicumarol and salicylic acid provide guidance as to how other materials will behave. The fact that the spray-dried salicylic acid and precipitated dicumarol samples are approximately the same size range and can be described with a similar slope as seen in Figure 5.8 supports the universality of the data. If we assume that the correlation between ^{1}H T_1 time and particle size displayed by dicumarol and salicylic acid is representative of the ranges occupied by the particles of each materials, we can propose a model that describes the correlation between particle size and ^{1}H T_1 time. The dicumarol line crosses the theoretical line at approximately a particle size of 100 nm, and the salicylic acid line at a particle size of about 74 μm. This suggests that up to 100 nm in size, the particles may follow the theoretical line. At particles 100 nm or greater, the slope of the line changes, indicating the crystal defects may start to increase. The change in slope again at approximately 74 μm indicates that there is a higher propensity for internal relaxation for these materials. As noted earlier the correlation between the ^{1}H T_1 time and the particle size of dicumarol and salicylic acid were thought to approach a linear and a cube correlation respectively. This translates into the following equations, where the y-intercepts obtained with our data were used in this proposed model.

Table 5.10 ^{1}H T_1 times of salicylic acid samples measured on a 300MHz and a 400 MHz spectrometer

Sieved salicylic acid 180-300 µm	
Magnet strength	^{1}H T_1
300 MHz	4000s ± 295
400 MHz	5074s ± 365

Sieved salicylic acid 300-425 µm	
Magnet strength	^{1}H T_1
300 MHz	4220s ± 485
400 MHz	4939s ± 382

$d < 100$ nm; $\log \sqrt{}^1H\ T_1 = \log d + 1.46$

$100\ nm < d < 74\ \mu m$; $\log \sqrt{}^1H\ T_1 = 0.5 \log d + 0.8$

$d > 74\ \mu m$; $\log \sqrt{}^1H\ T_1 = 0.16 \log d + 1.46$

The physical meaning behind these potential correlations is not clear at this point, but is believed to be due to defect density.

Although the spin diffusion theory as only been applied to polymeric systems, its theory is well established and based on the properties of nuclei and of the material (rigidity). As a result although a quadratic of cubic equation could potentially be employed to fit the salicylic acid and dicumarol data, such equation would have no physical meaning. Nonetheless, since the model is only based on two compounds, salicylic acid and dicumarol, investigation of other compounds would be helpful in determining the strength of the model proposed. Figure 5.11 is a plot of the proposed model overlapped with the salicylic acid and dicumarol data.

5.4 Conclusions

A correlation between the size of crystalline particles of dicumarol and salicylic acid and their proton spin-lattice relaxation time ($^1H\ T_1$) was shown to exist; however, it did not follow the theoretical spin diffusion description and as a result a model was proposed.

The potential implications of the findings presented here include the ability to evaluate the particle size distribution of crystalline powders using SSNMR. Significantly different particle sizes would be expected to have different $^1H\ T_1$ times that can be detected within the powders. Moreover, since SSNMR can be used to characterize APIs in the presence of the excipients in a formulation, such evaluation of the polydispersity of powders could be conducted on formulated drug products during drug development. The next chapter presents the characterization of the particle size distribution of crystalline powders of dicumarol by SSNMR.

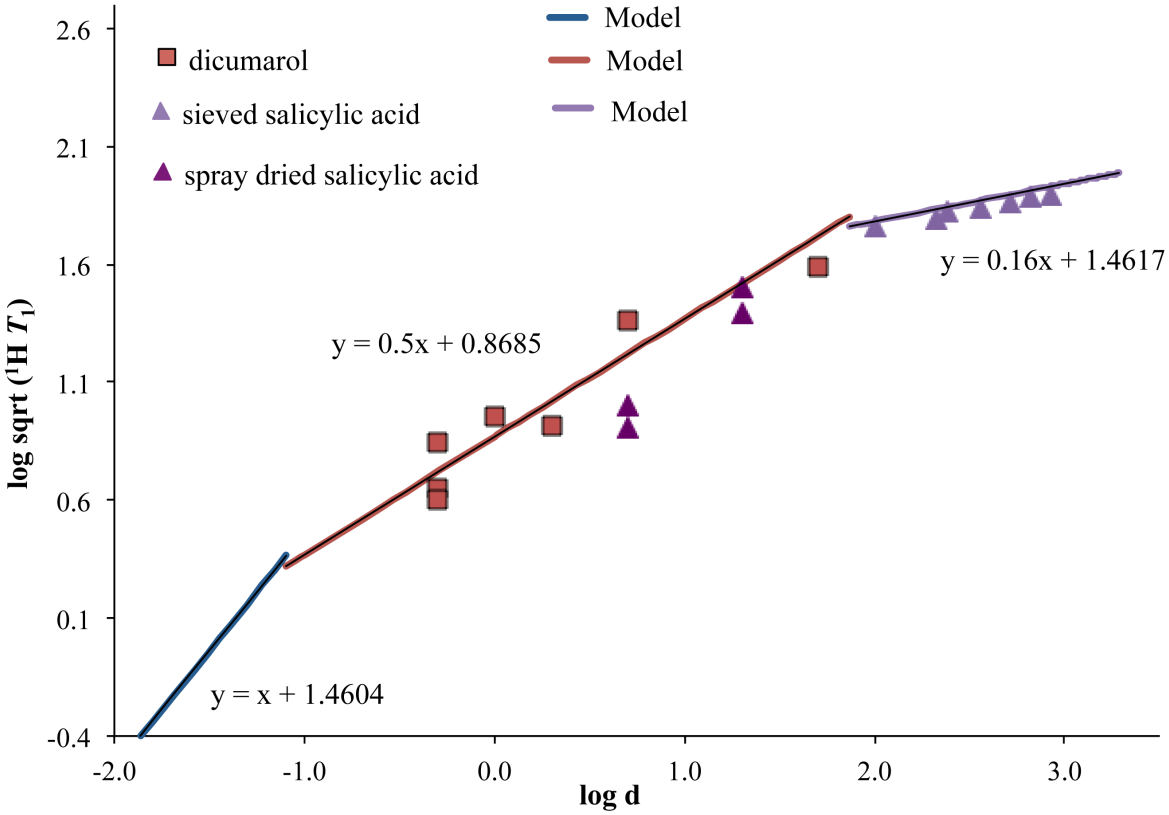

Figure 5.11 Proposed model; the markers represent the data presented earlier in this chapter, while the lines represent the proposed model

The ability to characterize the effect of tableting on the particle size of crystalline APIs and excipients by SSNMR is another ramification of the conclusions drawn here. Depending on the magnitude of the reduction in ^{1}H T_1 times observed upon tableting, if any, conclusions could be drawn on the impact of the compaction process on the particle size of the API or excipients. An investigation of the effect of compression forces on ^{1}H T_1 times will also be presented in the next chapter.

Finally, another possible implication of the results presented here is the ability to assess the relative amount of crystal defects present in a given crystalline material. If the decrease in ^{1}H T_1 time upon milling a crystalline solid is larger than expected for the particle size obtained, this could indicate a large density of defects, which in turn could lead to a reduction in chemical stability. That is because crystal defects are believed to be the starting points of chemical reactions in the solid state. An example of the potential of SSNMR ^{1}H T_1 time measurements to be indicators of the chemical stability of crystalline APIs is presented in Chapter 7.

5.5 References

1. Barich DH, Gorman EM, Zell MT, Munson EJ 2006. 3-Methylglutaric acid as a 13C solid-state NMR standard. Solid State Nuclear Magnetic Resonance 30(3-4):125-129.

2. Pines A 1973. Proton-enhanced NMR of dilute spins in solids. J Chem Phys 59(2):569.

3. Andrew ER, Bradbury A, Eades RG 1959. Removal of Dipolar Broadening of Nuclear Magnetic Resonance Spectra of Solids by Specimen Rotation. Nature 183(4678):1802-1803.

4. Lowe IJ 1959. Free Induction Decays of Rotating Solids. Physical Review Letters 2(7):285-287.

5. Dixon WT, Schaefer J, Sefcik MD, Stejskal EO, McKay RA 1982. Total suppression of sidebands in CPMAS C-13 NMR. Journal of Magnetic Resonance (1969) 49(2):341-345.

6. Chen Q, Schmidt-Rohr K 2006. Measurement of the local 1H spin-diffusion coefficient in polymers. Solid State Nuclear Magnetic Resonance 29(1-3):142-152.

7. Henrichs PM, Tribone J, Massa DJ, Hewitt JM 1988. Blend miscibility of bisphenol A polycarbonate and poly(ethylene terephthalate) as studied by solid-state high-resolution carbon-13 NMR spectroscopy. Macromolecules 21(5):1282-1291.

8. Pham TN, Watson SA, Edwards AJ, Chavda M, Clawson JS, Strohmeier M, Vogt FG 2010. Analysis of Amorphous Solid Dispersions Using 2D Solid-State NMR and ^{1}H T_1 Relaxation Measurements. Molecular Pharmaceutics 7(5):1667-1691.

9. Rabbani SR, Edmonds DT 1994. Nuclear spin-lattice relaxation-time reduction in small particles. Physical Review B 50(9):6184-6188.

10. Iacocca RG, Burcham CL, Hilden LR 2010. Particle engineering: A strategy for establishing drug substance physical property specifications during small molecule development. Journal of Pharmaceutical Sciences 99(1):51-75.

11. Klapper H. 2010. Generation and Propagation of Defects During Crystal Growth Springer Handbook of Crystal Growth. In Dhanaraj G, Byrappa K, Prasad V, Dudley M, editors., ed.: Springer Berlin Heidelberg. p 93-132.

12. Isbester PK, Jr. 1999. Development of an isolated flow variable-temperature magic-angle spinning (MAS) nuclear magnetic resonance (NMR) probe for heterogeneous catalysis studies and high-temperature high-speed 19F MAS NMR techniques applied to fluoropolymers. ed., United States -- Minnesota: University of Minnesota. p 179-179 p.

13. Dhanaraj G, Byrappa K, Prasad V, Dudley M. 2010. Crystal Growth Techniques and Characterization: An Overview
Springer Handbook of Crystal Growth. In Dhanaraj G, Byrappa K, Prasad V, Dudley M, editors., ed.: Springer Berlin Heidelberg. p 3-16.

14. Schieber LJ. 2010. Methods for increasing sensitivity and throughput of solid-state NMR spectroscopy of pharmaceutical solids. ed., United States -- Kansas: University of Kansas. p 242.

15. Gil AM, Alberti E 1998. The effect of Magic Angle Spinning on proton spin lattice relaxation times in some organic solids. Solid State Nuclear Magnetic Resonance 11(3,4):203-209.

16. Harris RK. 1983,1986. Nuclear Magnetic Resonance Spectroscopy. ed., New York: John Wiley & Sons, Inc. .

Chapter 6

Characterization of the polydispersity of powders and tablets using Solid-State NMR Spectroscopy

6.1 Introduction

In the previous chapter, it was shown that the particle size of crystalline dicumarol and salicylic acid could be quantitatively correlated to the SSNMR proton spin-lattice relaxation (^{1}H T_1) of the materials. In this chapter, the particle size distribution of crystalline dicumarol in powders, modeled by physical mixtures of crystalline samples of different particle sizes, is characterized using SSNMR proton spin-lattice relaxation time (^{1}H T_1) measurements, and the results are compared to laser diffraction. The impact of compaction forces on the particle-size distribution of salicylic acid in formulated tablets is also characterized using SSNMR and these results are then correlated to the dissolution profile of the API.

6.1.1 Relevance of polydispersity in pharmaceuticals

The particle size distribution, or polydispersity, of crystalline solid pharmaceuticals is an important property to characterize because it impacts the flow of the powder during manufacturing and the dose uniformity of the final drug product [1-3]. Highly polydisperse powders composed of larger and smaller particles are more likely to segregate during mixing. This results in a lack of dose uniformity in the final formulated drug product. The polydispersity of a material could also affect its ability to be made into a tablet [4]. Finally, the dissolution profile of a solid drug product can be impacted by the polydispersity of the particles in the powder as well. Smaller size particles are known to have a faster dissolution rate than larger particles, as described by the Noyes-Whitney equation:

$$\frac{dS}{dt} = \frac{DA(C_S - C)}{h} \qquad (6.1)$$

where dS/dt is the dissolution rate, D is the diffusion coefficient, A is the surface area, C_s is the concentration of the solid in the diffusion layer h immediately surrounding the drug particle, and

C is the concentration of the solid in the bulk medium. A powder composed of a very broad distribution of particles may not have a uniform dissolution profile, which might be detrimental to the bioavailability of the material. Conversely, a mixture of particles of different sizes could be used as a controlled-release drug delivery approach [5]. Polydispersity is generally assessed using laser diffraction; however, in samples composed of a mixture of materials, such as pharmaceutical formulations, it is not possible to obtain polydispersity information for a single component of the mixture by laser diffraction. Such information might be needed should the formulation not perform as expected.

6.2 Materials and Methods

6.2.1 Sample preparation

Cryogrinding

After a 15 min precooling period, about 1.5 g of dicumarol was cryoground with alternating cycles of 2 min of cooling and 2 min of grinding (SPEX SamplePrep 6770 Freezer/Mill, SamplePrep, Inc., Metuchen, NJ). The rate of grinding was 10 counts per second. Total grinding times were 4 and 10 min.

Preparation of physical mixtures.

Two and three-component physical mixtures of cryoground dicumarol and as-received dicumarol were prepared. Each of the components of the physical mixtures were weighed individually and then mixed gently with a spatula. The resulting mixture was then packed in a rotor.

Preparation of salicylic acid tablets.

The salicylic acid tablets were prepared in the laboratory of Dr. Gregory Amidon at the University of Michigan (Ann Arbor, MI). They were composed of sieved salicylic acid (125-300 μm) (50%) (125-300 μm), lactose monohydrate tabletose 80 (24.5%), microcrystalline cellulose (MCC) (24.5%), and magnesium stearate (1%) or sieved salicylic acid (50%) (125-300 μm), dicalcium phosphate (29.4%), microcrystalline cellulose (MCC) (19.6%), and magnesium stearate (1%). First, the excipients were blended together and then the API was added. The compaction forces used to prepare the tablets were varied resulting in tablets with different solid fractions. The solid fraction is equivalent to the density of the tablets. The diameter of all the tablets was approximately 5.6 mm.

6.2.2 Sample characterization

Differential Scanning Calorimetry (DSC)

Small amounts of sample (1-4 mg) were weighed in a standard, hermetic or T-Zero normal TA aluminum pan. Samples were heated from -10ºC to 300ºC using a 10ºC/min ramp (DSC Q2000, TA Instruments, New Castle, DE).

Solid-state NMR (SSNMR)

^{13}C SSNMR data were collected using a Tecmag Apollo (Tecmag, Inc., Houston, TX) spectrometer operating at a ^{13}C frequency of ~300 MHz ^{1}H frequency. The samples were packed in 7 mm zirconia rotors (Revolution NMR, Fort Collins, CO). A 2-module homebuilt probe was used. 3-methylglutaric acid (MGA) was used as an external standard, with the methyl peak referenced at 18.84 ppm [6]. All spectra were acquired using ramp cross polarization and magic angle spinning (CP/MAS) [7-9]. A SPINAL-64 decoupling pulse sequence was used, and the spinning side bands were suppressed using total sideband suppression (TOSS). The acquisition

length was 2048 points for all salicylic acid samples and 1024 points for all dicumarol samples. The contact time employed was 1 ms for both compounds. Proton relaxation time values, ^{1}H T_1, were measured via saturation recovery.

Fitting of ^1H T_1 data

The peaks in the SSNMR spectra obtained during the saturation recovery experiment were integrated in the Tecmag NMR software (Tecmag, Inc., Houston, TX) and exported, along with the corresponding tau time interval values used during the saturation recovery NMR experiment. Using KaleidaGraph (Synergy Software, version 4.1), the peak areas were plotted against the tau values and fitted to a curve using the known exponential equation for the ^{1}H T_1 relaxation:

$$Integrals = m_1\left(1 - e^{-\frac{\tau}{T_{1(1)}}}\right) \quad (6.2).$$

The m_1 coefficient and the ^{1}H T_1 are obtained from the fit.

Laser diffraction

Laser diffraction measurements were performed by Dr. Joseph Lubach at Genentech. A Malvern 2000 Mastersizer was used. The powders were suspended in hexane and sonicated for 2 min in the measuring chamber before each measurement. The refractive index of dicumarol was calculated using the ACD Labs software.

Dissolution

Dissolution profiles for salicylic acid powder and formulated tablets were obtained using a MicroDiss apparatus (pIon, Billerica, MA). High purity water was used as the dissolution medium. The API concentration was kept at approximately 0.2 mg/mL and the volume of water

used was adjusted accordingly depending on the amount of API initially present. UV detection was over the range 260-340 nm. The dissolution profile of two tablets of each solid fraction was obtained and the average was used to construct the plots.

6.3 Results and Discussion

6.3.1 Dicumarol

6.3.1.1 Effect of grinding on physical state and relaxation times of dicumarol

Figure 6.1 is an overlay of the DSC thermograms of as-received, 4 min, and 10 min cryoground dicumarol. An endotherm indicative of the melting of dicumarol around 290 ºC is the only thermal event present in the three thermograms. There are no events below 290 ºC. The melting endotherm of the 10 min cryoground dicumarol is slightly broader than the endotherm of the other two samples, possibly due to poor thermal contact between the samples and the pan or particle size effects. Regardless, the DSC results indicate that dicumarol remained crystalline upon being milled. The physical state of the samples was also characterized by SSNMR. Figure 6.2 shows the ^{13}C SSNMR spectra of dicumarol as received and dicumarol cryoground for 4 and 10 min. The three spectra contain the same number of peaks at the same chemical shifts, indicating that no polymorphic conversion occurred upon milling. The linewidths of the peaks in the three spectra are also very similar, although the peaks of the cryoground samples are slightly broader than the as-received material, as shown by the loss of resolution of the split peak at 115 ppm.

The ^{1}H T_1 time of dicumarol cryoground for 4 min was 13 s, and the ^{1}H T_1 time of the 10 min cryoground material was 8 s. Both of these relaxation times are significantly shorter than the

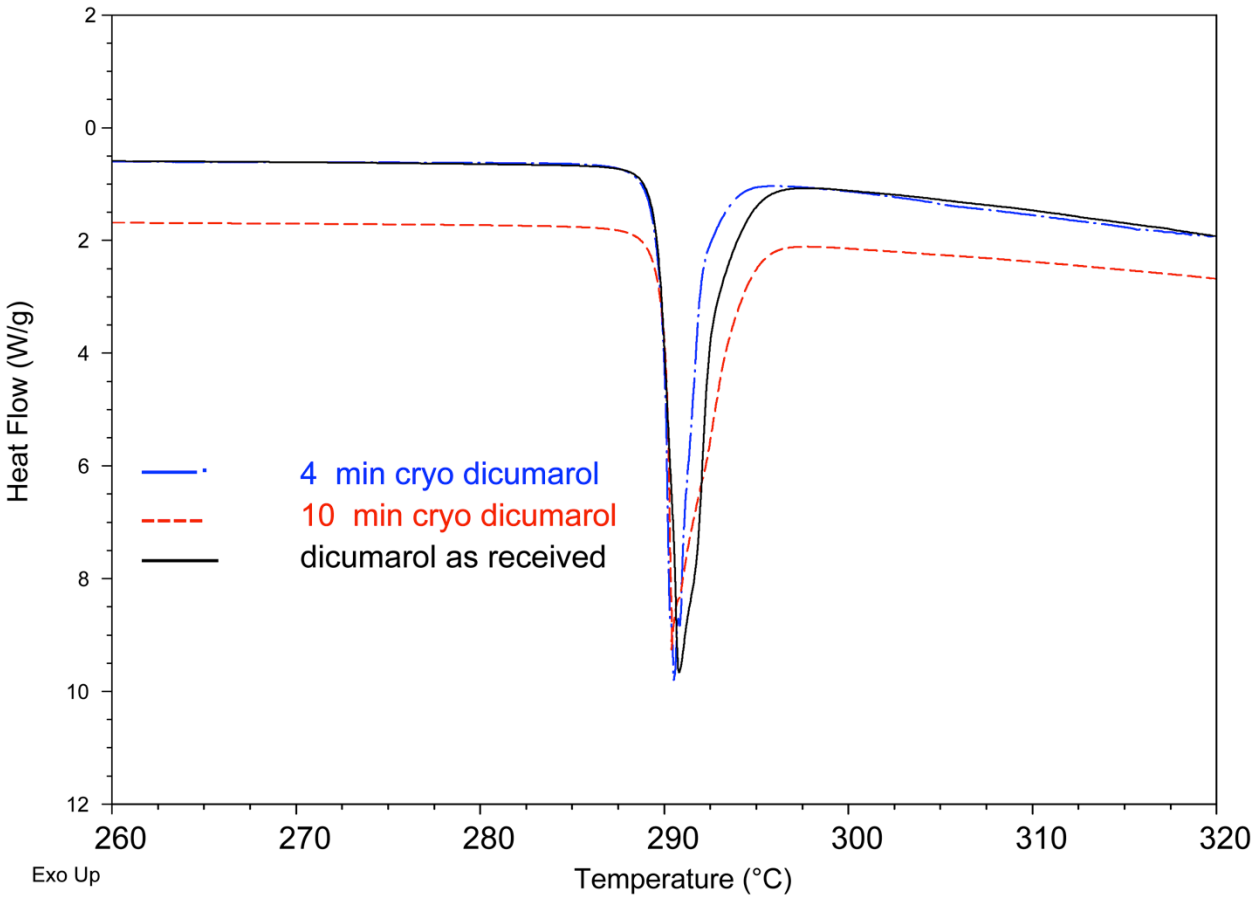

Figure 6.1. DSC thermograms of as received, 4 min cryoground and 10 min cryoground dicumarol

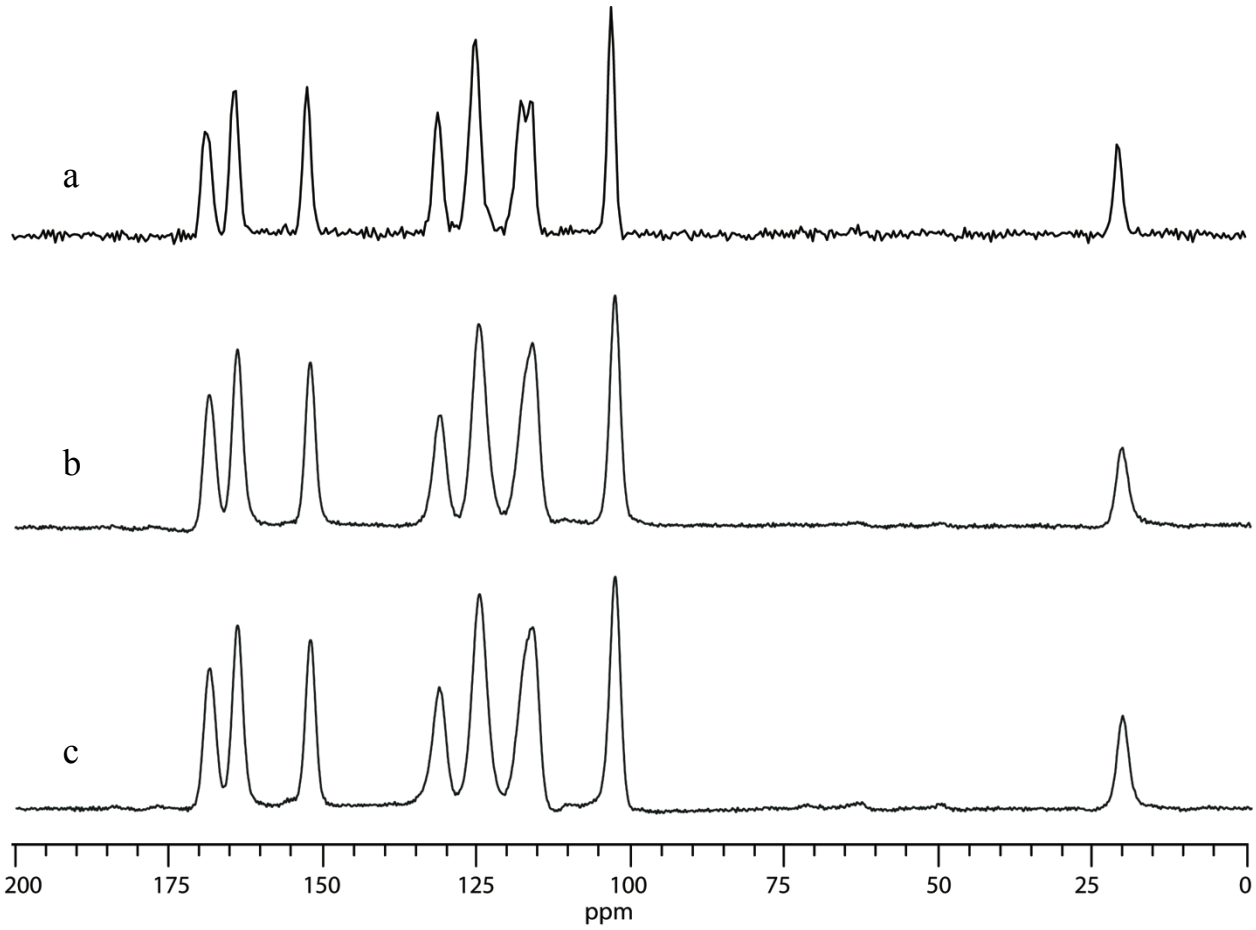

Figure 6.2. ^{13}C CP/MAS spectra of a. as received dicumarol; b. dicumarol cryoground for 4 min; c. dicumarol cryoground for 10 min

^{1}H T_1 of the as-received material (1500 s); this was expected since grinding decreased the size of the particles, and it was shown in the previous chapter that the ^{1}H T_1 time of crystalline dicumarol decreases with particle size. The cryoground samples and the as-received dicumarol were used to prepare physical mixtures that were used as a model to study the ^{1}H T_1 relaxation behavior of highly heterogeneous crystalline powders and determine if the amount of each component of the mixture can be quantified by SSNMR.

6.3.1.2 Characterization of 2-component physical mixtures of crystalline dicumarol by SSNMR relaxation measurements

Five physical mixtures of as-received and 10 min cryoground dicumarol were prepared with ratios ranging from 10:90 to 90:10 (as received: cryoground w/w) (Table 6.1). As discussed in the previous section, both the as-received and the cryoground dicumarol are crystalline, and mixing them in a physical mixture was not expected to alter their physical state, as confirmed by the ^{13}C SSNMR spectrum of the physical mixtures seen in Figure 6.3. Although the SSNMR spectra of all the mixtures are identical to each other and to the spectrum of as-received dicumarol, the relaxation times of the components of the mixtures are expected to be maintained in a physical mixture. This means that, unlike the individual pure materials, the relaxation behavior of the physical mixture will be best described with a bi-exponential equation, where each of the exponential term describes the relaxation of one of the components in the mixture. The following equation is used to fit the ^{1}H T_1 relaxation data of the two-component physical mixtures.

$$Integrals = m_1\left(1 - e^{-\frac{\tau}{T_{1(1)}}}\right) + m_2\left(1 - e^{-\frac{\tau}{T_{1(2)}}}\right) \quad (6.3)$$

The m_1 and m_2 pre-exponential coefficients are then used to calculate the ratio of each of the

Table 6.1. Theoretical ratios of physical mixtures of as-received and 10 min cryoground dicumarol

Sample	Theoretical fraction (by weight)
As-received	0.899
10-min cryoground	0.101
As-received	0.251
10-min cryoground	0.749
As-received	0.498
10-min cryoground	0.502
As-received	0.751
10-min cryoground	0.249
As-received	0.102
10-min cryoground	0.898

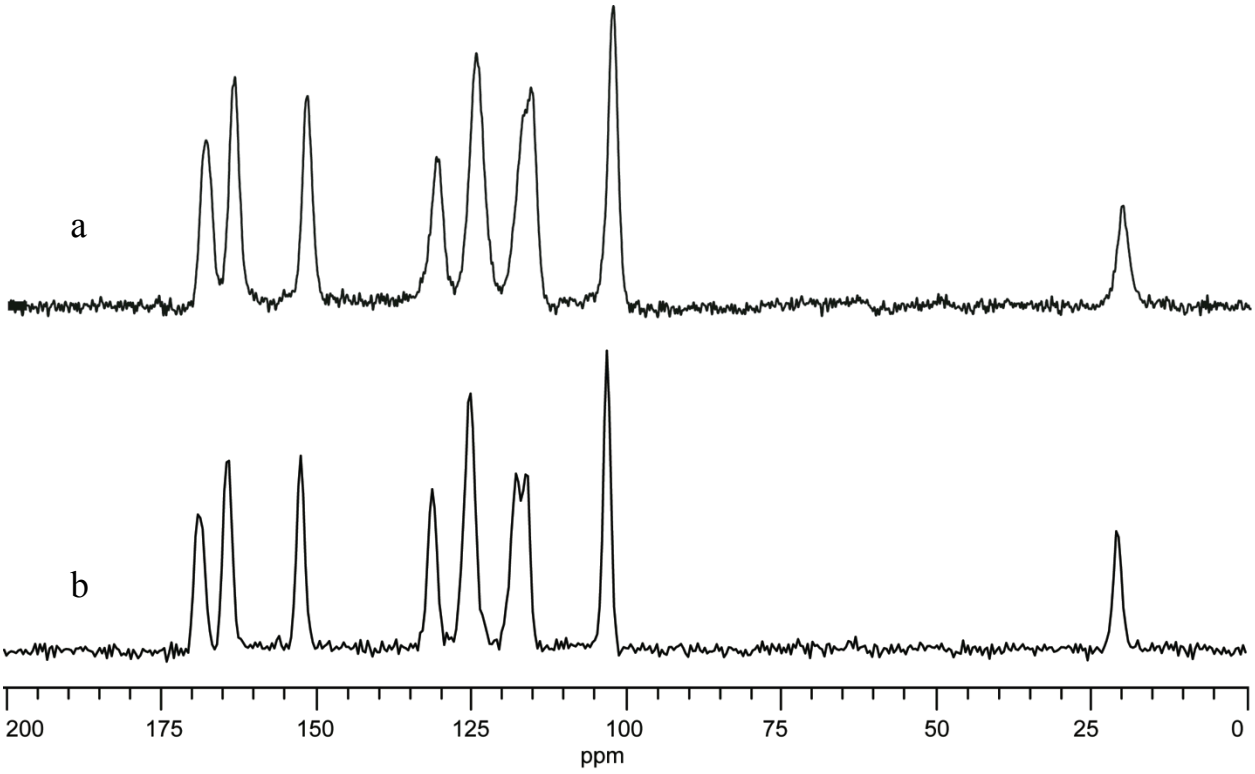

Figure 6.3 ^{13}C SSNMR spectra of **a.** physical mixture of as-received and 10 min cryoground dicumarol; 25:75 as-received:10 min cryoground dicumarol; **b.** as received dicumarol

components in the mixture using the following equations.

$$(1) = \frac{m_1}{m_1+m_2} \quad (6.4)$$

$$(2) = \frac{m_2}{m_1+m_2} \quad (6.5)$$

The physical mixtures were prepared with two components whose individual ^{1}H T_1 times were known, and therefore there are two options for fitting the data. In method 1, the ^{1}H T_1 curves could be fitted by setting the ^{1}H T_1 times in the equation to their known values and only letting the m_1 and m_2 coefficients be determined by the software fit. The ^{1}H T_1 time of as-received dicumarol was set at 1500 s and that of the 10 min cryoground dicumarol was set to be 8 s. The relative amounts of each material in the mixtures were calculated using equations 6.4 and 6.5.

In method 2, a value for the ^{1}H T_1 times is not set. In that case, the ^{1}H T_1 values obtained from the fit is used to determine which of the pre-exponential coefficients corresponds to the as-received dicumarol and which one corresponds to the cryoground sample. Since the pure as-received dicumarol has the longest ^{1}H T_1 time of the two components of the physical mixtures, the longer ^{1}H T_1 time was attributed to that material, and the shorter one to the cryoground sample. For example, when method 2 was used to fit the data of the 50:50 physical mixture, the following ^{1}H T_1 equation was obtained:

$$Integrals = m_1\left(1 - e^{-\frac{\tau}{2000\,s}}\right) + m_2\left(1 - e^{-\frac{\tau}{9.7\,s}}\right) \quad (6.6)$$

In equation 6.6, we attributed the 2000 s ^{1}H T_1 time to the as-received dicumarol and the 9.7 s ^{1}H T_1 time to the 10 min cryoground dicumarol; therefore, m_1 corresponds to as-received dicumarol and m_2 corresponds to the 10 min cryoground dicumarol.

The ratios of as-received and 10 min cryoground dicumarol in the physical mixtures were calculated using method 1 and method 2 and were compared to the theoretical ratios calculated from the weights of each of the materials in the mixtures. Table 6.2 summarizes the results. When using the first method, with the ^{1}H T_1 times set in the equation, the average difference between the theoretical and calculated ratios of as-received and cryoground dicumarol in the physical mixtures was 2.6% ± 2.1%. When the ^{1}H T_1 times are not set, as in method 2, the average difference between the theoretical and calculated ratios was 2.5% ± 3.1%.

The results presented up to this point were calculated by fitting the entire curve obtained from plotting the integrated SSNMR peak areas versus the time τ to equation 6.3. Alternatively, the long and the short tau times can be treated as two separate data sets. Each curve is then fit to a mono-exponential T_1 equation as defined in equation 6.2. At tau values longer than 50 s, the as-received dicumarol is expected to be the only component of the physical mixture whose nuclei have not yet reached equilibrium. Due to its shorter ^{1}H T_1 time, the cryoground material has already returned to equilibrium at tau values greater than 50 s and its contribution to the amount of signal detected is expected to be constant at these tau values. Figure 6.4 shows the resulting curve for the 25: 75 as received: cryoground sample. Since only the longer tau values are used, the y-intercept of the curve is not zero or approaching zero. Instead, that value corresponds to the amount of cryoground sample present in the mixture and was used to calculate the ratios of the components of the mixture using equations 6.4 and 6.5.

Table 6.2. Ratios of physical mixtures of as-received and 10 min cryoground dicumarol- obtained with and without set ^{1}H T_1 times- Method 1 and method 2, respectively

Sample	Theoretical fraction	Method 1		Method 2		^{1}H T_1 (Method 2)
		Calculated fraction	Δ	Calculated fraction	Δ	
As-received	0.899	0.843	0.056	0.819	0.079	1700s
10-min cryo	0.101	0.157		0.181		5.2s
As-received	0.751	0.743	0.008	0.745	0.006	1800s
10-min cryo	0.249	0.257		0.255		11s
As-received	0.498	0.460	0.038	0.471	0.027	2000s
10-min cryo	0.502	0.540		0.529		9.7s
As-received	0.251	0.243	0.008	0.253	0.002	1900s
10-min cryo	0.749	0.757		0.747		7.0s
As-received	0.102	0.123	0.021	0.114	0.013	890s
10-min cryo	0.898	0.877		0.886		8.7s

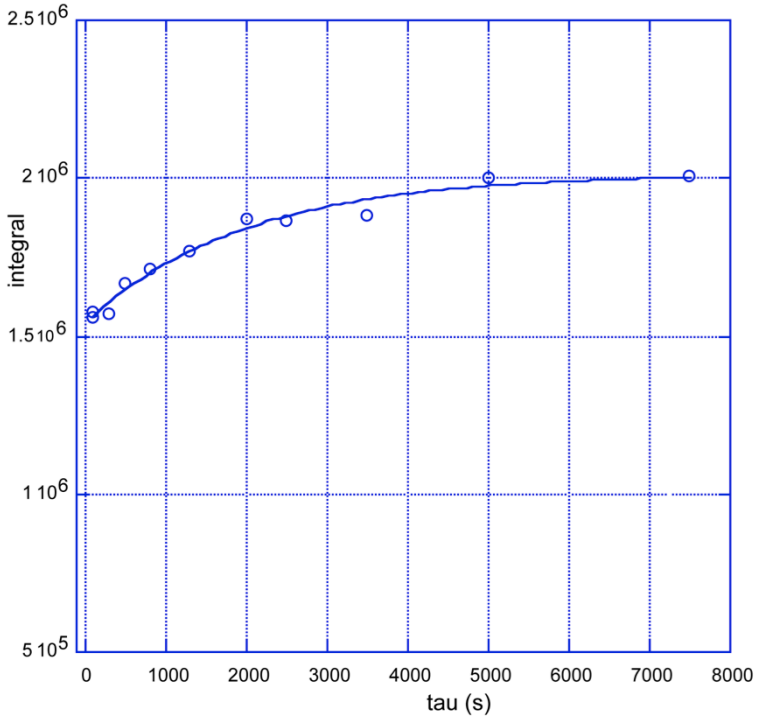

Figure 6.4 Curve of integrated peak areas versus tau values for the 25:75 as-received:10 min cryoground physical mixture using only the longer tau values (> 50 s) to construct the plot and perform the fitting.

Once again, the fitting could be performed using either method 1 or method 2, in which the ^{1}H T_1 times are specified or allowed to vary, specifically. The results are shown in Table 6.3. The average difference between the theoretical and calculated ratios was 2.7% ± 2.0% using method 1, and 3.1% ± 1.7% using method 2. The largest differences between the theoretical and calculated ratios were observed with the 50:50 physical mixture. These results are comparable to the ones obtained when the tau values were not treated as separate data sets.

The mixtures were only prepared once, therefore no standard deviation could be calculated. However, we can propose a few explanations for the difference observed between the calculated and the theoretical ratios. The first reason might be the quality of the fit, and the accuracy of the coefficients obtained from the fit. The Kaleidagraph software was used to fit the ^{1}H T_1 data obtained experimentally by SSNMR to equation 6.3, and the R^2 value obtained was used as an indicator of the quality of the fit; for all the mixtures, the R^2 values were close to 1 (>0.9). Therefore, the fit quality is likely not to blame. It is also possible that the weight-based theoretical ratios do not actually reflect the exact composition of the physical mixtures. This would be the case if the two powders were not homogeneously mixed before being packed in the rotor, and a small amount of powder was left on the weigh paper and did not get transferred to the rotor. Increasing the number of scans used to acquire the data, could also provide even better data through improving the signal to noise ratio of the spectra, as well as additional tau values.

Table 6.3. Calculated ratios and ^{1}H T_1 times of physical mixtures of as-received and 10 min cryoground dicumarol

Sample	Theoretical fraction	Method 1		Method 2		^{1}H T_1 (Method 2)
		Calculated fraction	Δ	Calculated fraction	Δ	
As-received	0.899	0.886	0.013	0.865	0.034	1900s
10-min cryo	0.101	0.114		0.135		-
As-received	0.751	0.717	0.034	0.710	0.041	1800s
10-min cryo	0.249	0.283		0.290		-
As-received	0.498	0.441	0.057	0.446	0.052	2000s
10-min cryo	0.502	0.559		0.554		-
As-received	0.251	0.243	0.022	0.234	0.017	2000s
10-min cryo	0.749	0.757		0.766		-
As-received	0.102	0.093	0.008	0.092	0.010	1100s
10-min cryo	0.898	0.907		0.908		-

6.3.1.3 Differences in ^1H T_1 times between pure materials and materials in the physical mixtures

When using method 2, the calculated ^{1}H T_1 times of as-received and ground dicumarol in the physical mixtures were used to identify the pre-exponential coefficient that corresponded to each of the components in the mixture. However, the ^{1}H T_1 times of the components in the mixture did not always exactly match the ^{1}H T_1 times of the pure materials, though the two values were close. The ^{1}H T_1 values are summarized in Table 6.2 and 6.3. In all physical mixtures containing 25% of more of as as-received dicumarol, the ^{1}H T_1 of as-received dicumarol was longer than the one obtained with the pure material, with values ranging from 1700 s to 1900 s; the ^{1}H T_1 time of the pure as-received dicumarol was 1500 s. In the mixture containing 10% as-received dicumarol, the ^{1}H T_1 time of this component were 890 s and 1100s. These differences in ^{1}H T_1 between the pure material and the material in the presence of another component were not expected. These differences suggest that it is more difficult to accurately determine the ^{1}H T_1 time of the minor component. Increasing the number of acquisitions collected during the proton-spin lattice relaxation experiment could potentially allow us to obtain more accurate ^{1}H T_1 times for the minor component.

6.3.1.4 Comparison to laser diffraction measurements

Figures 6.5 and 6.6 show the particle size distribution obtained by laser diffraction of two physical mixtures containing 50% and 10% by weight of as-received dicumarol. The 50:50 physical mixture shows a clear bimodal distribution, similar to two overlapping Gaussian distributions. The particles present in the sample range from approximately 0.3 μm to 79 μm in diameter, with maxima at about 1.7 and 17 μm. By looking at the graph, one can estimate that the two particle size distributions in the samples are present in approximately equal amounts

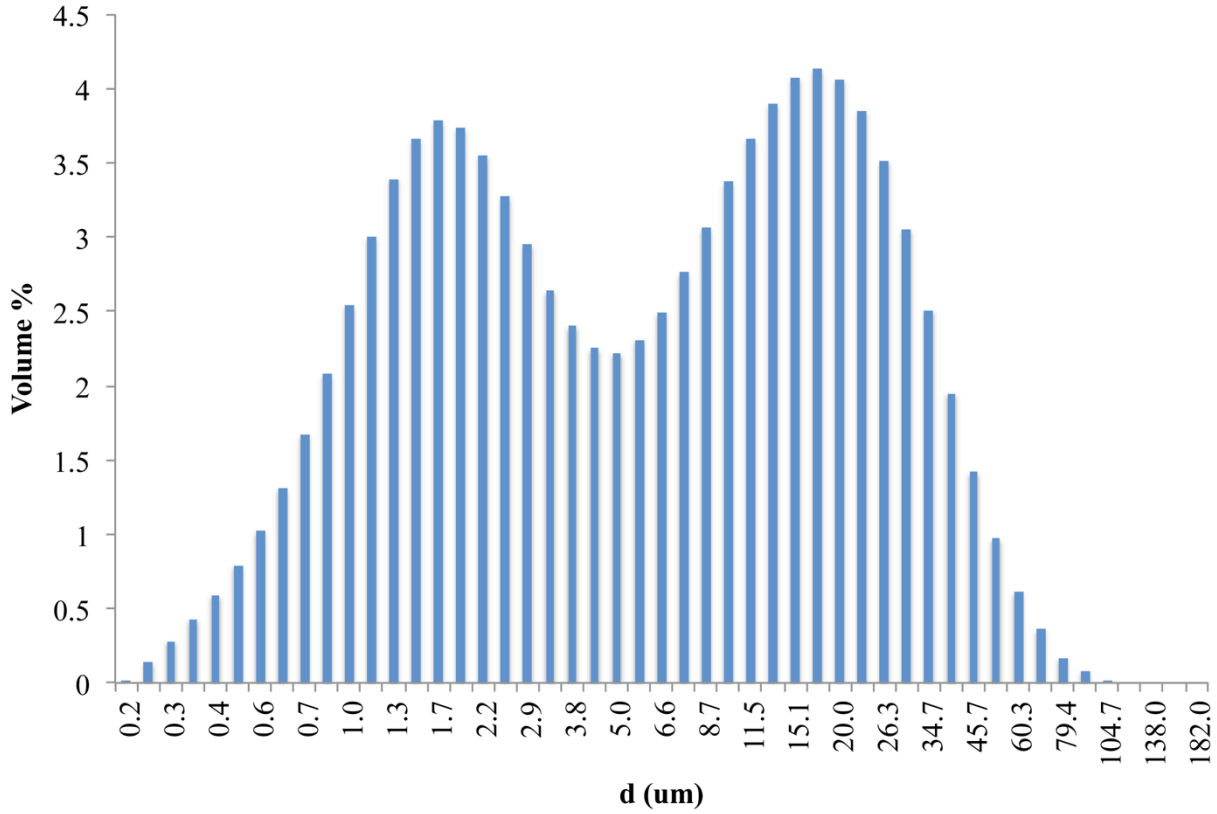

Figure 6.5 Particle size distribution obtained using laser diffraction of physical mixture of as-received and 10 min cryoground dicumarol; 50:50 as-received:10 min cryoground

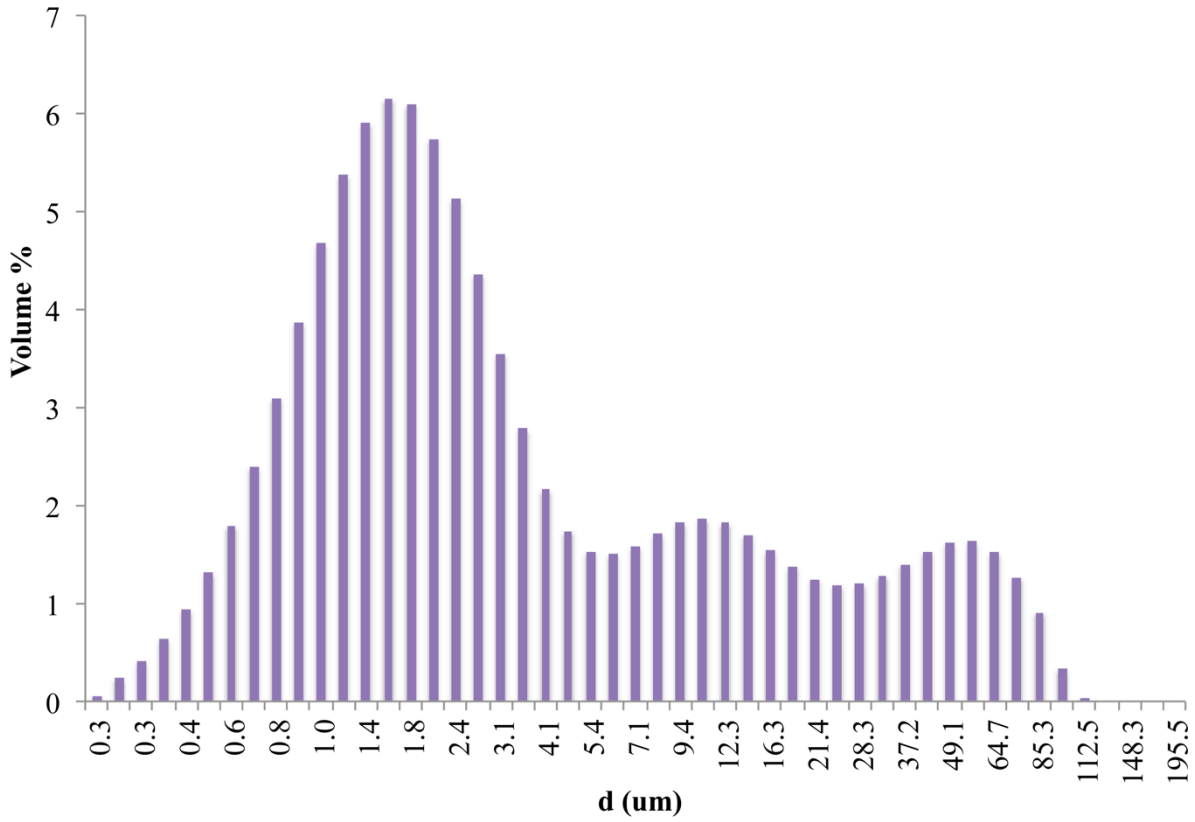

Figure 6.6. Particle size distribution using laser diffraction of physical mixture of as-received and 10 min cryoground dicumarol; 10:90 as-received:10 min cryoground

since the two distributions peak at approximately the same volume percentage. For the 10:90 physical mixture containing 10 % of as-received material (shown in Figure 6.6), instead of the expected bimodal distribution, a tri-modal distribution was obtained. The large Gaussian distribution has a maximum at about 1.7 μm and the two smaller distributions have maxima at approximately 10 and 60 μm. Though a trimodal distribution was unexpected, the data clearly shows that the smaller range of particles constitutes the largest part of the sample. These results indicate that the particle size distribution data obtained by laser diffraction mostly agree with the theory and the SSNMR results. Furthermore, the 50:50 distribution looks similar to the laser diffraction data obtained for two samples, Lot C and Lot D of precipitated dicumarol (Figure 5.4), prepared and characterized in the previous chapters. This supports the fact that the two distinct ^{1}H T_1 times obtained for these samples were due to a bimodal distribution in particle size.

6.3.1.5 Characterization of 3-component physical mixtures of crystalline dicumarol by SSNMR relaxation measurements

The two orders of magnitude difference between the ^{1}H T_1 time of as-received and 10 min cryoground dicumarol allowed us to distinguish and quantify them in the physical mixtures using SSNMR. In order to study a more complex case, and one in which the components of the mixture have ^{1}H T_1 times that are closer in magnitude, physical mixtures containing various ratios of as-received dicumarol, 4 min cryoground dicumarol, and 10 min cryoground dicumarol were prepared and characterized. Table 6.4 summarizes the composition of the mixtures prepared.

The ^{1}H T_1 time of the cryoground dicumarol samples are 8 s for the 10 min cryoground material and 13 s for the 4 min cryoground dicumarol. Because there are three different materials with different relaxation rates in the physical mixtures, the equation used to fit the spin lattice

Table 6.4 Theoretical ratios of physical mixtures of as-received, 4 min cryoground and 10 min cryoground dicumarol

Sample	Theoretical fraction (by weight)
As-received	0.50
4 min cryoground	0.25
10-min cryoground	0.25
As-received	0.10
4 min cryoground	0.60
10-min cryoground	0.30
As-received	0.40
4 min cryoground	0.10
10-min cryoground	0.50

relaxation data contains three exponential terms.

$$Integrals = m_1\left(1 - e^{-\frac{\tau}{T_{1(1)}}}\right) + m_2\left(1 - e^{-\frac{\tau}{T_{1(2)}}}\right) + m_3\left(1 - e^{-\frac{\tau}{T_{1(3)}}}\right) \quad (6.7)$$

Similarly to what was described with the bi-exponential equation, the pre-exponential coefficients m_1, m_2, and m_3 can be used to calculate the ratio of each of the components in the mixture with the following equations.

$$(1) = \frac{m_1}{m_1+m_2+m_3} \quad (6.8)$$

$$(2) = \frac{m_2}{m_1+m_2+m_3} \quad (6.9)$$

$$(3) = \frac{m_3}{m_1+m_2+m_3} \quad (6.10)$$

Again, the data could be fitted two different ways: by setting a value for the ^{1}H T_1 times (method 1), or letting that value vary (method 2). However, when a value was set for ^{1}H T_1 times, the pre-exponential coefficients observed for the 4 min cryoground sample were negative. This is physically impossible therefore only method 1 was used and the longest ^{1}H T_1 time was attributed to the as-received dicumarol and the shortest one to the 10 min cryoground material since the ^{1}H T_1 times of the pure samples follow that trend. Table 6.5 summarizes the theoretical and calculated ratios. Both ratios agreed within 10% or less of each other only for as-received dicumarol. The calculated ratios of each of the cryoground materials in the physical mixtures were significantly over- or underestimated. In particular, the ratios of the cryoground materials calculated using the NMR coefficients in the physical mixture composed of 40, 50 and 10% of as-received, 10 min cryoground, and 4 min cryoground dicumarol, respectively, differed by more than 35% from the theoretical ones. We believe that the poor agreement between the two values

Table 6.5. Ratios and ^{1}H T_1 times of physical mixtures of as-received, 4 min cryoground and 10 min cryoground dicumarol

Sample	Theoretical fraction	Calculated fraction	Absolute difference	^{1}H T_1
As-received	0.50	0.450	0.052	2100s
4 min cryo	0.25	0.189	0.059	53s
10-min cryo	0.25	0.361	0.112	6.9s
As-received	0.10	0.105	0.001	1600s
4 min cryo	0.60	0.734	0.140	15s
10-min cryo	0.30	0.161	0.141	5s
As-received	0.40	0.414	0.013	2700s
4 min cryo	0.10	0.470	0.365	14s
10-min cryo	0.50	0.116	0.379	4s

is due to the assumption that we made earlier that the shortest ^{1}H T_1 time obtained when fitting the data of the physical mixture is from the 10-min cryoground dicumarol. When that assumption is not made, and the pre-exponential m coefficients used to calculate the relative amounts of 4 min and 10 min cryoground dicumarol in the mixture are switched, there is better agreement between the theoretical and the calculated ratios. This result suggests that it is difficult to distinguish components of a highly heterogeneous powder whose ^{1}H T_1 times are very close to each other. Furthermore, the ^{1}H T_1 time of the 4 min cryoground dicumarol in the mixtures ranged from 14 s to 53 s, while the ^{1}H T_1 time of the 10 min cryoground material ranged from 4 s to 6.9 s. Those values are unexpectedly very far from the ^{1}H T_1 values of 4 min and 10 min cryoground dicumarol alone: 13 s and 8 s, respectively.

In order to determine if the agreement between theoretical and calculated numbers would improve when the cryoground samples were treated as one material, a bi-exponential equation was used to fit the ^{1}H T_1 data. Again, either method 1 or method 2 could be used to fit the data, and the results obtained with both methods are presented in Table 6.6. The calculated amounts of total cryoground material in the physical mixtures are within 1-3 % of the theoretical amount. While SSNMR can distinguish between relaxation time that differ by one order of magnitude or more, this result demonstrates that SSNMR cannot differentiate between materials with very similar relaxation behavior.

Table 6.6. Ratios and ^{1}H T_1 times of physical mixtures of as-received, 4 min cryoground and 10 min cryoground dicumarol treated as 2-component physical mixtures, analyzed with or without setting a value for the ^{1}H T_1 time of as-received dicumarol- Method 1 and method 2, respectively

Sample	Theoretical fraction	Method 1		Method 2		^{1}H T_1 (Method 2)
		Calculated fraction	Δ	Calculated fraction	Δ	
As-received	0.502	0.465	0.037	0.489	0.013	1500s
4+10-min cryo	0.498	0.535		0.511		-
As-received	0.104	0.113	0.009	0.113	0.009	1010s
4+10-min cryo	0.896	0.887		0.887		-
As-received	0.401	0.362	0.039	0.428	0.027	2600s
4+10-min cryo	0.599	0.638		0.572		-

6.3.2 Salicylic acid formulations

Tableting is a commonly used manufacturing process that can affect the polydispersity of solid pharmaceuticals. While the previous sections focused on characterizing the polydispersity of dicumarol in powders, in the following sections the effect of compaction forces on the poydispersity of another API, salicylic acid, in formulated tablets will be studied using SSNMR ^{1}H T_1 times measurements and the results will be correlated to the dissolution rate of the material.

6.3.2.1 Effect of compaction force and excipient type on the ^{1}H T_1 times of salicylic acid in formulated tablets

Two formulations were tableted using different compaction forces and the ^{1}H T_1 time of salicylic acid in the tablets was obtained. Table 6.7 summarizes the compaction forces used for each formulation and the solid fraction, or density, of the resulting tablets. Formulation A was composed of sieved salicylic acid (125-300 μm), lactose monohydrate, MCC, and magnesium stearate, and Formulation B was composed of sieved salicylic acid (125-300 μm), dicalcium phosphate, MCC, and magnesium stearate. The ^{1}H T_1 time of the 125-300 μm sieved fraction of salicylic acid is 3900 s. The spin-lattice relaxation behavior of as-received α-lactose monohydrate tabletose was best modeled with two ^{1}H T_1 times: 60 s and 200 s, and the ratios of material at the origin of each ^{1}H T_1 were 63% and 37 %, respectively. However, after blending with the other excipients, only one ^{1}H T_1 time was obtained for lactose: 89 s. This suggests that blending increased the homogeneity of the lactose. In order to measure the ^{1}H T_1 times of salicylic acid and lactose monohydrate in the tablets, we first identified the peaks in the spectra that could be integrated to perform the ^{1}H T_1 time measurements.

Table 6.7. Compression forces used to prepare the salicylic acid tablets from a. Formulation A; b. Formulation B

a.

Tablet set	Punch applied force (lbs)	Solid Fraction
1	350	0.81
2	550	0.86
3	1000	0.90
4	2500	0.93

b.

Table set	Punch applied force (lbs)	Solid Fraction
1	350	0.79
2	1000	0.86
3	2500	0.91

Figure 6.7 shows the ^{13}C SSNMR spectra of as-received lactose monohydrate and microcrystalline cellulose (MCC). A ^{13}C SSNMR spectrum of dicalcium phosphate cannot be obtained because that material does not contain any ^{13}C. Lactose is crystalline and is present as its α polymorph; this polymorphic identification can be made based on work previously done on lactose in our laboratory [10]. MCC contains broad peaks indicating that it is amorphous. The peaks of both of these excipients are contained within the 112-50 ppm region of the spectrum.

Figure 6.8 shows the ^{13}C SSNMR spectra of as-received salicylic acid and representative spectra of salicylic acid tablets prepared from Formulation A and Formulation B. The peaks below 112 ppm in Figure 6.8b are from MCC, and in Figure 6.8c they are from both MCC and α-lactose monohydrate. Lactose remained crystalline after blending and compaction, as evidenced by the sharp peak at 92 ppm in the ^{13}C SSNMR spectrum obtained from the tablets. The peaks between 200 and 112 ppm belong to salicylic acid. They are sharp and narrow indicating that processing did not change the crystalline state of salicylic acid either. The salicylic acid peaks between 200 and 112 ppm and the lactose peak at about 92 ppm were used to obtain the ^{1}H T_1 times of the two materials.

The ^{1}H T_1 times of salicylic acid and lactose monohydrate prepared from Formulation A are presented in Tables 6.8a and 6.8b. The ^{1}H T_1 data for both salicylic acid and lactose in the tablets prepared from Formulation A were first fitted with a mono-exponential equation (Table 6.7a). However, the spin-lattice relaxation curves of salicylic acid in the Formulation A tablets prepared with compaction forces of 550 and 1000 lbs, and of lactose in the tablets prepared with compaction forces of 550, 1000 and 2500 lbs were found to be best fitted using two distinct ^{1}H T_1 times (Table 6.7b). When the other sets of tablets were fitted with bi-exponential equations the ^{1}H T_1 times obtained had large errors associated with them. The tablets better described with two

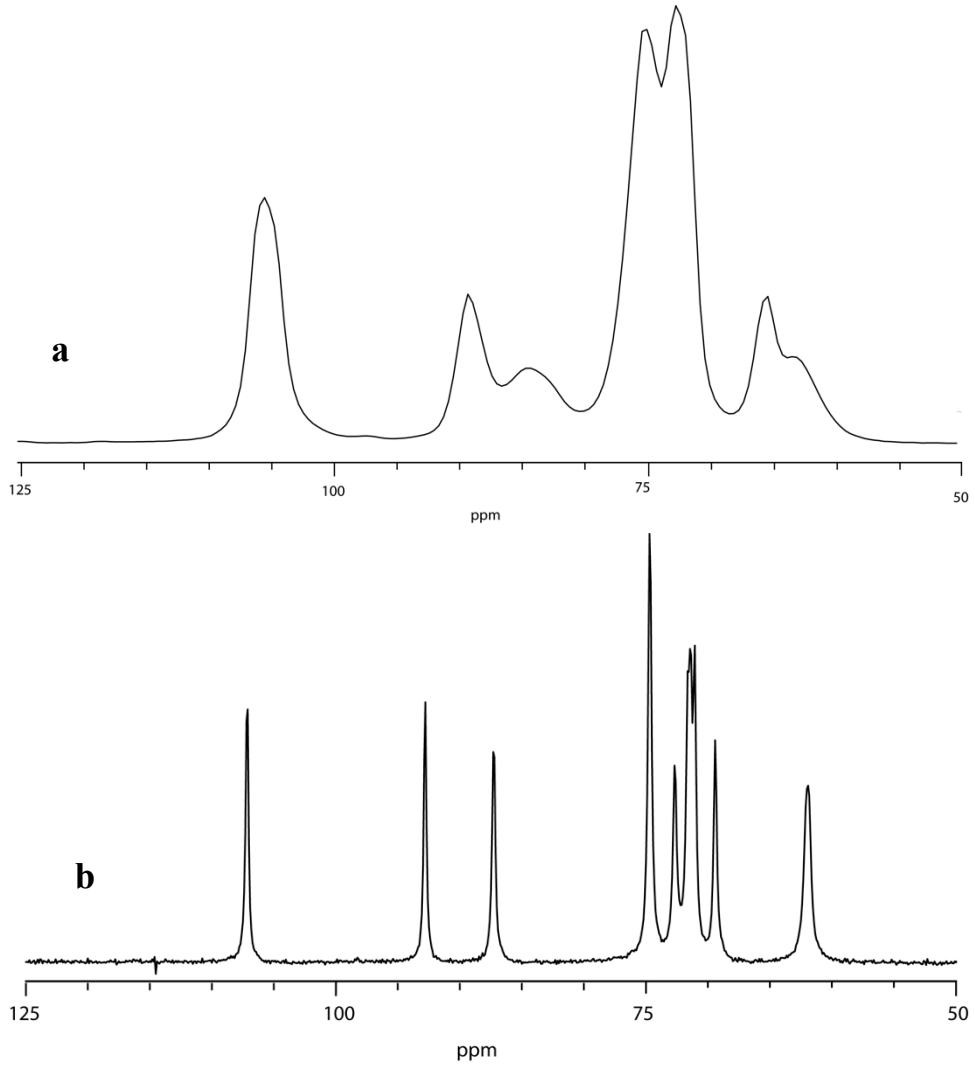

Figure 6.7. ^{13}C CP/MAS spectrum of **a.** microcrystalline cellulose (MCC); **b.** α-lactose monohydrate tabletose 80

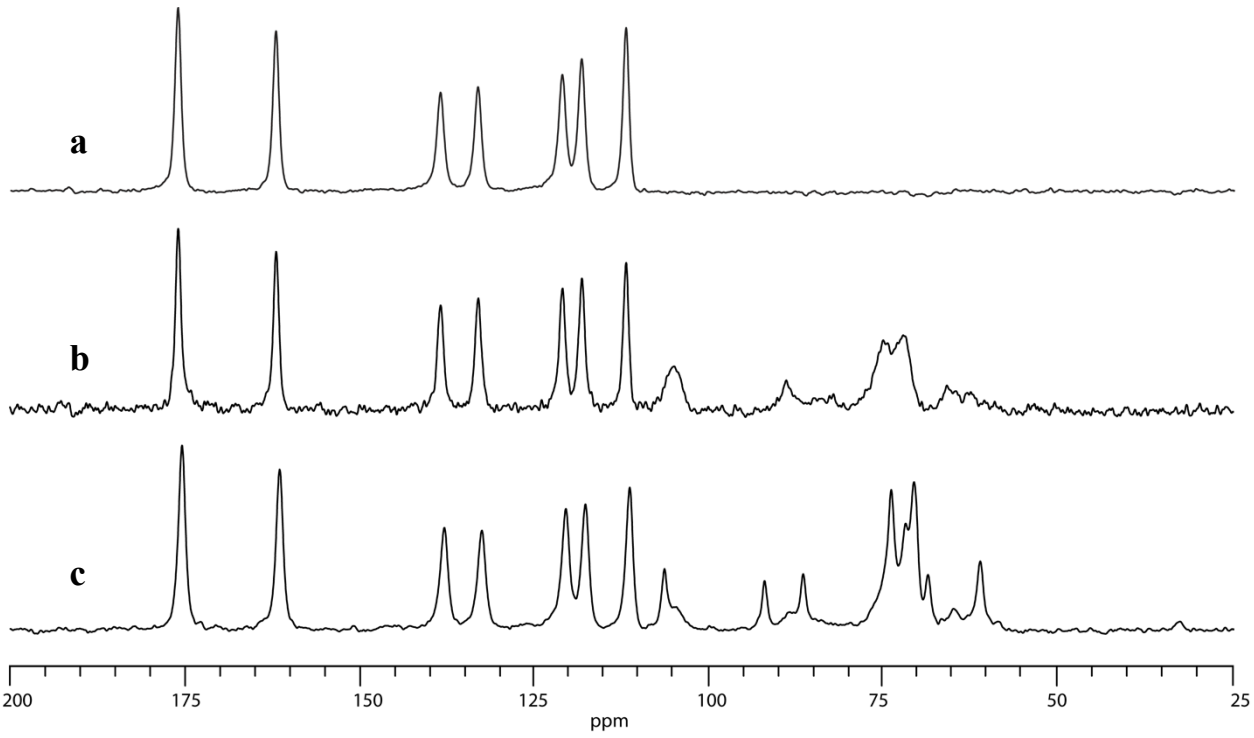

Figure 6.8 ^{13}C SSNMR spectra of **a.** as-received salicylic acid **b.** representative tablet of salicylic acid with dicalcium phosphate **c.** representative tablet of salicylic acid with lactose

Table 6.8 ^{1}H T_1 times of lactose and salicylic acid in the Formulation A tablets obtained using mono-exponential **(a)** and bi-exponential fits **(b)**; the errors indicated are the errors of the fit. The percentages in parenthesis indicate the amount of material at the origin of that ^{1}H T_1 time.

a.

Tablet set	Solid Fraction	Punch applied force (lbs)	Salicylic acid ^{1}H T_1	Lactose ^{1}H T_1
		0	3900 s	89 s
1	0.81	350	2200 s ± 370	83 s ± 5
2	0.86	550	2100 s ± 350	73 s ± 5
3	0.90	1000	2000 s ± 290	79 s ± 7
4	0.93	2500	1400 s ± 126	51 s ± 6

b.

Tablet set	Solid Fraction	Punch applied force (lbs)	Salicylic acid ^{1}H T_1		Lactose ^{1}H T_1	
		0	-	-	-	-
1	0.81	350	-	-	-	-
2	0.86	550	560 s ± 180 (41%)	5300 s ± 1900 (59%)	13 s ± 8 (19%)	93 s ± 14 (81%)
3	0.90	1000	500 s ± 240 (36 %)	3500 s ± 1100 (64%)	16 s ± 6 (31%)	120 s ± 26 (69%)
4	0.93	2500	-	-	5 s ± 2 (27%)	68 s ± 6 (73%)

^{1}H T_1 times may contain both smaller and larger particles that differ significantly in their size. The smaller particles would likely result from larger chunks fragmenting during the tableting process. It is not possible to determine using the SSNMR data if segregated domains of each type of particle exist in the tablets or if they are intimately mixed. A large error is associated with the ^{1}H T_1 times of salicylic acid resulting from 2-component fits, rendering it difficult to establish a trend between the compaction forces and the ^{1}H T_1 times using that set of data. This is somewhat not surprising since it was shown earlier, with the dicumarol physical mixtures (§6.3.1.3), that it could be difficult to obtain accurate ^{1}H T_1 times for the components of heterogeneous materials: the ^{1}H T_1 times of as-received and cryoground dicumarol in the physical mixture were not always the expected values However, some observations on the changes in ^{1}H T_1 times with compaction forces can be made.

The ^{1}H T_1 times of lactose monohydrate and salicylic acid in the tablets are shorter than the ^{1}H T_1 times of the materials before tableting. The shortest ^{1}H T_1 time obtained for salicylic acid was 1400 s, and it was 51 s for lactose monohydrate compared to 3900 s and 89 s for the untableted materials. Generally, the ^{1}H T_1 times of both materials decreased with increasing compaction forces and increasing solid fraction; however, the lactose in the set of tablets # 3 seems to be an outlier to this trend: its ^{1}H T_1 time (79 s) is longer than the ^{1}H T_1 times of lactose in tablet set #4 (51s).

Salicylic acid in the tablets prepared using Formulation B were best fitted using two distinct ^{1}H T_1 times; the values obtained are presented in Table 6.9. Again, the fact that two ^{1}H T_1 times were needed to accurately describe the spin-lattice relaxation of the tablets suggests that smaller and larger particle size distributions are present in the tablets. Similarly to the tablets

Table 6.9 ^{1}H T_1 times of salicylic acid in the Formulation B tablets. The percentages in parenthesis indicate the amount of material at the origin of that ^{1}H T_1 time calculated using equations 6.4 and 6.5.

Table set	Solid Fraction	Punch applied force (lbs)	Salicylic acid ^{1}H T_1	
1	0.79	350	760s ± 800 (21%)	3600s ± 1300 (79%)
2	0.86	1000	390s ± 150 (39%)	3800s ± 1300 (69%)
3	0.91	2500	260s ± 74 (28%)	2200s ± 240 (72%)

prepared using Formulation A, higher compaction forces were associated with shorter ^{1}H T_1 times. For sets of tablets 1 and 2, the longer ^{1}H T_1 time of the two ^{1}H T_1 times detected was approximately the same as the 3900 s ^{1}H T_1 time of untableted sieved salicylic acid. The long ^{1}H T_1 time of the tablets prepared with compaction forces of 2500 lbs was 2200s. The shorter ^{1}H T_1 times were more significantly different, and the tablets prepared with the stronger compaction force had the shortest ^{1}H T_1 time overall (260 s).

6.3.2.2 Effect of compaction forces and excipient type on the dissolution rate of salicylic acid in tablets

Figure 6.9a is an overlay of the dissolution curves of the 125-300 μm sieved salicylic acid fraction and tablets of salicylic acid prepared from Formulation A, the lactose-containing formulation. The relative amount of salicylic acid dissolved is plotted versus the time in seconds. The set 1 of Formulation A tablets (350 lbs) were damaged during shipping and even more while in the spinning rotor during the SSNMR experiment; as a result, no dissolution data was obtained on these tablets. The sieved salicylic acid has the fastest dissolution rate of all the materials, and approximately 90 % of the salicylic acid was dissolved after 500 s. About 92 % of the salicylic acid initially present in the tablets was dissolved after 1920 s, at the end of the dissolution study. The shape of the dissolution curves of all the tablets is sinusoidal indicating that there is a short lag before salicylic acid starts dissolving into solution. That lag time lasted approximately 70- 80 s for the tablets and is believed to be the time that it takes the tablets to disintegrate. Between 80 and 500 s, the dissolution rate of salicylic in the tablets is fastest for tablets set 4 (solid fraction of 0.93) and slowest for the tablet set 3 (solid fraction equal to 0.90). The dissolution rate of salicylic acid from the tablets in set 2 (solid fraction of 0.86) is between these two although it is closer to that of the tablets with a solid fraction of 0.93. For both the tablet set 4 and tablet set 2,

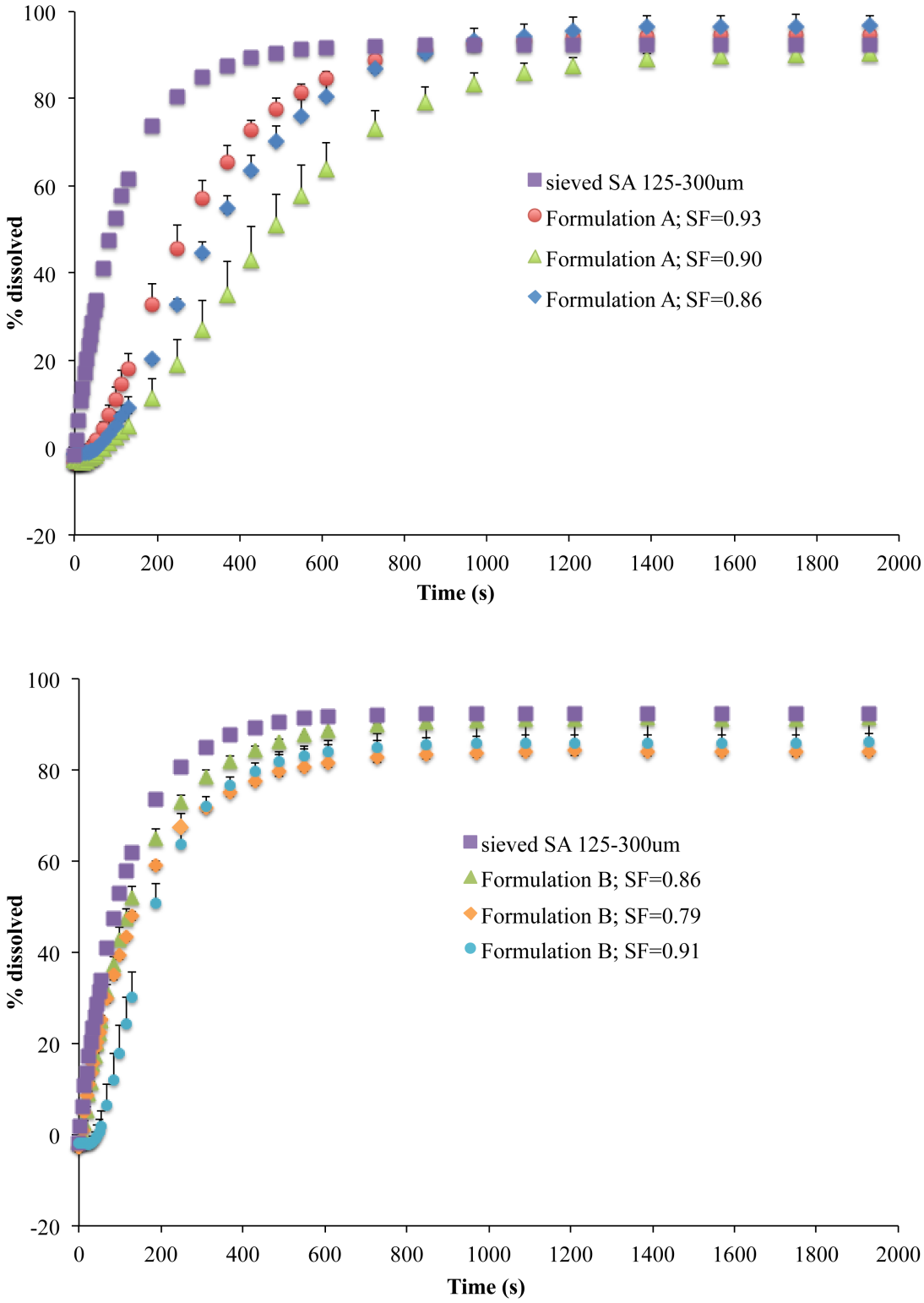

Figure 6.9. Dissolution profile of salicylic acid in tablets; n=2. The error bars represent the deviation from the mean

approxiately 90% of the salicylic acid initially present in the tablets was dissolved after 800 s. After that point the curves start to plateau out and the final amount of salicylic acid present insolution after 2100 s is about 95% of the nominal amount present initially. For the tablets with a 0.90 solid fraction, only about 85% of the salicylic acid initially present in the tablets was in solution after about 800 s. The dissolution curve begins to plateau out near 1100 s and about 90% of the relative amount of salicylic acid initially present in the tablets is in solution at the end of the dissolution study.

Figure 6.9b in an overlay of the dissolution profile of sieved salicylic acid and the salicylic acid tablets prepared using dicalcium phosphate (Formulation B). No lag time is present in the dissolution curves of the tablets prepared with the lowest compaction forces, tablets set 1 and 2 (350 and 1000 lbs), while a short lag time of ~40s exists with the tablets prepared with the strongest compaction forces (tablet set 3) (2500 lbs). After that time the three sets of tablets have similar dissolution profiles and follow the same type of dissolution profile as the free powder.

During the dissolution experiments it was also noted that the tablets containing dicalcium phosphate almost immediately disintegrated once placed in water, with the exception of the tablet prepared with the strongest compaction forces. This observation is consistent with the explanation that the lag time observed with the tablets containing lactose is due to the slower disintegration of the tablets. Very little difference exists between the different tablets in terms of amounts of salicylic acid dissolved at the end of the dissolution study. However, the dissolution rate of salicylic acid was slightly faster in the tablet set 2 (solid fraction of 0.86). The percentage of salicylic acid present in solution after 500 s for the tablets sets 1 and 2 (solid fraction of 0.79 and 0.86) was approximately 80% and 88%, respectively. It was also about 80 % for tablet set 3. The final relative amounts of salicylic acid in solution at the end of the study were only slightly

higher than those values. For both formulations, a larger tablet solid fraction was associated with faster dissolution of salicylic acid. Only the tablets of lactose and salicylic acid with a solid fraction of 0.90 did not follow this trend. An explanation for this was not immediately apparent.

6.3.2.3 Relationship between dissolution profile and ^1H T_1 times of salicylic acid and lactose monohydrate in formulated tablets

For all the tablets, the ^{1}H T_1 time of salicylic acid and the dissolution rate seemed to correlate: a shorter ^{1}H T_1 time was associated with a faster dissolution rate. This was more easily seen with the tablets prepared with lactose (Formulation A), since the tablets containing lactose all have very similar dissolution profiles. In Chapter 5, it was shown that shorter ^{1}H T_1 times were associated with smaller particles, and it is possible that compaction caused some of the particles of salicylic acid to fragment into smaller particles with stronger compaction forces generating smaller particles. It is interesting to note that the set number 3 of tablets containing lactose did not follow the trends associated with increasing compaction forces causing either a decrease in ^{1}H T_1 times of lactose monohydrate or faster dissolution rates. The ^{1}H T_1 time of lactose in the tablet set 3 of Formulation A (1000 lbs compression forces, solid fraction of 0.90) was higher than the ^{1}H T_1 time of lactose in the tablet set 4; a value of about 60 s was expected and instead the ^{1}H T_1 time of lactose obtained is 120 s. This indicates that the ^{1}H T_1 time of lactose, not of salicylic acid, could be used to predict the dissolution behavior of salicylic acid. Further supporting the significant influence of lactose monohydrate on the dissolution profile of the API is the fact that in the tablets where lactose is not present, the dissolution profile of salicylic acid closely mirrors the profile of the free powder. The differences in water solubility between MCC and lactose could help explain these observations. Lactose is soluble in water while MCC is not, as a result the presence of lactose would be expected to impact the dissolution

profile of salicylic acid from the tablet as it would be dissolving also. Conversely, MCC does not dissolve, hence the similarity between the dissolution profile of the salicylic acid in powder form and the salicylic acid in the MCC-containing tablets.

These observations strongly suggest that lactose is a major factor in the dissolution behavior of tablets in solution and that ^{1}H T_1 times measurements could potentially be used to predict that behavior. However, more data on more samples is likely needed in order to be able to draw firmer conclusions.

6.4 Conclusions

The findings presented in this chapter indicate that highly polydisperse crystalline samples can be distinguished from homogeneous samples based on the number of ^{1}H T_1 times detected. The relative amount of each phase can also be quantified. The effect of compaction forces on the tablets homogeneity can also be assessed in the same way, and it was found that stronger compaction forces were associated with shorter ^{1}H T_1 times. Decreases in ^{1}H T_1 times after compaction have previously been observed with pure lactose monohydrate, however only one compaction force was studied [10]. Here, the different compaction forces appear to have different effects on the formulated API as in addition to the reduction in ^{1}H T_1 time, some of them have generated materials whose spin lattice relaxation is best described using two ^{1}H T_1 times. This suggests that these tablets contain both larger and smaller particles.

Finally, a relationship between compaction forces, ^{1}H T_1 times and dissolution rate was found, and the influence of the excipients on the dissolution profile of the API was underlined. These results highlight the potential for ^{1}H T_1 times measurements of crystalline solid pharmaceuticals to be used for the prediction of physicochemical properties such as mixing level and dissolution rate.

6.5 References

1. Johnson MC 1972. Particle size distribution of the active ingredient for solid dosage forms of low dosage. Pharm Acta Helv 47(8):546-559.

2. Swaminathan V, Kildsig D 2002. Polydisperse Powder Mixtures: Effect of Particle Size and Shape on Mixture Stability. Drug Development & Industrial Pharmacy 28(1):41-48.

3. Yalkowsky SH, Bolton S 1990. Particle size and content uniformity. Pharm Res 7(Copyright (C) 2012 U.S. National Library of Medicine.):962-966.

4. Yajima T, Itai S, Hayashi H, Takayama K, Nagi T 1996. Optimization of size distribution of granules for tablet compression. Chem Pharm Bull 44(Copyright (C) 2012 American Chemical Society (ACS). All Rights Reserved.):1056-1060.

5. Iacocca RG, Burcham CL, Hilden LR 2010. Particle engineering: A strategy for establishing drug substance physical property specifications during small molecule development. Journal of Pharmaceutical Sciences 99(1):51-75.

6. Barich DH, Gorman EM, Zell MT, Munson EJ 2006. 3-Methylglutaric acid as a 13C solid-state NMR standard. Solid State Nuclear Magnetic Resonance 30(3-4):125-129.

7. Pines A 1973. Proton-enhanced NMR of dilute spins in solids. J Chem Phys 59(2):569.

8. Andrew ER, Bradbury A, Eades RG 1959. Removal of Dipolar Broadening of Nuclear Magnetic Resonance Spectra of Solids by Specimen Rotation. Nature 183(4678):1802-1803.

9. Lowe IJ 1959. Free Induction Decays of Rotating Solids. Physical Review Letters 2(7):285-287.

10. Lubach JW, Xu D, Segmuller BE, Munson EJ 2007. Investigation of the effects of pharmaceutical processing upon solid-state NMR relaxation times and implications to solid-state formulation stability. Journal of Pharmaceutical Sciences 96(4):777-787.

Chapter 7

Investigation of the effect of milling on gabapentin physical and chemical stability

7.1 Introduction

The previous chapters focused on the correlation between the particle size of crystalline solids and their SSNMR proton-spin-lattice relaxation (^{1}H T_1) times using dicumarol and salicylic acid as model compounds. In Chapter 6, the ability to use ^{1}H T_1 times to determine the polydispersity of powders was shown, as well as the ability to predict the dissolution behavior of a tableted crystalline API. In this chapter, the correlation between the proton spin-lattice relaxation (^{1}H T_1) time, the amounts of defects present in a ground API, and the chemical stability of the material is demonstrated, thus highlighting further the relevance and utility of using ^{1}H T_1 times to characterize pharmaceutical solids.

7.1.1 Chemical stability in solids

The chemical stability of pharmaceutical solids is currently assessed and predicted by submitting the material to lengthy stability tests and using kinetic models to fit the data. However, solids do not behave as homogeneous systems, rendering their solid-state chemical kinetics difficult to predict, and extrapolations from the kinetic model to the actual stability of the material at ambient conditions difficult to make. One of the most common kinetic models is the Prout-Tompkins model. It was first proposed in 1944 to describe the thermal decomposition of crystals of potassium permanganate, and since then it has been widely applied to pharmaceutical systems [1,2]. The Prout-Tompkins equation assumes that the rate of chemical degradation reaction is controlled by linearly growing nuclei that spread from the nucleation site through the crystal by branching. This makes the presence of nucleating sites a critical aspect of the solid-state reaction mechanism. Carstensen has extensively studied the kinetics of the solid-state degradation of aspirin using a Prout-Tompkins model [3,4].

Changes in the chemical stability of solid pharmaceuticals can occur as a result of manufacturing processes such as milling [5-9]. Previous studies in the Munson laboratory have investigated the correlation between the presence of crystal defects in milled aspirin, the chemical stability of the material, and its proton spin-lattice relaxation time ^{1}H T_1 [10]. In that study, aspirin was cryoground for up to 60 min and the ^{1}H T_1 times and ^{13}C SSNMR spectra of the ground materials were collected. The ^{13}C SSNMR spectra indicated that all the materials were still crystalline after grinding. However, a stability study of the ground materials revealed that 60 min of cryogrinding created a very unstable material that completely degraded to salicylic acid and acetic acid after 3 days under stability conditions (50% RH, 75ºC). That material also had the lowest ^{1}H T_1 time of all the aspirin samples. The aspirin sample that was ground for the shortest amount of time had the longest ^{1}H T_1 time and was the most chemically stable. It still contained more than 80% of aspirin after 3 days under stability conditions. This study highlighted the potential for ^{1}H T_1 times to serve as stability predictors of crystalline materials. In this chapter we extend the work of Lubach on aspirin to another API: gabapentin.

7.1.2 Gabapentin as a model compound

Gabapentin is an excellent model compound for this study because it has known chemical stability issues [11]. It is known to degrade to a cyclic lactam via a dehydration reaction. Recently, Zong and coworkers investigated the effect of milling on both the physical and chemical stability of gabapentin [11]. They milled Form II for 15-60 min and stored the samples at 50 ºC, at relative humidity values ranging from 5 to 80%. The chemical stability was assessed by the amount of gabapentin lactam formed. While milling did not cause any physical transformation, the amount of lactam formed increased with milling time. Moisture had an unusual stabilizing effect and prevented further degradation to the lactam. They concluded that while milling is known to

introduce lattice disorder, moisture may bring about recrystallization ("healing of the crystal defects") and thereby stabilize the material.

Gabapentin also has several known crystal forms that may impact its stability. Three polymorphic forms of gabapentin and a hydrate have been reported in the literature: Forms II, III, and IV are anhydrous forms, while Form I was later discovered to be a monohydrate therefore not an actual polymorph of the material [12,13]. Form II is the most thermodynamically stable form under ambient conditions. Form III and Form IV are metastable, and the latter has not been well characterized. A number of groups have studied the interconversion of gabapentin crystalline forms as a result of milling and other stress factors such as heating [13-15]. Fourier-Transform Infrared spectroscopy (FT-IR), differential scanning calorimetry (DSC), thermogravimetric analysis (TGA) and powder X-Ray diffraction (PXRD) were the techniques used to characterize gabapentin forms in all the reports.

In this chapter, solid-state NMR (SSNMR), along with PXRD and DSC, were used to characterize the physical state of gabapentin, and SSNMR relaxation times were correlated to the propensity of gabapentin to chemically degrade to its lactam upon being milled.

7.2 Materials and Methods

Gabapentin (Form II) was obtained from Hangzhou Starshine Pharmaceutical Co. LTD (Hangzhou, China). Gabapentin lactam was purchased from Sigma Aldrich (St. Louis, MO). Because this work was a collaborative project performed in the context of NIPTE (National Institute for Pharmaceutical Technology and Education) some of the sample preparation and characterization was performed at the University of Minnesota or the University of Iowa.

7.2.1 Sample preparation

Preparation of Form III and Form I

Gabapentin Form I was prepared using the method of Ibers by dissolving 160 mg of gabapentin Form II in 1 mL of water, adding 3 mL of 2-propanol, and keeping it in the freezer for six days [16]. The crystals were then harvested. Thermogravimetric analysis (TGA) of Form I revealed a weight loss of ~9%, close to the stoichiometric water content of 10% for the monohydrate. Gabapentin Form III was crystallized from a saturated 95% ethanol solution at 60 ºC. The temperature was kept constant throughout the crystallization process. These samples and the milled samples were prepared at the University of Iowa.

Spray-drying

A 5% solution (w/w) of gabapentin in a solution of water: ethanol (1:2) was spray dried in a Buchi spray dryer. The inlet temperature was 60ºC, the aspiration rate was 100% of the pump capacity and the pump rate was 5% of the pump capacity. The spray drying was performed at the University of Minnesota in the laboratory of Dr. Suryanarayanan.

Milling

Gabapentin Form II was milled in a planeraty mill for 45 min with four hardened steel balls (Pulviserette 7, Planetary Micro Mill)

7.2.2 Sample characterization

Polarized Light Microscopy (PLM)

Samples were imaged on a polarized light Olympus microscope (Center Valley, PA) under a 20X objective.

Powder X-Ray Diffraction

The diffraction patterns were collected using a wide angle X-ray diffractometer (model D5005, Bruker, Madison, WI) at ambient temperature. The instrument was operated in a step-scan mode, in 0.05º2θ steps, and counts were accumulated for 1.0 second at each step over the range of 5 to 40°2θ. The PXRD patterns were obtained at the University of Minnesota in the laboratory of Dr. Suryanarayanan.

High-Performance Liquid Chromatography (HPLC)

A Thermo Spectrum HPLC System (P4000 pump, AS3000 auto injector, and UV 6000 LP photodiode array detection system) was used to quantify gabapentin and gabapentin lactam. The results are reported as a mole percentage (w/w) of total gabapentin (gabapentin + gabapentin lactam). The amount of gabapentin lactam generated during milling was determined from HPLC of samples before and after milling. A small amount of each of the gabapentin samples was stored at 50 ºC and 0% relative humidity for 24 hours and then subjected to HPLC. HPLC measurements on these samples were used to determine the amount of chemical degradation occurring upon thermal stress. The HPLC stability studies were performed in the laboratory of Dr. Kirsch at the University of Iowa.

Solid State Nuclear Magnetic Resonance (SSNMR) Spectroscopy

^{13}C SSNMR spectra were collected using either a Chemagnetics CMX300 (Varian, Palo Alto, CA), a Bruker Avance 300 (Bruker, Billerica, MA) or a Tecmag Apollo (Tecmag, Inc., Houston, TX) spectrometer all operating at a ^{13}C frequency of ~75 MHz. Each sample was packed under ambient conditions in a 7 mm zirconia rotor (Revolution NMR, Fort Collins, CO). 3-methylglutaric acid was used as an external standard, with methyl peak referenced to 18.84 ppm

[17]. All spectra were acquired using ramp cross polarization and magic angle spinning (CP/MAS) [18-20]. A SPINAL-64 decoupling pulse sequence was used, and the spinning side bands were suppressed using total sideband suppression (TOSS). A contact time of 1 ms, MAS frequency of 4.0 kHz and a ^{1}H decoupling field of 70-80 kHz were used. Proton relaxation time values, ^{1}H T_1, were measured by saturation recovery.

7.3 Results and discussion

Before studying the chemical degradation induced by milling of gabapentin Form II, all the known forms of gabapentin were first characterized. During the characterization process, one new form was identified.

7.3.1 Gabapentin forms characterization by SSNMR

Figure 7.1 shows the ^{13}C SSNMR spectrum of Form II of gabapentin. The spectrum has one peak in the carbonyl region at 179 ppm, and eight peaks in the aliphatic region between 20 and 60 ppm. The peak at 39 ppm is broadened due to coupling with ^{14}N. This peak is useful for identifying different crystalline forms of gabapentin because of its distinctive line shape. The linewidths of the other peaks vary from 10-15 Hz. Because the carbonyl peak is separate from the aliphatic peaks, only the aliphatic region is shown in the spectra presented in the rest of this chapter.

Figure 7.2 shows the aliphatic region of the ^{13}C SSNMR spectra of the known crystalline forms of gabapentin that have been analyzed in our laboratory, as well as gabapentin lactam. In contrast to gabapentin Form II, the crystalline Forms I and III only have seven peaks in the aliphatic region of their spectra. This is likely due to overlapping peaks of two carbons between 20-25 ppm, which results in a broader peak at 22 ppm for Form III and 22.5 ppm for Form I. In

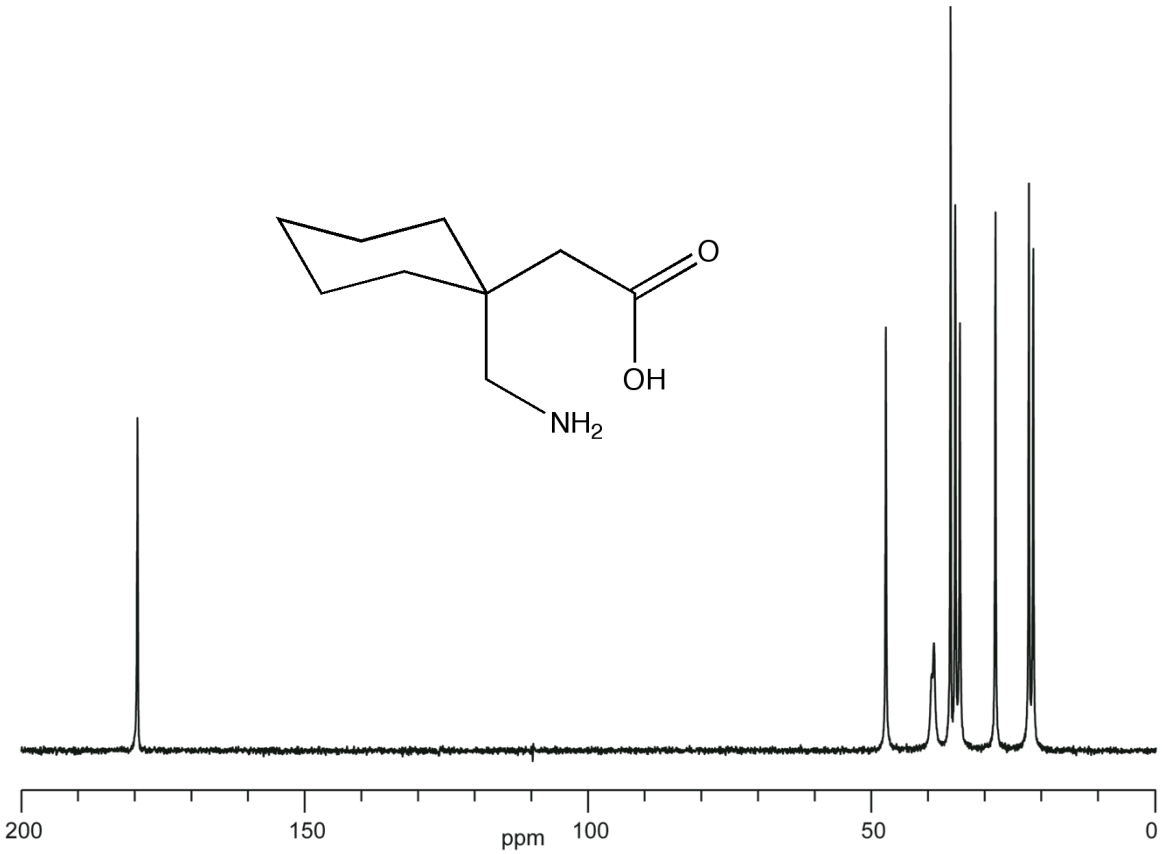

Figure 7.1 ^{13}C CP/MAS SSNMR spectrum of gabapentin Form II and chemical structure of gabapentin

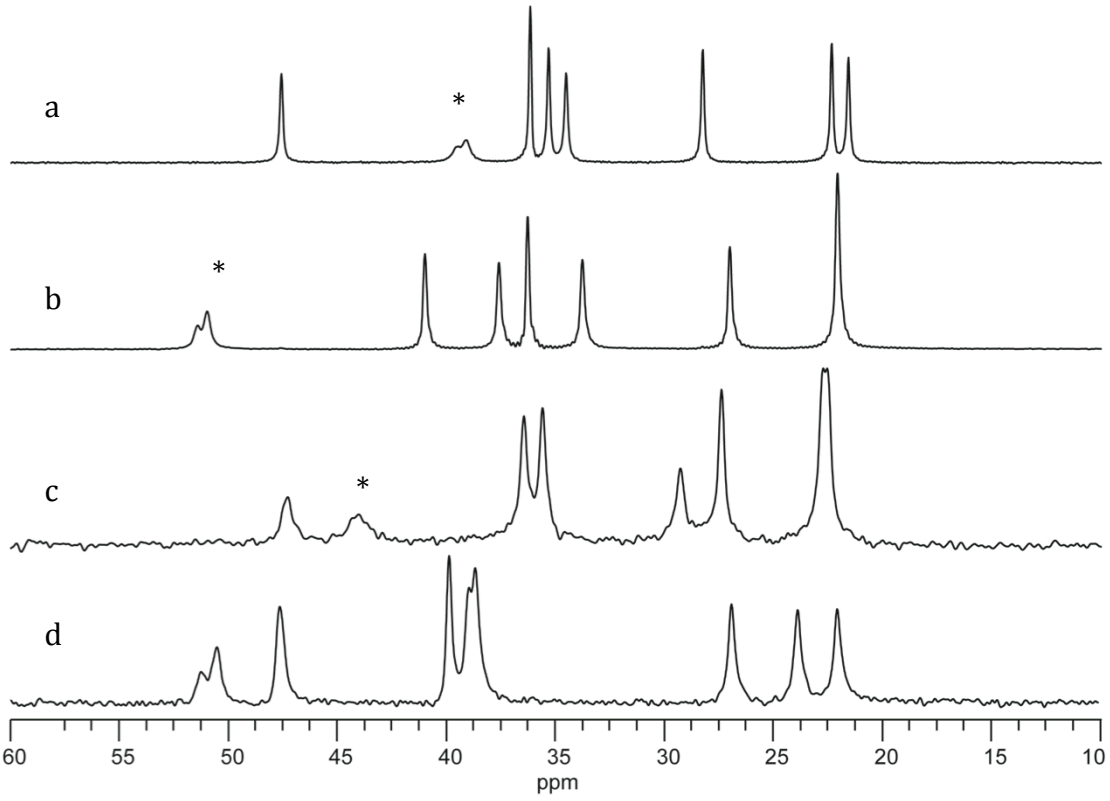

Figure 7.2 Aliphatic region of ^{13}C CP/MAS SSNMR spectra of **a.** gabapentin Form II; **b.** gabapentin Form III; **c.** gabapentin Form I; d. gabapentin lactam
(*) indicates the nitrogen-split peak.

Form III, the carbon peak that is broadened due to ^{14}N coupling is located at 51 ppm. There is a 12 ppm difference between the location of that peak in Form II and Form III. The ^{13}C SSNMR spectrum of Form I, the monohydrate, presented in Figure 7.2c has a different set of chemical shifts than observed for Forms II and III. The ^{13}C SSNMR spectrum of the degradation product of gabapentin, gabapentin lactam is presented in Figure 7.2d. The lactam's aliphatic region has seven peaks; two of these peaks (51 ppm and 38 ppm) are broadened due to coupling with the adjacent ^{14}N nucleus. Table 7.1 summarizes the ^{13}C SSNMR chemical shifts of the known gabapentin forms as well as gabapentin lactam. A new form of gabapentin was discovered while characterizing the known forms; it is presented in the following section.

7.3.2 New form of gabapentin

The ^{13}C SSNMR spectrum of spray-dried gabapentin shown in Figure 7.3b (aliphatic region only) indicates that it is a mixture of forms. Some of the peaks in the spectrum align with Form III, while the other ones do not align with either of the other known forms of gabapentin, suggesting that they belong to an unknown form of gabapentin. However, a PXRD pattern of the same material (Figure 7.4) indicates that it is a mixture of Form I and another form. Since the PXRD peaks of the new form were identical to the ones of Form I, that new polymorph was denoted the isomorphous desolvate. That form has never been reported to the best of our knowledge.

The isomorphous desolvate was also generated by in-situ dehydration of the monohydrate (Form I) inside the NMR spectrometer. Figure 7.3c shows the aliphatic region of the ^{13}C SSNMR spectrum of the material obtained after spinning gabapentin monohydrate in the NMR rotor for an extended period of time during the NMR experiment; it is a mixture of Form I (22.8

Table 7.1. SSNMR chemical shifts of gabapentin forms and gabapentin lactam. The peaks are listed in the order that they appear in the spectra.

	Chemical shifts (ppm)								
Form I	178.5	47.4	44.0	36.4	35.6	29.3	27.4	22.6	
Form II	179.5	47.6	39.1	36.2	35.3	34.5	28.2	22.4	21.6
Form III	177.4	51.2	41.0	37.6	36.3	33.8	27.0	22.1	
Lactam	179.1	50.9	47.6	39.9	38.8	26.9	23.9	22.0	

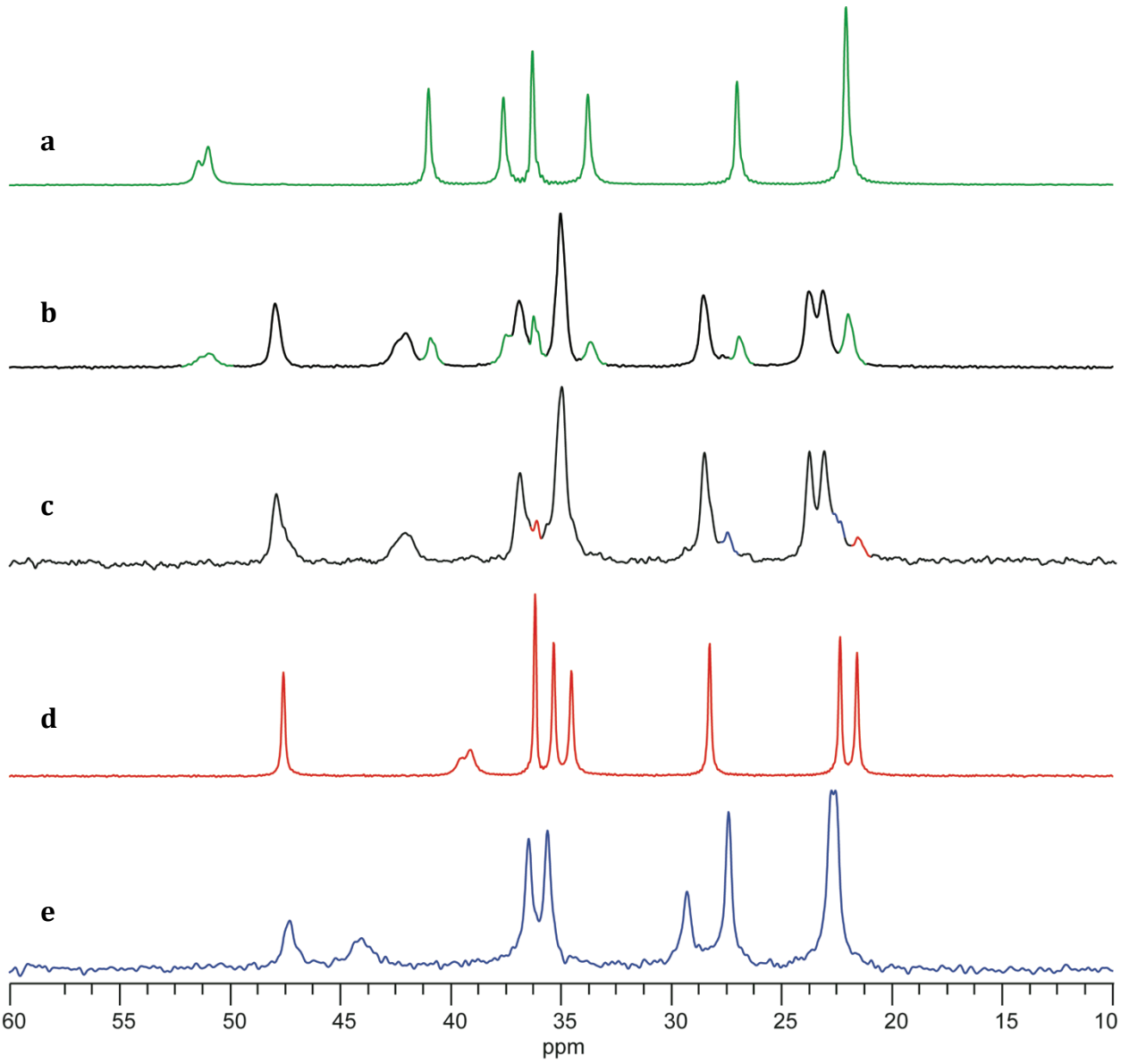

Figure 7.3 Aliphatic region of ^{13}C CP/MAS SSNMR spectra of **a.** gabapentin Form III; **b.** gabapentin spray-dried; **c.** the mixture of forms generated in situ; **d.** gabapentin Form II; **e.** gabapentin Form I

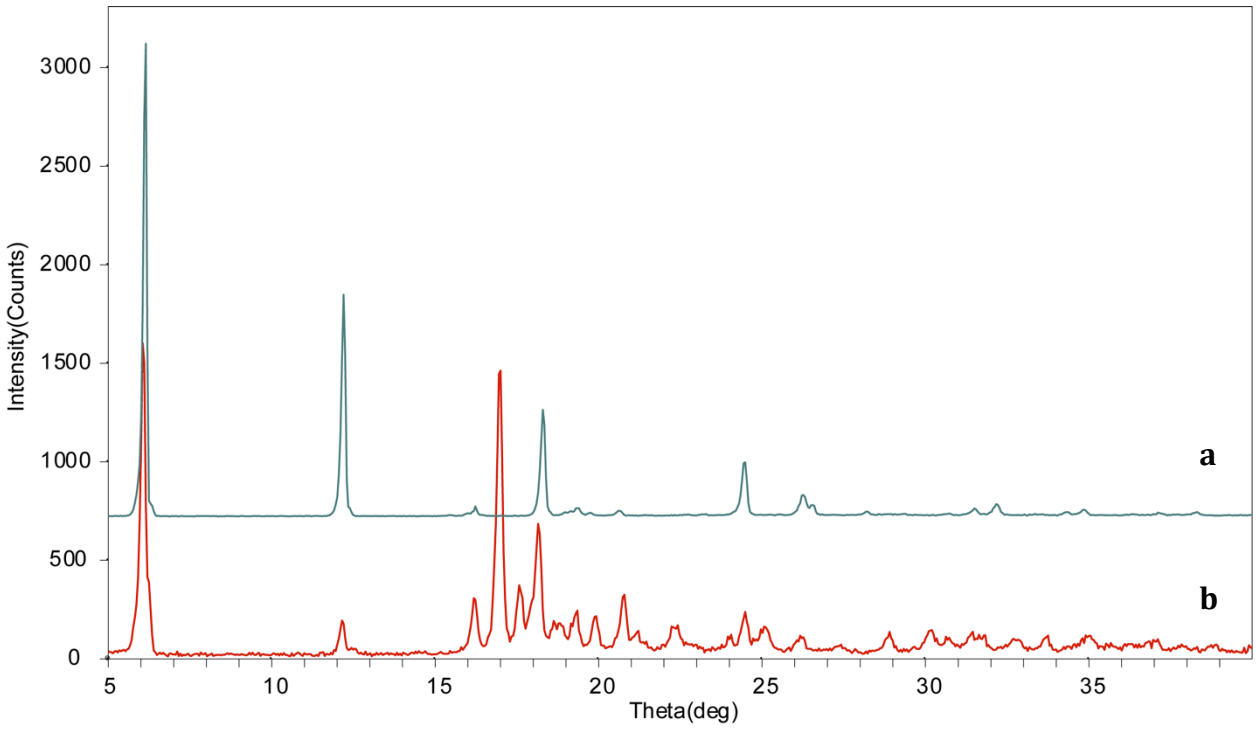

Figure 7.4 PXRD patterns of **a.** gabapentin form I; **b**. gabapentin spray dried

and 27.4 ppm), Form II (21.6 and 36.2 ppm), as well as the isomorphous desolvate. The Form II and Form I peaks are significantly smaller than the peaks of the isomorphous desolvate, suggesting that these forms are present in a lesser amount. It is not possible to accurately quantitate the amount of each form present in the material because differences in relaxation behaviors between the forms have not been accounted for when acquiring the spectrum. The peaks belonging to Form I are present because the conversion from Form I to the isomorphous desolvate was not complete, while peaks from Form II are present because the isomorphous desolvate is a metastable form that rapidly converts to the most thermodynamically stable Form II in the course of the NMR experiment. The proposed sequence of conversion is the following: Form I →Isomorphous desolvate →Form II.

The differences in chemical shifts, or peak position, in the ^{13}C SSNMR spectra of the previously known forms of gabapentin allowed us to distinguish between them. Also, the appearance of new peaks permitted us to identify a new form of gabapentin, the isomorphous desolvate, which is not identifiable by PXRD. Another helpful parameter in the identification of the forms of gabapentin by SSNMR is their proton spin-lattice relaxation (^1H T_1) times.

7.3.3 ^1H T_1 times of the forms of gabapentin

The ^1H T_1 of as-received gabapentin Form II is 134 s. Gabapentin Form III has a ^1H T_1 value of 63 s. The ^1H T_1 of gabapentin Form I is 378s suggesting very low mobility. It is possible that a hydrogen bonding network between the water and the gabapentin molecules causes this form to have this low a molecular mobility. Water can act as a relaxation sink and cause shorter ^1H T_1 times when it is mobile in the structure such as in non-stoichiometric hydrates or channel hydrates; however, when water is fixed in the crystal lattice, presumably by hydrogen bonding, relaxation times can be longer.

7.3.4 Effect of milling and hydroxy propylcellulose (HPC) on gabapentin Form II physical form conversion

Gabapentin Form II was milled for 45 min to determine the influence of milling on the physical and chemical stability of the material. It was also mixed with a small amount of hydroxypropylcellulose (HPC) and subjected to the same treatment. All the samples were then placed under stability conditions for 24h (50 ºC/ 0% RH). Table 7.2 describes the preparation method for each sample.

Figure 7.5 shows the ^{13}C SSNMR spectra of gabapentin Form II and gabapentin Form II-HPC mixtures before and after milling. The spectra of as-received gabapentin Form II (Figure 7.5a), and gabapentin Form II mixed with 6.5% HPC (Figure 7.5b) display the same carbon chemical shifts and similar linewidths of approximately 12-14 Hz. This indicates that HPC has no effect on the physical form of gabapentin in an unground physical mixture. This was expected since physically mixing materials, without milling, generally does not cause changes in physical state of the components of the mixture. The spectra of gabapentin Form II milled alone and of gabapentin Form II mixed with 6.5% HPC and milled have eight peaks with chemical shifts corresponding to gabapentin Form II. The spectrum in Figure 7.5d contains small peaks at 37 ppm and 41 ppm. Gabapentin milled alone shows no such peaks.

Figure 7.6 shows that these small peaks align with two of the peaks of Form III. This means that when milled in the presence of HPC (6.5% w/v), a small fraction of gabapentin Form II converted to Form III. Figure 7.7 shows the aliphatic region of the ^{13}C SSNMR spectrum of the unmilled and milled physical mixtures of gabapentin Form II and HPC and confirms this observation. Other groups have also observed gabapentin form conversion in the presence of a

Table 7.2 Summary of preparation conditions of gabapentin samples and sample notation

Preparation Conditions	**Sample**
Gabapentin Form II	A
Gabapentin Form II milled for 45 min	B
Gabapentin Form II milled for 45 min and exposed to 50 °C/0% RH for 24 h	C
Gabapentin Form II – HPC (6.5%) mixture	D
Gabapentin Form II – HPC (6.5%) mixture milled for 45 min	E
Gabapentin Form II – HPC (6.5%) milled for 45 min and exposed to 50°C/0% RH for 24 h	F

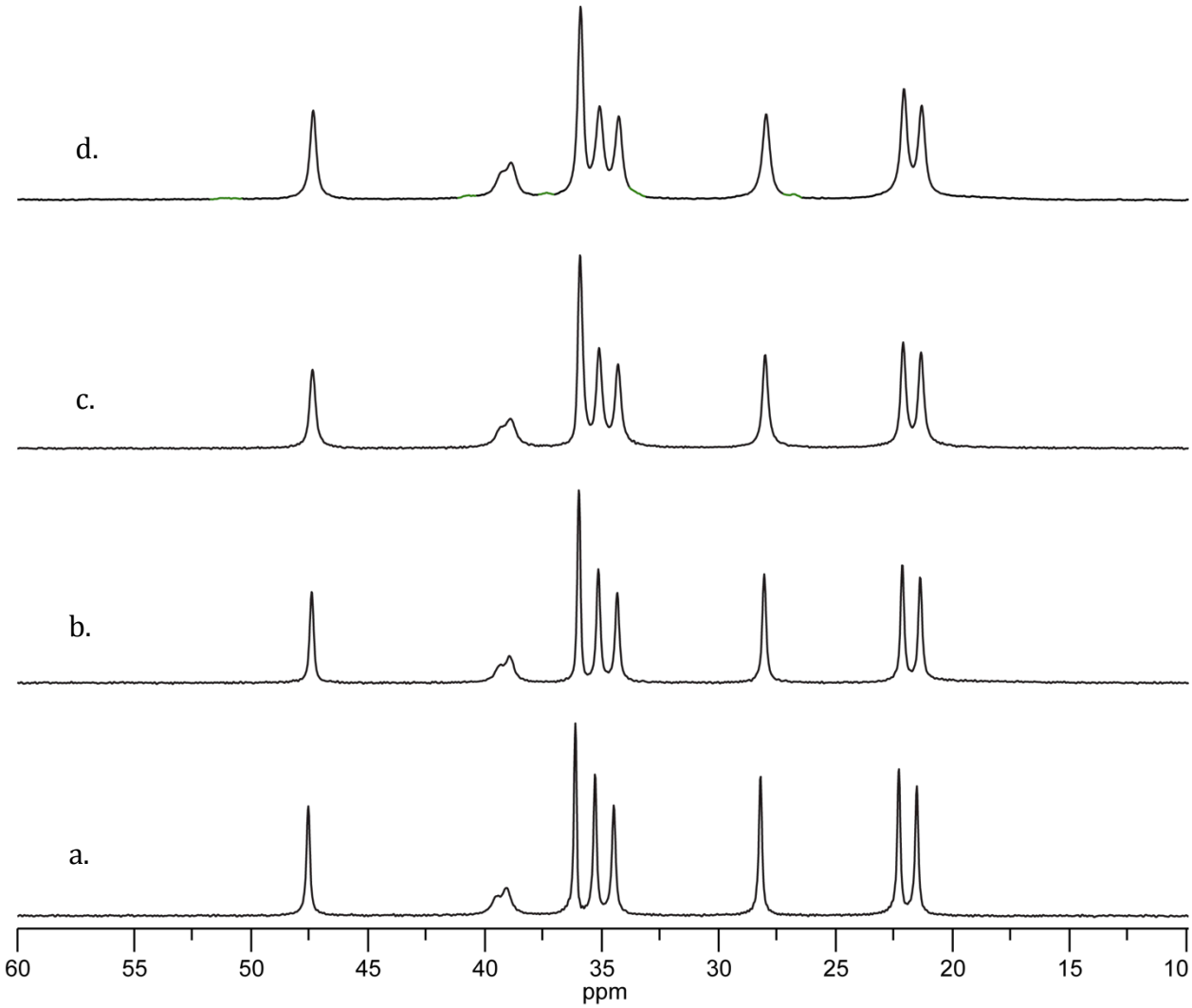

Figure 7.5 Aliphatic region of ^{13}C CP/MAS SSNMR spectra of **a**. gabapentin Form II (Sample A); **b** gabapentin Form II mixed with 6.5% HPC (Sample D); **c**. gabapentin Form II milled for 45 min (Sample B); **d**. gabapentin Form II mixed with 6.5% HPC and milled for 45 min (Sample E). The peaks in red correspond to Form III

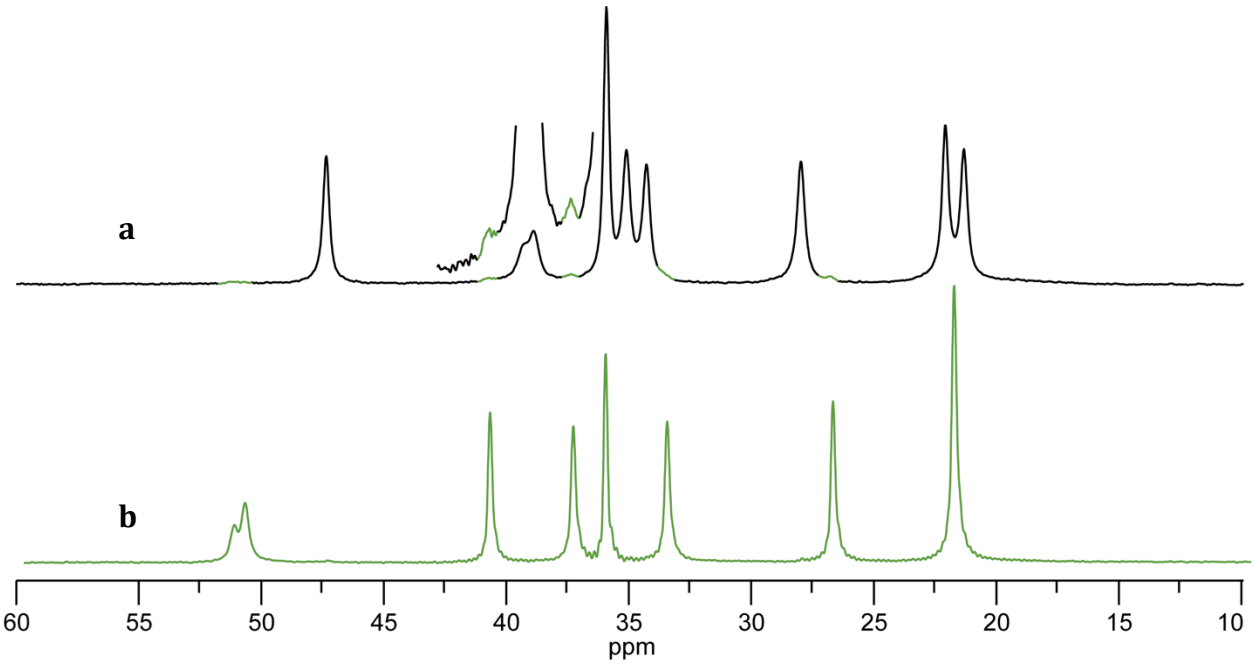

Figure 7.6 Aliphatic region of ^{13}C CP/MAS SSNMR spectra of **a**. gabapentin Form II mixed with 6.5% HPC and milled for 45 min (Sample E); **b**. gabapentin Form III

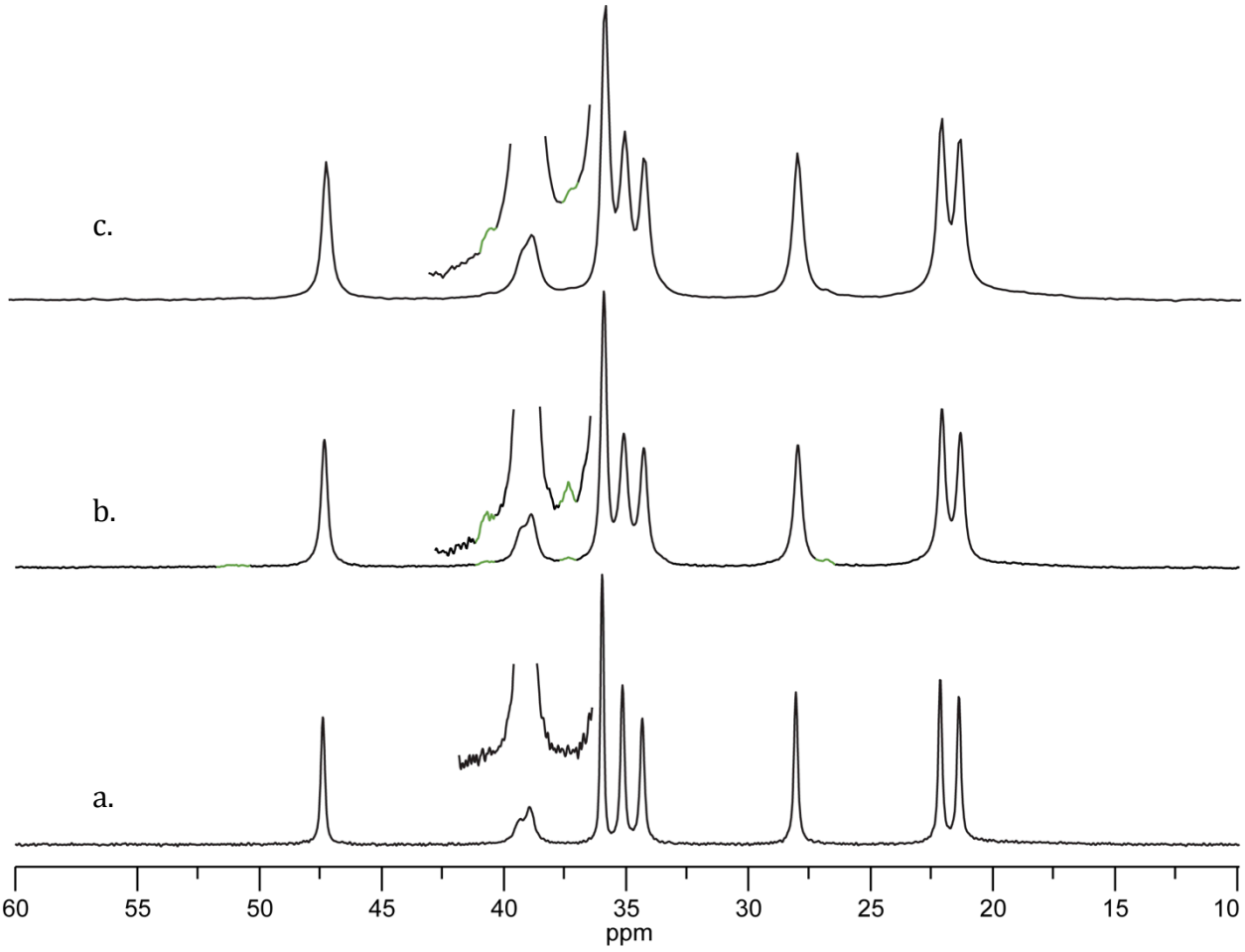

Figure 7.7 Aliphatic region of ^{13}C CP/MAS SSNMR spectra of **a**. gabapentin Form II mixed with 6.5% HPC (Sample D); **b**. gabapentin Form II mixed with 6.5% HPC and milled for 45 min (Sample E); **c**. gabapentin Form II mixed with 6.5% HPC, milled for 45 min, and exposed to 50ºC/0% RH (Sample F)

variety of excipients [13]. It is possible that the heat generated during milling combined with the presence of an excipient possibly acting as a stabilizer of the metastable form generated are responsible for these observed polymorphic conversions.

7.3.5 Effect of milling and HPC on lactam formation (chemical stability) and ^1H T_1 times

The ^1H T_1 times of the samples were measured before they were submitted to stability conditions. Despite the fact that all the milled and unmilled gabapentin and gabapentin-HPC samples are mainly composed of crystalline gabapentin Form II, their ^1H T_1 values are significantly different (Table 7.3). Gabapentin and the gabapentin-HPC mixture (Samples A and D) have the same ^1H T_1 value of ~ 130 s. The ^1H T_1 of gabapentin milled alone (Sample B) was 41 s, while that of Form II milled and exposed to 50ºC/0% RH (Sample C) was 61 s. The two gabapentin-HPC milled samples (Samples E and F) have significantly lower ^1H T_1 values than any of the other gabapentin samples: 11s and 14s.

The lactam content in all the milled and unmilled samples described above was measured before and after thermal stress (50ºC/ 0% RH/ 24h). Those conditions are different from typical stress conditions that use high relative humidity because the presence of water has been shown to stabilize gabapentin instead of causing it to be less stable [11]. Table 7.3 summarizes the results of the stability study. The samples that have been milled, Samples B, C, E and F have generated some lactam during the milling process as their initial lactam levels, before stability testing, are not zero. For all the samples except pure gabapentin Form II (Sample A), some lactam was generated during stability studies. Samples E and F generated approximately the same relative amount of lactam during stability (~0.5%). They also generated the largest relative amount of lactam of all the samples. Comparing the amounts of lactam generated during stability in

Table 7.3 Summary of gabapentin stability study and ^{1}H T_1 times. The amount of lactam generated during the stability study (Δ lactam) is presented in the last column

Preparation conditions	**Sample**	**^{1}H T_1 (s)**	**Initial lactam (%w/w)**	**Δ lactam**
Gabapentin Form II	A	134	0.000	0.000
Gabapentin Form II milled for 45 min	B	41	0.048	0.109
Gabapentin Form II milled for 45 min and exposed to 50 °C/0% RH for 24 h	C	61	0.098	0.134
Gabapentin Form II – HPC (6.5%) mixture	D	130	0.003	0.011
Gabapentin Form II – HPC (6.5%) mixture milled for 45 min	E	11	0.110	0.464
Gabapentin Form II – HPC (6.5%) milled for 45 min and exposed to 50°C/0% RH for 24 h	F	14	0.453	0.467

Samples B and C allows us to assess the effect of milling and thermal stress on the chemical stability of gabapentin Form II. Comparing those amounts to the ones generated in Samples E and F, that contain HPC, suggests that the presence of HPC has a significant impact on the chemical stability of gabapentin as more lactam was generated in the latter samples. Moreover, these results indicate that unless the materials were milled, exposure to high temperature and low humidity conditions did not cause formation of significant amounts of gabapentin lactam (<0.2%). Based on the lactam levels generated in the samples during thermal stress, three categories of materials emerge: low, medium and high relative chemical stability. The high stability group contained less than 0.01% of lactam. It includes as-received gabapentin Form II and gabapentin Form II mixed but not milled with 6.5% HPC. The medium stability group is composed of samples that contained between 0.01% and 0.1% of lactam, and includes the milled gabapentin Form II samples. Finally the low stability group generated more than 0.4% lactam and is made up of the milled Form II –HPC samples. 0.4% is the limit placed by the US Pharmacopeia on the amount of gabapentin lactam that can be present in tablets of gabapentin.

7.4 Discussion

The milled gabapentin Form II samples had shorter ^{1}H T_1 times and were less chemically stable than the unmilled materials (Table 7.3). The magnitudes of the ^{1}H T_1 times obtained for each sample correlate well with the low, medium, and high chemically stable groups defined earlier. The high stability group (Samples A and D) has ^{1}H T_1 times of ~130s, the medium stability group (Samples B and C) has ^{1}H T_1 times of 40-60s while the most unstable group has the shortest ^{1}H T_1 times observed: 11-14s (Samples E and F). These results suggest that a correlation exists between ^{1}H T_1 time and chemical stability of the gabapentin samples: unless milling caused a decrease of the ^{1}H T_1 time of gabapentin by more than an order of

magnitude, the material generated was not significantly less chemically stable than the unmilled as-received material.

The most unstable milled materials with HPC (Samples E and F) also contained small amounts of metastable gabapentin Form III, as such it is possible that it is that form that then converts to gabapentin lactam during stability studies. It is also possible that the presence of amorphous HPC creates regions of higher mobility in the material where chemical reactions can take place more readily.

The work presented in the earlier chapters of this dissertation indicate that particle size and the presence of defects are some of the physical explanation for the decrease in ^{1}H T_1 time observed when milling a crystalline material; therefore we can speculate that the decrease in particle size that occurred as a result of milling, which obviously led to an increase in surface area, could potentially be responsible for the decrease in chemical stability of gabapentin by providing more molecules on the surface that could undergo the dehydration reaction and generate the degradation product gabapentin lactam. However, since materials that were milled for the same amount of time, and presumably contain similarly sized particles, presented different ^{1}H T_1 times, it is safe to assume that another factor might be affecting the chemical stability of the material as well; that factor might be the presence of crystal defects that are the sites of chemical degradations. These crystal defects would also act as relaxation sinks and would explain the decrease in ^{1}H T_1 time observed.

Zong and coworkers developed a kinetic model based on the presence of nucleating sites, or defects, to describe the solid-state chemical degradation of gabapentin [21]. Their model included a parameter denoted gaba* that represents a crystalline gabapentin that is thought to be in a disordered state, yet not amorphous, and is likely to generate the degradation product

gabapentin lactam. A collaboration with that group has allowed us to measure the ^{1}H T_1 times of samples for which the amount of gaba*, abbreviated as G^*_0, had been measured. A correlation between the ^{1}H T_1 times and the G^*_0 term appears to exist. The plot correlating the two parameters is presented in Figure 7.8; it shows a linear correlation; however, the significance of each of the terms in the equation is not yet known. That plot includes ball-milled gabapentin Form II, gabapentin Form II milled and kept at 50ºC /0%RH for 24h, as well as tablets of gabapentin Form II. The tablets contain the least amount of gaba* and also had the longest ^{1}H T_1 times. Although more data is most likely needed in order to definitely establish that correlation, this result again supports the existence of a correlation between API chemical stability and SSNMR ^{1}H T_1 times. The mechanistic explanation behind such a correlation would rely on a Prout-Tompkins kind of chemical stability model, where crystal defects are considered the sites of chemical degradation in solids. These crystal defects are also partially responsible for the decrease in ^{1}H T_1 times observed when milling a material.

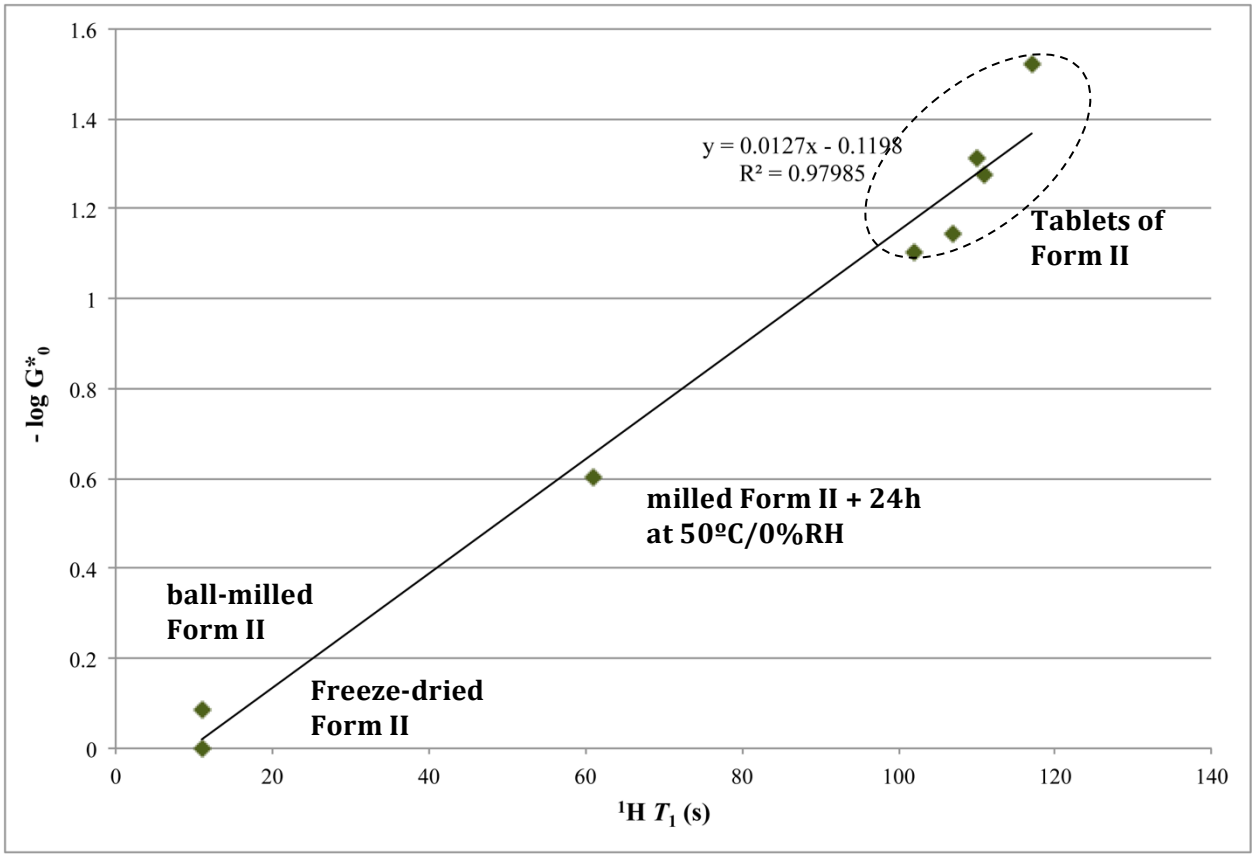

Figure 7.8 Plot of the log plot of "reactive gabapentin" as defined in (21) versus ^{1}H T_1 time for a few powdered samples and tablets of gabapentin Form II

7.5 Conclusion

We showed that milling gabapentin Form II in the presence of a small amount of HPC created a chemically unstable crystalline Form II material. The material with the shortest SSNMR ^{1}H T_1 times also had the lowest chemical stability. The results presented in this chapter reinforce the potential for ^{1}H T_1 to be used as a possible tool for correlating chemical stability predictor for solid crystalline pharmaceuticals. Combined with the results presented in the previous chapters, the results presented here allowed us to formulate potential hypotheses of the physical basis for the chemical instability of a crystalline API including the decrease in particle size occurred upon milling and possible crystal defects created upon milling and other processing.

7.6 References

1. Haskell RJ 1998. Characterization of submicron systems via optical methods. Journal of Pharmaceutical Sciences 87(2):125-129.

2. Beekman A, Shan D, Ali A, Dai W, Ward-Smith S, Goldenberg M 2005. Micrometer-Scale Particle Sizing by Laser Diffraction: Critical Impact of the Imaginary Component of Refractive Index. Pharmaceutical Research 22(4):518-522.

3. Carstensen JT, Attarchi F, Hou XP 1985. Decomposition of aspirin in the solid state in the presence of limited amounts of moisture. J Pharm Sci 74(7):741-745.

4. Carstensen JT, Attarchi F 1988. Decomposition of aspirin in the solid state in the presence of limited amounts of moisture III: Effect of temperature and a possible mechanism. J Pharm Sci 77(4):318-321.

5. Iacocca RG, Burcham CL, Hilden LR 2010. Particle engineering: A strategy for establishing drug substance physical property specifications during small molecule development. Journal of Pharmaceutical Sciences 99(1):51-75.

6. Wöstheinrich K, Schmidt PC 2001. Polymorphic Changes of Thiamine Hydrochloride During Granulation and Tableting. Drug Development and Industrial Pharmacy 27(6):481-489.

7. Zhang GGZ, Law D, Schmitt EA, Qiu Y 2004. Phase transformation considerations during process development and manufacture of solid oral dosage forms. Advanced Drug Delivery Reviews 56(3):371-390.

8. Ward GH, Schultz RK 1995. Process-Induced Crystallinity Changes in Albuterol Sulfate and Its Effect on Powder Physical Stability. Pharmaceutical Research 12(5):773-779.

9. Brittain HG 2002. Effects of mechanical processing on phase composition. Journal of Pharmaceutical Sciences 91(7):1573-1580.

10. Lubach JW. 2007. Applications of nuclear magnetic resonance spectroscopy to pharmaceutical solids. ed., United States -- Kansas: University of Kansas. p 376.

11. Zong Z, Desai SD, Kaushal AM, Barich DH, Huang H-S, Munson EJ, Suryanarayanan R, Kirsch LE 2011. The Stabilizing Effect of Moisture on the Solid-State Degradation of Gabapentin. AAPS PharmSciTech 12(Copyright (C) 2011 American Chemical Society (ACS). All Rights Reserved.):924-931.

12. Reece HA, Levendis DC 2008. Polymorphs of gabapentin. Acta Crystallographica Section C 64(3):o105-o108.

13. Lin S-Y, Hsu C-H, Ke W-T 2010. Solid-state transformation of different gabapentin polymorphs upon milling and co-milling. International Journal of Pharmaceutics 396(1-2):83-90.

14. Braga D, Grepioni F, Maini L, Rubini K, Polito M, Brescello R, Cotarca L, Duarte MT, Andre V, Piedade MFM 2008. Polymorphic gabapentin: thermal behaviour, reactivity and interconversion of forms in solution and solid-state. New Journal of Chemistry 32(10):1788-1795.

15. Hsu CH, Ke, W. T., Lin, S. Y. 2010. Progressive steps of polymorphic transformation of gabapentin polymorphs studied by hot-stage FTIR microspectroscopy. Journal of Pharmacy and Pharmaceutical Sciences 13(1).

16. Ibers JA 2001. Gabapentin and gabapentin monohydrate. Acta Crystallographica Section C 57(5):641-643.

17. Barich DH, Gorman EM, Zell MT, Munson EJ 2006. 3-Methylglutaric acid as a 13C solid-state NMR standard. Solid State Nuclear Magnetic Resonance 30(3-4):125-129.

18. Pines A 1973. Proton-enhanced NMR of dilute spins in solids. J Chem Phys 59(2):569.

19. Andrew ER, Bradbury A, Eades RG 1959. Removal of Dipolar Broadening of Nuclear Magnetic Resonance Spectra of Solids by Specimen Rotation. Nature 183(4678):1802-1803.

20. Lowe IJ 1959. Free Induction Decays of Rotating Solids. Physical Review Letters 2(7):285-287.

21. Zong Z, Qiu J, Tinmanee R, Kirsch LE 2012. Kinetic model for solid-state degradation of gabapentin. Journal of Pharmaceutical Sciences 101(6):2123-2133.

Chapter 8

Conclusions and Future Directions

8.1 Summary

The particle size of solid APIs and the presence of crystal defects impacts important pharmaceutical properties such as their dissolution rate and the drug bioavailability, as well as their chemical and physical stability. The particle size of solid materials also influences the ability to manufacture them. Poor manufacturability can lead to powder segregation and lack of dose uniformity in the final drug product. As a result, it is important that it be well characterized. A number of particle sizing techniques exist but none allow the size characterization of the API in the presence of excipients. Solid-state NMR spectroscopy (SSNMR), because it is selective, can be used to characterize solid APIs in a formulation. In this dissertation the correlation between the particle size of crystalline APIs and their proton spin-lattice relaxation times (^{1}H T_1) was investigated using model compounds. Dicumarol and salicylic acid were selected as model compounds for this study because of their long ^{1}H T_1 times and the fact that when ground they maintained the same crystalline form while their ^{1}H T_1 times decreased. For substances with short ^{1}H T_1 times, the investigation and findings presented here have less applicability. Crystalline samples of the model compounds containing particles with sizes ranging from 1 um-800 um were prepared by sieving, spray-drying, and anti-solvent precipitation. These preparation techniques were chosen because, unlike grinding, they do not involve mechanical attrition of the material, which is known to result in crystal defects being created (1). These defects are known to cause decreases in ^{1}H T_1 times therefore their presence would interfere with our investigation of the effect of particle size on ^{1}H T_1 times.

The model compounds selection and the preparation and physical state characterization of the samples of dicumarol and salicylic acid were presented in chapter 4. In Chapter 5 the size of the particles in the samples was characterized using two accepted particle-sizing methods:

laser diffraction and scanning electron microscopy, and then correlated with the ^{1}H T_1 times of the materials. Chapter 5 also presented a model that describes the correlation observed between the ^{1}H T_1 time of the dicumarol and the salicylic acid materials and their particle size. The model was based on the assumption that spin diffusion is the main spin-lattice relaxation mechanism. In Chapter 6 we presented how SSNMR relaxation time measurements could be used to characterize the polydispersity of crystalline powders, using physical mixtures of dicumarol. We extended this study to the investigation of the effect of different compaction forces on the homogeneity of formulated tablets of salicylic acid. Different ^{1}H T_1 times were obtained for salicylic acid at all compaction forces, and heavier compaction forces lead to a larger decrease in ^{1}H T_1 time. Also at certain compaction forces, the relaxation of salicylic acid was best described with two ^{1}H T_1 times. The ^{1}H T_1 time of lactose, one of the main excipients in some of the tablets was also found to correlate with the dissolution rate of salicylic acid in the tablets. Finally, in Chapter 7 we showed that changes in ^{1}H T_1 times of ground crystalline gabapentin Form II were correlated with the chemical stability of the material: samples with shorter ^{1}H T_1 times were the least chemical stable. The physical meaning for the reduction in ^{1}H T_1 time observed was believed to be both the presence of crystal defects and the decrease in particle size of the material.

8.2 Conclusion

The work presented here showed that pharmaceutically relevant bulk properties of crystalline solids can be characterized by solid-state NMR. It also increased our understanding of the physical meaning of changes in proton-spin lattice relaxation times observed in crystalline solids. Finally, it reinforces the potential for SSNMR to be used as a prediction tool for the behavior of pharmaceutical solids such as dissolution rate, or chemical stability.

8.3 Suggestions for future work

8.3.1 Improvements to the ^1H T_1 time-particle size model proposed

A few studies are briefly discussed that could be performed in order to improve the model proposed in Chapter 5 and establish its limitations.

- *Study more particle sizes of model system dicumarol and salicylic acid*

In the work presented here, we attempted to generate particles that spanned as wide a size range as possible and spent considerable amounts of time attempting to prepare particles of dicumarol by trial and error using anti-solvent precipitation. One avenue that was not explored is the preparation of crystalline particles with sizes ranging from 1-10 μm by precipitation followed by recrystallization of the dicumarol. This would be performed by just letting the dicumarol suspension prepared by anti-solvent precipitation sit at room temperatures for various amounts of time. Varying the length of times allowed for recrystallization could lead to crystals of a variety of sizes.

- *Establish the validity of the model in other systems*

In order to determine how applicable the findings presented here are to other molecules, other compounds need to be studied. Niflumic acid was once considered for use in this study and is one system that could be investigated further. The structure and ^{13}C SSNMR spectra of niflumic acid are presented in Figure 8.1. Niflumic acid has only one known polymorph and the ^1H T_1 time of as-received niflumic acid is 76 s, which is relatively short, however now that the correlation has been proposed it would be fairly straight forward to determine whether niflumic acid follows the trend of decreasing ^1H T_1 times with particle size.

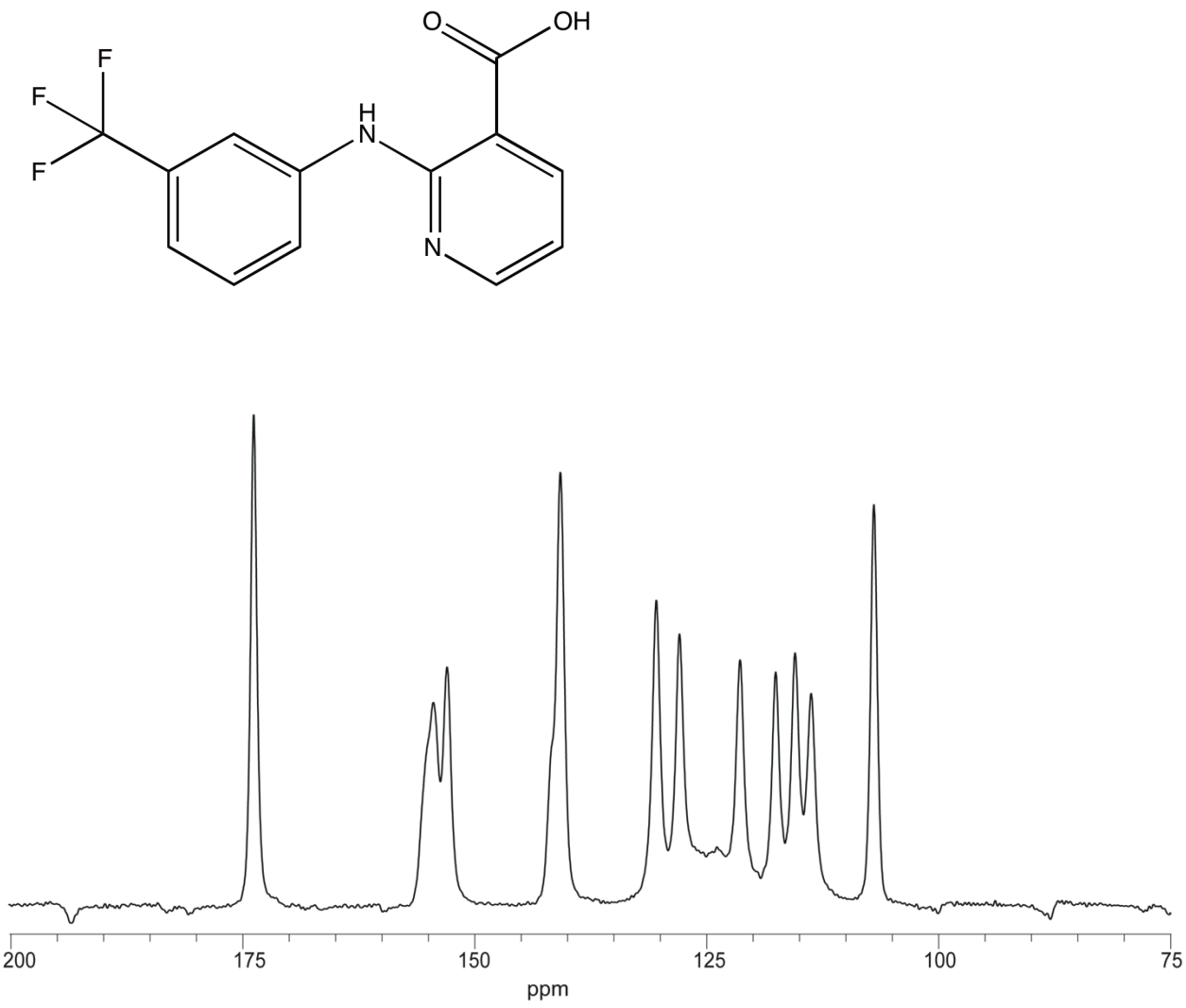

Figure 8.1 Structure and ^{13}C SSNMR spectrum of as-received niflumic acid

Figure 8.2 shows scanning electron microscope images of as-received niflumic acid and a sample prepared by precipitating a solution of niflumic acid in ethanol into an aqueous solution of Pluronics F 127. The particles obtained have a rod-like morphology. The effect of this type of morphology on the ^{1}H T_1 time is not known; however likely due to the different sizes present in the samples, two ^{1}H T_1 times were detected: 6 s and 36 s. Those values are smaller than the ^{1}H T_1 time of as-received niflumic acid. The DSC thermograms of the as-received and precipitated niflumic acid are shown in Figure 8.3. An endotherm due to the melting of niflumic acid is present in the thermograms around 205 ºC indicating that the precipitated material is crystalline.

8.3.2 Further explore the implications of the work presented here

- *Study the effect of different excipients on the tablet homogeneity and API dissolution rate*

In chapter 6, we showed that the ^{1}H T_1 time of salicylic acid in tablets changed with the compaction forces used to prepare the tablets. The number of ^{1}H T_1 time values detected was also dependent on the compression forces used. The two other major components of the tablets were lactose monohydrate and microcrystalline cellulose (MCC) or dicalcium phosphate and MCC. Different APIs and excipients could be studied in order to determine if the trend of decreasing ^{1}H T_1 time with increasing compaction forces holds, as well as investigate further the influence of lactose monohydrate on the dissolution rate of the API. Materials are often described as hard or soft; a studying using excipients from each of these categories would be interesting. It might enable the study of mechanisms such as deformation or fragmentation that may occur during tableting.

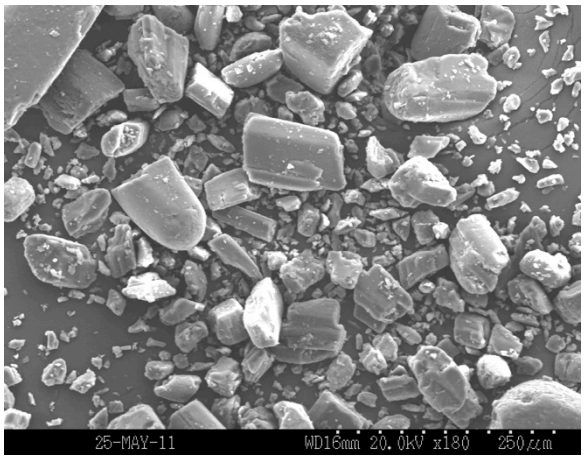

a

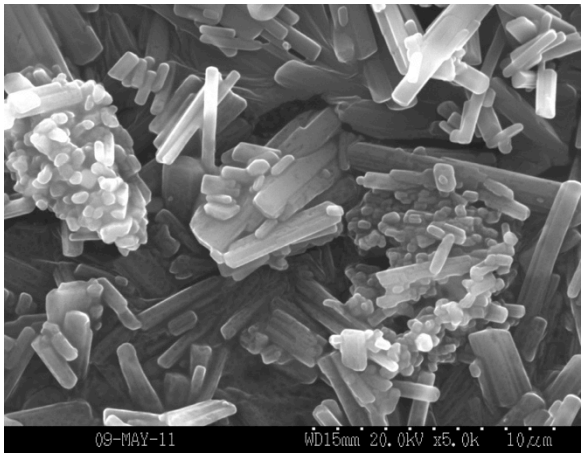

b

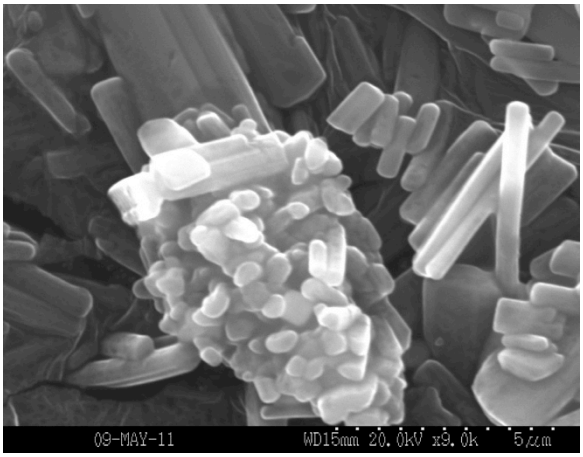

c

Figure 8.2 SEM micrograph of a.as-received niflumic acid; b-c. precipitated niflumic acid

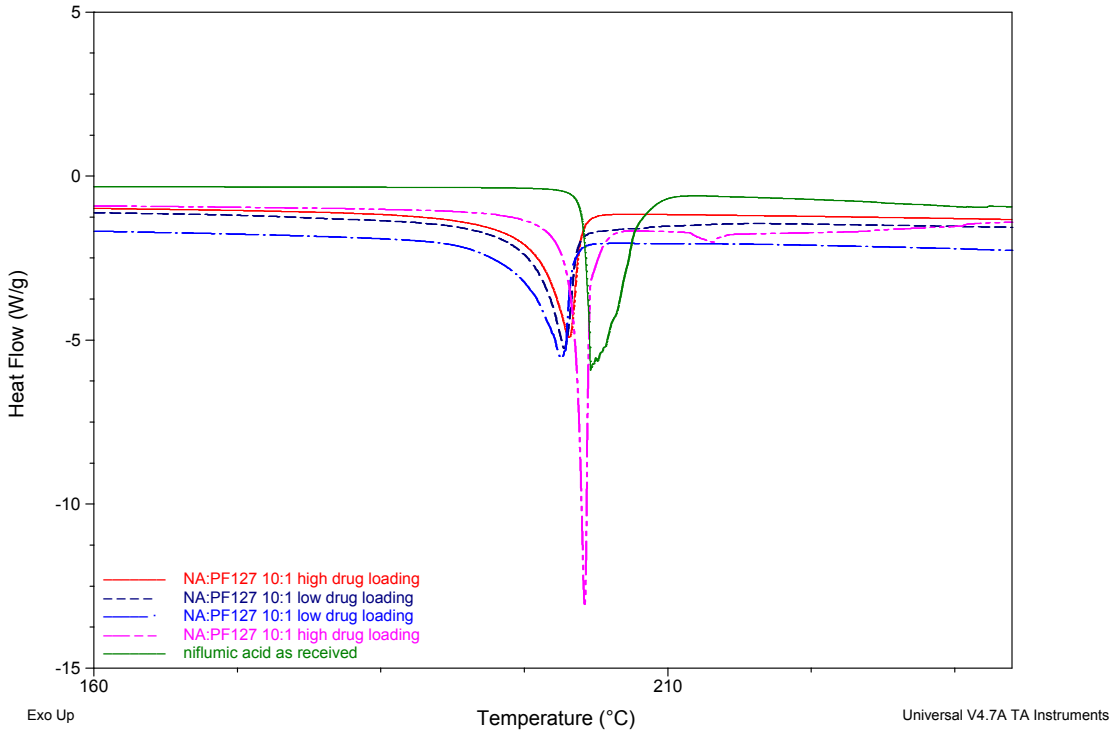

Figure 8.3 DSC thermograms of as-received niflumic acid and precipitated niflumic acid

- *Investigate further the correlation between ^1H T_1 time and chemical stability*

In Chapter 7 we showed that the ^{1}H T_1 time of ground crystalline gabapentin was correlated with the chemical stability of the material, most likely because this stability is dependent on the presence of crystal defects that are the sites of chemical degradation reactions. Investigating how changes in particle size in gabapentin influenced its chemical stability and its ^{1}H T_1 time could provide some insights on mechanisms of solid-state chemical degradation. However, the challenge with using gabapentin to perform this investigation will lie in finding a method to engineer the size of particles without causing polymorphic conversions. Aspirin is another compound that could be used to perform that study, although it might be difficult to detect changes in its ^{1}H T_1 time since it is relatively short compared to gabapentin (60 s).

8.4 Implications of this work

The implications of the work presented here include being able to better characterize solid pharmaceutical drug candidates throughout the different manufacturing steps and all the way to the final formulated drug product. This could result in better drug products, and potentially faster drug development thanks to the potential ability for SSNMR to be used as a prediction tool for the behavior or solid pharmaceuticals throughout manufacturing.

8.5 References

1. Wildfong PLD, Hancock BC, Moore MD, Morris KR. Towards an understanding of the structurally based potential for mechanically activated disordering of small molecule organic crystals. Journal of Pharmaceutical Sciences. 2006;95(12):2645-56.